THE USE OF MICROFINE CEMENT TO ENHANCE THE EFFICACY OF CARBON NANOFIBERS AND MICROFIBERS IN PORTLAND CEMENT MORTARS

A Dissertation

by

JOSHUA RYAN HOGANCAMP

Submitted to the Office of Graduate and Professional Studies of
Texas A&M University
in partial fulfillment of the requirements for the degree of

DOCTOR OF PHILOSOPHY

Chair of Committee	Zachary Grasley
Committee Members	Philip Park
	Ankit Srivastava
	Marcelo Sanchez
Head of Department	Robin Autenrieth

August 2017

Major Subject: Civil Engineering

ABSTRACT

The research herein discusses the mixing techniques for multi-scale fiber-reinforced Portland cement-based materials and their results on the mechanical properties of the overall composite with emphasis on drying shrinkage cracking resistance. The primary fibers used in this dissertation were carbon nanofibers (CNFs) and milled carbon microfibers (MCMFs). Ordinary Type I/II Portland cement (OPC) was found to limit the concentration of CNFs that can be successfully incorporated into the material due to geometric clustering. Using a microfine Portland cement eliminated geometric clustering of CNFs and stabilized the mixture, allowing for high concentrations of CNFs up to 5% by weight of cement. CNFs were dispersed in the cement by sonicating the CNFs with the cement in pure ethyl alcohol in fixed proportions, and then the alcohol was evaporated and recaptured with a distillation column. The hybrid CNF/cement powder produced was used to make high-concentration fiber-reinforced mortars. MCMFs were added during sonication for multi-scale fiber reinforcement in concentrations up to an additional 5% by weight of cement, and larger microfibers were added during mixing for up to 13% total fibers by weight of cement.

Dispersion of CNFs in cement was analyzed using a theoretical model and a finite element algorithm that utilized SEM images of the hybrid powders. In both scenarios, CNF dispersion was hindered in OPC but not in microfine cement. Restrained ring drying shrinkage tests revealed that high concentrations of CNFs did not significantly

benefit hybrid OPC mortar, but the CNFs did bridge microcracks in the hybrid microfine cement mortar and extended time until failure by up to 640%. The addition of MCMFs to the hybrid microfine cement mortar extended time until failure and peak microstrain in the restraining ring by at least 5,200% and 390%, respectively. Further testing revealed that high concentrations of CNFs can prove detrimental to OPC while high concentrations of MCMFs could prove highly beneficial. Multiple experiments also revealed that while high concentrations of CNFs can prove beneficial, the addition of high concentrations of MCMFs with CNFs can provide compounded benefits that are greater than the sum of the benefits from CNFs or MCMFs alone.

DEDICATION

Here's to the fools who dream,

foolish as they may seem.

–Benj Pasek and Justin Paul

ACKNOWLEDGEMENTS

I thank my committee chair, Dr. Grasley, for his guidance, patience, and support in my work. I cannot overstate the impact of his leeway—and, I daresay, excitement—for creativity while I followed my crazy ideas. I would also like to thank my committee members, Dr. Park, Dr. Sanchez, and Dr. Srivastava, for their continuing support and encouragement.

I also thank my colleagues, friends, and the department faculty and staff. My colleagues, for their comradery while we travel this road together. My friends, for the reminders to work hard and play harder (do *not* forget the latter). The department faculty and staff, for tolerating my antics, bearing my unceasing questions, and forgiving my general forgetfulness towards pesky paperwork.

I thank my family for their support and encouragement through my entire education. My siblings, while proud of my achievements, have always kept me grounded and relish in reminding me that doctors of philosophy do not, in fact, know everything. My parents have encouraged me in my endeavors and helped pack (and usually unpack) the moving trailer at every university; they have always been excited about my work and beam when they hear of my new accomplishments. Their support has been and is still invaluable; from the depths of my soul, thank you both for being you.

Finally, I thank my wife for her unfailing friendship, companionship, and faith that I could do this. Tess, I would not be who or where I am without you. Here's to us.

CONTRIBUTORS AND FUNDING SOURCES

Contributors

This work was supervised by a dissertation committee consisting of advising Professor Zachary Grasley, Professors Philip Park and Marcelo Sanchez of the Department of Civil Engineering, and Ankit Srivastava of the Department of Materials Science & Engineering.

The cement oxide compositions listed in Table 3 were determined by Kai-Wie Liu of the Department of Civil Engineering. The crack-mouth opening displacement data in Section 4.7 was determined with the assistance and supervision of Xijun Shi of the Department of Civil Engineering. Many experiments were conducted with the assistance of Bhavik Shah of the Department of Civil Engineering. All other work was completed independently by the student. Use of the Texas A&M Materials Characterization Facility is acknowledged.

Funding Sources

This work was made possible in part by the Qatar National Research Fund National Priorities Research Program No. 4-1142-2-440 and the National Science Foundation Division of Civil, Mechanical and Manufacturing Innovation No. 1562123. Its contents are solely the responsibility of the authors and do not necessarily represent the official views of the Qatar National Research Fund or the National Science Foundation.

Chemical admixtures were donated by Grace Construction Products of Cambridge, Massachusetts. Milled carbon microfibers and chopped carbon microfibers were donated by ZOLTEK of Bridgeton, Missouri. Microfine cement was donated by Capitol Cement of San Antonio, Texas.

NOMENCLATURE

Aspect ratio	fiber length/fiber diameter
CCMF	Chopped carbon microfiber
CMF	Carbon microfiber
CMOD	Crack-mouth opening displacement
CNF	Carbon nanofiber
CNT	Carbon nanotube
D	Dispersion parameter
E	Young's modulus (generic)
FE	Finite element
FRC	Fiber-reinforced cement/concrete/cementitious material
l_c	Critical fiber length
Macrofiber	Fibers with diameters approximately >0.5mm
MCMF	Milled carbon microfiber
Microfiber	Fibers with diameters ranging approximately from 1-500μm
MSE	Mean square error of data set
n	Number of samples in a data set
Nanofiber	Fibers with diameters ~100-200nm
Nanotube	Fibers with diameters ~2-10nm
OPC	Ordinary Portland cement
P	Applied load

PCBM	Portland cement-based material
PVA	Polyvinyl alcohol
q	q-value in Tukey's statistical analysis
RH	Relative humidity
R_{xx}	A radius (see Equation 5)
SEM	Scanning electron microscopy
S_i	Work vector to move a particle to a fully uniform dispersion
Sp	Spacing between cracks
V_f	Volume fraction of fibers
V_m	Volume fraction of matrix
vol%	Percent by volume, by volume of cement unless otherwise stated
W	Watts
w/c ratio	Mass ratio of water to cement
W_i	Work vector to move a particle to a fully non-uniform dispersion
wt%	Percent by weight, by weight of cement unless otherwise stated
α	Significance value in Tukey's statistical analysis
γ_r	Degree of restraint
ε	Strain (generic)
η	Crack width
μ	Data set mean
σ	Stress (generic)
σ_{fixed}	Theoretical maximum stress for a fully restrained specimen

σ_{fu}	Ultimate tensile strength of a fiber
σ_{mu}	Ultimate tensile strength of a cementitious matrix
τ_{fu}	Ultimate bond/slip strength between fibers and matrix
ϕ	Ratio of increase of permeability and diffusivity due to cracking

Mixture Designation

'Cement type' 'w/c ratio' – 'wt% CNFs' . 'wt% MCMFs' . 'wt% Other fiber'.

Example 1: OPC0.4-2.0 is an OPC mortar with a w/c ratio of 0.4, 2wt% CNFs, 0wt% MCMFs, and no other fibers.

Example 2: F0.5-2.2 is a microfine cement mortar with a w/c ratio of 0.5, 2wt% CNFs, 2wt% MCMFs, and no other fibers.

Example 3: F0.6-5.5.3 PVA is a microfine cement mortar with a w/c ratio of 0.6, 5wt% CNFs, 5wt% MCMFs, and 3wt% PVA microfibers.

TABLE OF CONTENTS

Page

LIST OF FIGURES

Page

LIST OF EQUATIONS

Page

LIST OF TABLES

Page

1. INTRODUCTION

1.1 Problem Statement

Portland cement based materials (PCBMs), the single most consumed material in the world after water [1], are quasi-brittle materials that have limited tensile strengths and strain capacities. Cracks often form in concrete during structural loading, foundation settlement, when exposed to fatigue, and when exposed to harsh environments. Concrete structures in the United States predominantly fail not from structural defects or excessive loading but from corrosion. Cracks in concrete allow water and deleterious chemicals such as deicing salts to penetrate and subsequently degrade the material as well as the reinforcing steel commonly used in concrete. According to research from NACE International, the estimated annual direct and indirect cost of concrete corrosion in the US is $7.8 billion* [2].

Concrete cracking can be caused by either internal or external forces. External forces are encountered in structural applications and include wind loads, vehicles on roads, structural dead weight loads, etc. Pavements and slabs are susceptible to foundation settlement and subgrade heave or erosion; high-rise structures are susceptible to wind forces that bend the structure and place the outer layers of concrete in tension, causing

* Corrected for inflation to match 2016 currency.

cracks on the outermost surfaces. Internal forces are found in almost all applications of concrete and are caused by drying shrinkage, autogenous shrinkage, sulfate attack, corrosion of reinforcing steel, and thermal gradients. Drying shrinkage and thermal gradients place the concrete under a non-uniform tension profile with high tension at the exposed surface and no tension inside the material, causing cracks on the exposed surface. Autogenous shrinkage causes the cement paste to shrink around aggregates and crack. Sulfate attack and reinforcing steel corrosion cause the inclusions (either aggregates or steel) to expand, placing the surrounding cement paste in tension which leads to cracking.

One of the best ways to mitigate concrete degradation is to limit the amount of water that can penetrate through the outermost layer of material by minimizing the size of the cracks that form. Such crack size minimization is often attempted by using macrofibers such as steel, polyvinyl alcohol, polypropylene, or others to bridge the cracks after formation. The size of fibers strongly dictates the number of cracks and the average crack widths that form in brittle matrices like Portland cement paste, mortar, and concrete; the larger (longer, larger diameter) a fiber, the fewer (but larger) the cracks that form. Commonly used microfibers such as polyvinyl alcohol (PVA) restrain cracks after they form in the material, but the cracks are large enough to see with the unaided eye (>0.1mm). Since transport properties through a cracked material roughly scale with the cube of crack width [3], it is preferable from a durability perspective to have a material with many very small cracks rather than a few larger cracks. In fiber reinforced concrete,

it has been proposed that the distance between cracks (and therefore the size of the cracks themselves) is directly proportional to the radius of the fibers [4, 5], so the use of nanofibers should theoretically result in multitudinous micro/nanocracks in concrete that are too small to be seen with the unaided eye.

One of the most difficult challenges in using microfibers and nanofibers in concrete and other PCBMs is thoroughly dispersing the fibers throughout the mixture. Microfibers can be adequately mixed throughout the material with more strenuous mechanical mixing (either longer mixing times with typical mixing techniques or higher energy input into mixing per unit time). However, the susceptibility of nanoparticles and nanofibers to thermal effects and van der Waals' forces, especially in water where materials such as carbon nanofibers (CNFs) and carbon nanotubes (CNTs) display hydrophobic tendencies, creates a ubiquitous hindrance to successfully incorporating CNFs and CNTs into PCBMs since the nanoparticles readily agglomerate together to form clumps on the order of micrometers or millimeters. These clumps lead to inconsistent material properties and potentially diminished material strength and stiffness [6]. The tendency of CNFs to agglomerate also severely limits the concentration of CNFs that can be included in an ordinary Portland cement (OPC) composite without clumping.

Another challenge in dispersing nanofibers throughout PCBMs is an effect called geometric clustering. Geometric clustering occurs when a mixture has constituents that

greatly vary in size and/or shape—see Figure 1. Figure 1a shows a representative 2D image of a typical OPC grain size distribution with a circle area fraction of 0.6 and an image edge length that is 5x larger than the largest circle. Figure 1b shows smaller 'nanoparticles' placed around the OPC grains subject to the constraint that no nanoparticle's centroid could be placed inside of an OPC grain. Figure 1c is Figure 1b with the OPC grains removed to show the large regions that do not contain nanoparticles. This geometric clustering can occur in OPC reinforced with nanofibers.

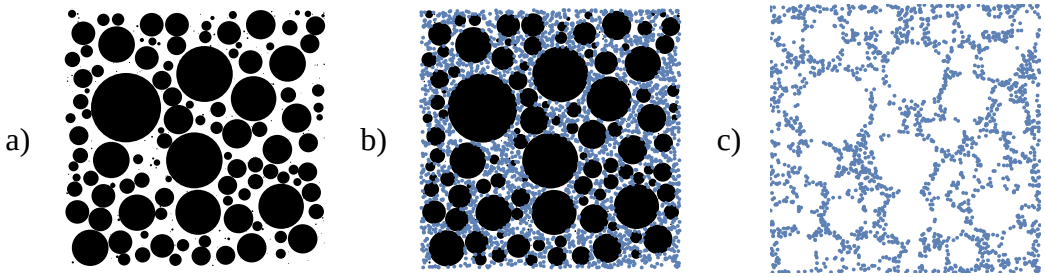

Figure 1: Geometric clustering of nanoparticles (blue) due to OPC grains (black). In (c), regions previously occupied by cement grains that are unreinforced by nanoparticles are clearly seen as empty voids.

1.2 Scope of Dissertation

It is desirable from a concrete durability perspective to decrease the width of cracks that form in PCBMs while maintaining or improving mechanical properties such as compressive strength, flexural strength, and impact toughness. While many researchers have used CNFs and CNTs in PCBMs for improving mechanical properties and cracking resistance with varying degrees of success, none have yet successfully made a 'crack-

proof' concrete. The results presented in this research make progressive headway in creating a PCBM with extreme resistance to cracking using CNFs while maintaining or improving other mechanical properties of the composite.

This dissertation details the development of a new Portland cement composite material with extreme resistance to cracking that includes high concentrations of CNFs and carbon microfibers (CMFs). Past research and literature reviews suggest that the primary factor in CNF PCBMs is the dispersion of the CNFs throughout the matrix; therefore, dispersion of CNFs was the first topic analyzed through experimental and computational methods. Scanning electron microscopy (SEM) imaging was utilized to determine the efficacy and dispersion of CNFs in preliminary OPC mortar experiments and in the final materials developed. It was discovered that using a cement with a grain size much finer than OPC improved and stabilized the dispersion of high concentrations of CNFs throughout the matrix. The use of microfine cement allowed for much higher concentrations of CNFs with a stable dispersion in the cement, but methods of dispersing CNFs commonly used in the PCBM industry do not permit higher concentrations of CNFs. A method new to the PCBM industry was explored and utilized to successfully disperse concentrations of CNFs in microfine cement 50x higher than the recommended concentrations in current literature.

The high-concentration CNF microfine cements were put through a battery of mechanical testing to determine the effect of the CNFs on the behavior of the composite material. The most important test used in this project was a miniaturized restrained ring

drying shrinkage test that used the porous nature of cement to place the outer surface of the specimens in tension. The exact time of cracking was recorded by monitoring the strain levels in the inner surface of the ring test setup. This test had highly repeatable results, and it allowed for detailed comparisons between cement mortars with differing amounts of CNFs and other fibers. Other tests used in this project included compressive strength, flexural strength, elastic modulus, free drying shrinkage, Izod fracture toughness, and crack-mouth opening displacement (CMOD) tests.

A distinct difference was found between CNF microfine cement and CNF OPC mortars with high concentrations of CNFs in all tests performed with CNF microfine cement mortars performing better than OPC mortars, especially regarding cracking resistance. CNF microfine cements extended cracking times by up to 640%, and the next step in testing involved using multiple fiber sizes to further increase cracking resistance. Milled carbon microfibers (MCMF) were added to the CNF microfine cement, also in high concentrations, and the cracking resistance of the multi-scale fiber-reinforced microfine cement was found to have benefits greater than the sum of contributions from CNFs or MCMFs separately. By combining CNFs and MCMFs with microfine cement, the cracking resistance of the composite was increased by 5,200% compared to the control mixtures.

The primary contributions of the research included in this dissertation are summarized as follows:

- Introduced a new dispersion method to the PCBM industry for dispersing high concentrations of CNFs and/or MCMFs into PCBMs.
- Determined that there is a maximum achievable dispersion of CNFs in OPC due to an effect called geometric clustering.
- Determined that using a microfine cement increases the maximum achievable dispersion of CNFs in PCBMs and stabilizes the mixture.
- Determined that SEM imaging is susceptible to bias and should not be used as a sole source of quantitative data, especially in mixtures whose constituents' sizes range over several orders of magnitude.
- Developed a miniaturized restrained ring drying shrinkage test for use with cement pastes or mortars to determine the efficacy of CNFs in preventing cracking.
- Determined that using a microfine cement enhances the efficacy of CNFs in the matrix, and that high concentrations of CNFs in microfine cement effectively bridge microcracks that form and delay the formation of a macrocrack.
- Determined that adding CNFs and MCMFs increases the cracking resistance in microfine cement mortars a greater amount than the sum of the individual cracking resistances provided by CNFs and MCMFs separately.
- Further characterized the effect of CNFs and MCMFs in OPC and microfine cement mortars with compressive strength, flexure, Izod impact toughness, and crack-mouth opening displacement tests.

1.3 Dissertation Outline

This dissertation is organized as follows. Chapter 2 reviews the current literature in the field of fiber-reinforced PCBMs and CNT/CNT cementitious materials. The literature covered in Sections 2.1-2.3 focuses on mechanical properties of FRCs and dispersion techniques for CNFs and CNTs in PCBMs and other materials. Section 2.4 discusses a concept known as geometric clustering that has a major influence on the dispersion of nanomaterials in PCBMs. Section 2.5 introduces the primary test method used in this research: the restrained ring drying shrinkage test. Chapter 3 covers the techniques of dispersing CNFs into cements, both OPC and microfine, and computational analyses thereof. Chapter 4 presents the procedures and results of mechanical testing performed on OPC and microfine cement mortars with high concentrations of CNFs and/or MCMFs. The restrained ring drying shrinkage test is the primary test, but it needs supplemental information to properly analyze the results and, hence, Chapter 4 is presented before the restrained ring drying shrinkage test results that are presented in Chapter 5. Chapter 5 discusses in detail the effects of high concentrations of CNFs and MCMFs in OPC and microfine cements, and the end of the Chapter 5 adds larger microfibers to microfine cement mortars that already have high concentrations of CNFs and MCMFs for up to 13% total fibers by weight of cement. Chapter 6 discusses the summary of the dissertation and primary conclusions, the shortcomings of the included research, and possible future work. Appendix A lists the material used in this research, and Appendix B presents SEM images of CNFs in the cements in this research.

2. LITERATURE REVIEWS

This chapter discusses background information and research already completed in fields related to those in this dissertation. The literature reviews cover fiber-reinforced cementitious materials (FRCs); the use of CNFs in other materials; dispersion techniques for CNFs in cements and other materials; the concept of geometric clustering; the restrained ring drying shrinkage test; cement calorimetry; and other experimental tests of PCBMs including free drying shrinkage prisms, mortar cubes, flexure prisms, Izod fracture toughness, and crack mouth opening displacement prisms.

2.1 Fiber-reinforced Cementitious Materials

The use of fibers in concrete and other brittle materials to increase strength and cracking resistance has existed since Biblical times as shown in *Exodus* 5:6-7:

> "And Pharaoh commanded the same day the task-masters of the people and their foremen, 'You shall no longer give the people straw to make bricks, as in the past; let them go and gather straw for themselves.'"

Other examples of the use of fibers in ancient times include bricks reinforced with straw near present-day Baghdad and concrete enhanced with horse hair for shrinkage resistance in the Roman era. A pueblo house built circa 1540, believed to be one of the oldest houses in the United States, is constructed with sunbaked adobe reinforced with straw [7]. Asbestos fibers were used in concrete in the 1900s with the development of

the Hatschek process but were later discontinued due to health hazards. By the 1960s, fiber types included glass, steel, and synthetic such as polypropylene. As of 2001, over 76 million m^3 (100 million yd^3) of FRC were produced annually with principal applications being slabs on grade, shotcrete, and precast members [8].

Some FRCs can be pre-manufactured as thin sheet components using, for example, asbestos or glass fibers. Most FRCs, both past and present, are randomly-oriented fibers in a cementitious matrix produced by adding fibers into the regular concrete mixer. The purpose of the fibers is not to increase strength but to bridge cracks during matrix failure and increase the energy required to completely break the material, thereby providing post-cracking ductility. It is important to note that while structural reinforcement in concrete such as rebar is included in structural concretes, fibers and steel reinforcement play different roles. Reinforcing bars are used to increase the load-bearing capacity of the structure while fibers are used for crack mitigation. Fibers cannot yet replace structural reinforcement, but they can be used in conjunction to improve overall performance in applications such as blast or seismic loading. An example of the increased ductility in FRC is shown in Figure 2 [9].

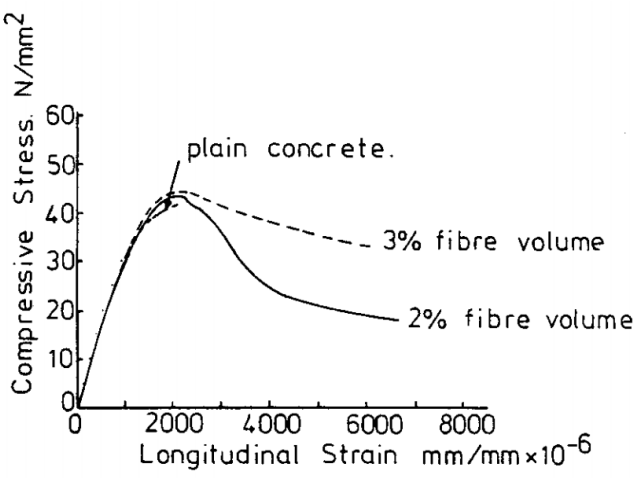

Figure 2: Stress-strain deformation in compression of steel-fiber concrete. The addition of fibers allows for post-peak sustained compressive stress. [9]

2.1.1 Failure Mechanics

Fibers in FRCs have two primary failure methods: fiber fracture and fiber pullout. Fiber pullout occurs when the tensile strength of the fiber exceeds the bond strength between the concrete and the fiber as shown in Figure 3. In Figure 3, an applied load *P* causes a crack in the FRC of maximum crack width η_p. As the crack grows, fibers are completely pulled out of the material in the traction-free crack length and no longer give strength at a crack width above η_{max}^{f}. Fibers in the fiber-bridging length are in tension and apply pressure on the material to bring the crack closed. The aggregate bridging length is the portion of the FRC where the cement matrix is cracked but inter-aggregate friction holds the composite at a crack width below η_{max}^{m}. This failure mode often occurs in composites that have high-strength fibers or fibers with low aspect ratios (length/diameter). Fiber pullout is the most energy-absorbent and ductile failure mode

for FRCs and is therefore the preferred method for designing FRC (fiber type, surface treatments, fiber content). For reasons of workability and dispersion in the matrix, the aspect ratio of most modern fibers is between 50-150.

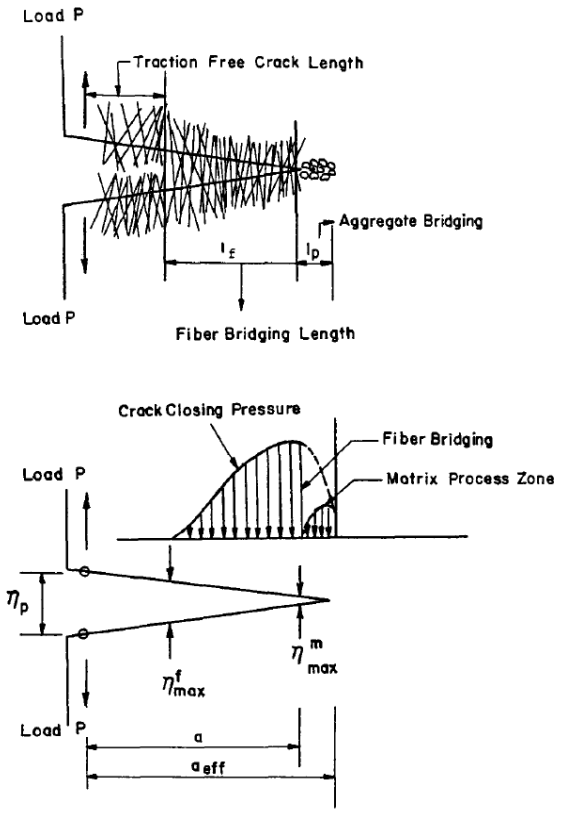

Figure 3: An idealized representation of a crack. The crack is bridged by fibers when small/narrow (l_f) creating a pressure to bring the crack closed. If the crack is too large/wide ($l > l_f$), the fibers no longer bridge the crack and no pressure is exerted.

Fiber fracture occurs when the bond strength between the fiber and the concrete is greater than the tensile strength of the fiber. Since this failure mode does not permit any

fiber slip before failure, the fibers and the cementitious matrix fail simultaneously and catastrophically without ductility or warning. While the flexural and tensile strength of the composite may be higher than that without fibers, an FRC with fiber fracture failure is most often avoided in practice due to its lack of ductility. Other fiber failure modes exist, such as fiber stripping wherein the outer surface of the fiber peels away, but these other modes resemble fiber fracture or pullout on the composite scale and are not discussed herein.

The mechanics that describe whether the fibers in an FRC will fracture or pullout involve a critical length, l_c, as shown in Figure 4. The critical length is the length above which the fiber will fracture rather than pull out when a crack intersects the fiber at its midpoint. For frictional shear stress transfer along a circular fiber, the calculated value of l_c *is*

Equation 1: Fiber critical length

$$l_c = \frac{\sigma_{fu} r}{\tau_{fu}}$$

where σ_{fu} is the ultimate stress of the fiber, r is the fiber radius, and τ_{fu} is the maximum frictional shear stress or bond strength. In Figure 4a, the length of the fiber is below l_c, and the ultimate strength of the fiber cannot be achieved resulting in a fiber pullout failure. Figure 4b shows the length of the fiber is l_c, and σ_{fu} is achieved. Figure 4c

shows when the length of the fiber is greater than l_c, and the fiber will fracture instead of pullout.

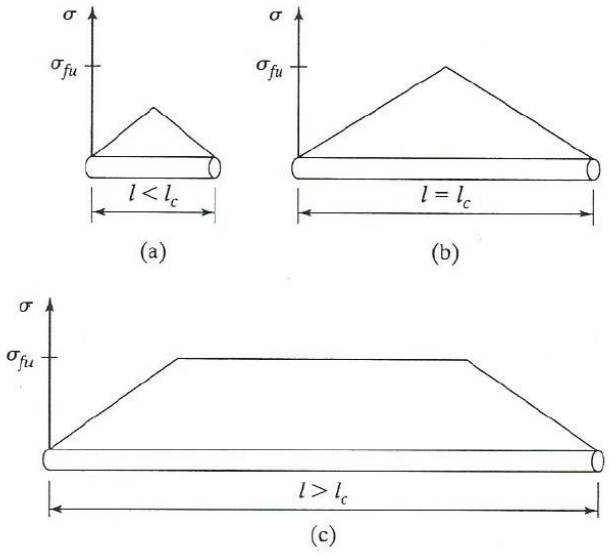

Figure 4: Effect of fiber length on shear stress transfer in a cement matrix. Fiber lengths less than l_c do not allow the fibers to reach the failure stress. [8]

One of the primary purposes for FRC in bridge decks and hydraulic structures is to mitigate cracking and prevent water inflow through the concrete. Concrete fails in the field mostly due to material degradation, and reinforced concrete structures corrode when water flows through the material. Water flowing through concrete can leech our calcium hydroxide and increase permeability, allow salts and other deleterious chemicals to corrode the concrete, cause the steel reinforcement to rust, and increase potential freeze-thaw damage. It has been shown in FRC that transport properties through a

cracked material increase proportional to the radius of the crack width cubed as shown in Equation 2 wherein k_c is a dependent on various thermodynamic properties, *S* is the crack spacing, and η is the crack width [3].

Equation 2: Transport properties

$$\phi = 1 + k_c \frac{\eta^3}{Sp}$$

Equation 2 demonstrates that the most important parameter on flow through a cracked material is the width of the cracks. It has been proposed that the size of a crack that forms in fiber reinforced concretes (and PCBMs) is directly proportional to the size of the reinforcing fibers as shown in Equation 3 [4] wherein *Sp* is the spacing between cracks; V_m and V_f are the volume fractions of matrix and fibers, respectively; *r* is the radius of the reinforcing fiber; σ_{mu} is the matrix failure stress; and τ_{fu} is the slip stress required to break the bond between fiber and matrix.

Equation 3: Crack spacing

$$Sp = \frac{V_m}{V_f} \frac{\sigma_{mu} r}{2\tau_{fu}}$$

Equation 3 suggests that if the spacing between the cracks is reduced, the size of the cracks themselves will also be reduced. Rebar, the largest fibers, allow large cracks that are measured in millimeters or centimeters, while microfibers reduce the crack size to a millimeter or less.

2.1.2 Macrofibers and Microfibers

FRCs use a wide variety of fiber types depending on the application, environmental factors, and cost. Table 1 shows typical fibers and their properties. The term *macrofiber* refers to fibers that have diameters that can be measured in millimeters, most typically steel. Macrofiber diameters range from ~0.5mm to ~2mm. The term *microfiber* refers to fibers that have diameters that can be measured in micrometers. Most fibers used today in FRC fall into this category. Steel FRC has been used for pavements and for highway and airport runway overlays to reduce both thickness and cracking; it is also used extensively in shotcrete for applications such as rock-face stabilization and tunnel linings. Traditional steel fibers were straight and smooth, but poor bond issues between the fibers and the concrete have led to using oddly-shaped fibers, ribbed fibers, or fibers with crimped or bent ends to enhance bond strength. Glass fibers are typically used in thin sheet components, and not all glass fibers are applicable in concrete since the highly alkaline environment will deteriorate the fibers. Synthetic fibers such as polypropylene or polyvinyl alcohol are used largely to reduce cracking due to plastic shrinkage, to improve the watertightness of structures, and to improve the toughness of structures. Synthetic fibers often have low elastic moduli and a high elongation at break, making them excellent at absorbing energy in structural failure [10].

Table 1: Typical properties of common fibers and cement matrix.

Fiber	Diameter (μm)	Specific Gravity	Modulus of Elasticity (GPa)	Tensile Strength (GPa)	Elongation at Break (%)
Steel	5-500	7.84	200	0.5-2.0	0.5-3.5
Glass	9-15	2.60	70-80	2-4	2.0-3.5
Asbestos					
Crocidolite	0.02-0.4	3.4	196	3.5	2.0-3.0
Chrysotile	0.02-0.4	2.6	164	3.1	2.0-3.0
Polypropylene	6-200	0.91	5-77	0.15-0.75	15
Aramid (Kevlar)	10	1.45	65-133	3.6	2.1-4.0
Carbon					
PAN*	7-9	1.6-1.7	230-380	2.5-4.0	0.5-1.5
Pitch	9-18	1.6-2.15	28-480	0.5-3.0	0.5-2.4
Nanofiber	0.05-0.20	2.0	240	2.92	--
SWCNT**	.0006-.0008	~1.3	1500	50-500	16
MWCNT***	.005-.05	~1.75	1000	10-60	~10
Nylon	20-200	1.1	4.0	0.9	13-15
Cellulose	--	1.2	10	0.3-05	--
Polyethylene	25-1000	0.95	0.3	0.08-0.6	3-80
Wood fiber	25-75	1.5	71	0.7-0.9	--
Cement matrix (for comparison)	--	2.5	10-45	0.004	0.02

*Polyacrylonitrile based
**Single-walled carbon nanotube (data from [11])
***Multiwalled carbon nanotube (data from [11, 12])
Data is from [8] except as noted otherwise

2.1.2.1 Strength

In modern FRCs, the purpose of fibers is not to increase compressive or flexural strengths. Compressive strengths of FRCs can have increases of ~25% compared to concretes without fibers, but the cost of fibers does not warrant their use for such low strength gains [7, 8, 13, 14]. Tensile strength of FRCs likewise has minimal gains with

the addition of fibers [8, 15]. The flexural strength of FRCs can increase with increasing concentrations of fibers that are adequately dispersed, but gains are minimal. Figure 5 shows the influence of fiber content on flexural load-deflection curves with 50mm long fibers with hooked ends; peak load before cracking was not increased by more than 25%, but the post-peak behavior showed strain-hardening effects and an increase in load capacity after the matrix cracked.

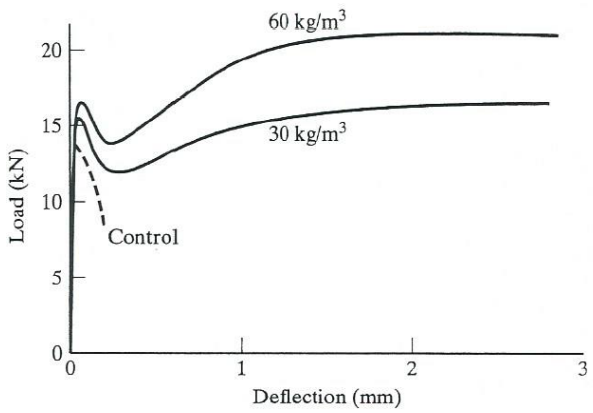

Figure 5: Influence of fiber content on flexural load-deflection curves for 50mm long fibers. [16]

2.1.2.2 Toughness

The principal role of fibers in FRC is to bridge cracks as the concrete cracks or dries. Figure 5 shows a strain-hardening effect in concrete specimens, but an equally important aspect is strain-softening wherein the applied load gradually decreases as the material

deforms as shown in Figure 6. Both strain-hardening and strain-softening are important in FRC since both absorb much more energy during material failure than would a concrete without fibers, also known as the material toughness. Figure 6 shows the ASTM C1018 method for determining the toughness of an FRC flexural specimen by comparing the area under the initial and post-peak load-deflection curve with the area under the pre-cracking load-deflection curve [17]. Toughness indices can increase by as much as 300% with polypropylene fibers by increasing the fiber concentration from 0.1% to 0.4% by volume [15].

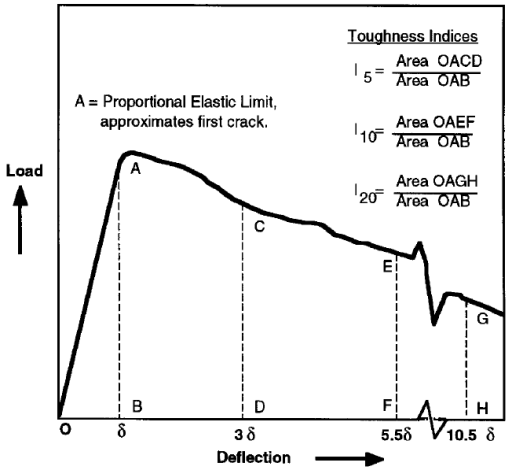

Figure 6: Flexural toughness indices as proposed in ASTM C1018. $I_5 < I_{10} < I_{20}$. [7]

2.1.2.3 Impact Resistance

The impact resistance of concrete can be increased by more than an order of magnitude by the addition of fibers [7]. It should be noted since the loading rates associated with

fracture and impact tests are dramatically higher than standard compressive or flexure tests, the fibers tend to fracture rather than pullout. Steel and carbon fibers are more effective for impact resistance than synthetic fibers, but most fiber types increase the fracture energy and the peak loads under impact [8]. The most common tests used in FRC impact tests are the Charpy (pendulum) test, drop-weight tests, and explosive loading tests [18]. Figure 7 shows the results for a drop-weight impact test where the number of blows required to create a crack in a specimen was recorded for specimens with four different fiber types [19]. Fiber Types A and C (steel fibers with hooked ends or corrugated shape, respectively) performed best compared to Types B and D (straight low-grade steel and polypropylene, respectively), but all fiber types outperformed the control mixture.

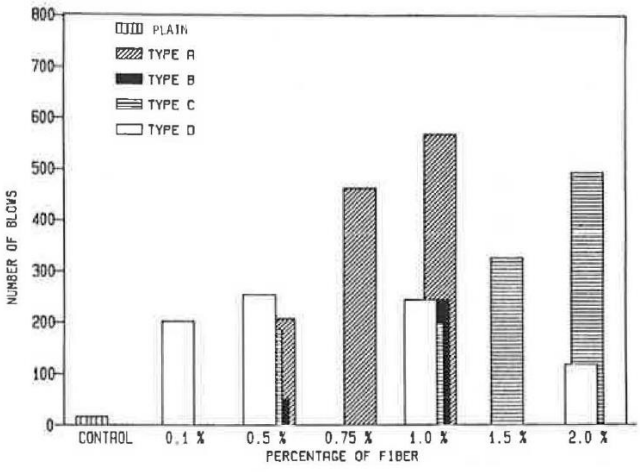

Figure 7: Drop-weight impact results for number of blows until first crack for concretes with various fiber types and concentrations. [19]

2.1.3 Mechanical Properties of PCBMs with CNFs and CNTs

One of the most important properties of CNFs in PCBMs is their effect on the macroscopic mechanical properties of the material. Adding CNFs to cement and concrete for its effect on electrical properties will be a niche field if the compressive strength is drastically reduced. The addition of CNFs to PCBMs has had mixed results in the early stages of research predominately because adequate dispersion was so difficult to achieve, but many research groups have overcome that obstacle and are making excellent progress in advancing CNF PCBMs.

At first glance, it is difficult to determine a set effect that CNFs have on PCBMs. There can be huge increments of change as improvements [20-24], as diminished properties [25, 26], or there can be no significant effect [6, 27]. The wide variety of results is primarily caused by dispersion, chemical treatment of the fibers, and total concentration of fibers.

A poor dispersion of CNFs or CNTs throughout a cement matrix almost always has a negative effect on the mechanical properties of the composite. Sanchez et al have, in multiple references presented early in the field, attempted to add CNF to cement paste as a dry powder without sonication, resulting in decreased split tensile capacities and no change in compressive strengths at best [27, 28]. Most researchers choose to sonicate the CNFs with a surfactant in the mix water, typically leading to increases in flexural strength and toughness [29-32], though some researchers have obtained mixed results

[33] or decreases [34] in flexural strength with the same sonication technique. Literature shows that increases in compressive strength are more difficult to achieve and occur only with the most careful dispersion techniques, either using sonication with a surfactant [35, 36] or by growing CNFs or CNTs directly onto the cement grains [23, 37]. Elastic modulus, either in flexure or compression, typically follows the trend of flexural or compressive strength, respectively.

Depending on the manufacturing process, CNFs and CNTs can have smooth sides which do not bind well to the cementitious matrix, and the fibers pull out of the matrix under low stress. Therefore, several researchers have treated the CNFs with, for example, nitric or sulfuric acid to introduce functional groups onto the surface of the fibers. The fibers must then be washed to remove the treatment chemicals, and the cleanliness of the fibers after treatment mandates the performance of the composite. Treated fibers that are thoroughly washed often perform on par or better than untreated fibers [29, 38], and treated fibers that are improperly cleansed perform far worse than untreated fibers [32].

Current literature uses concentrations of CNFs and CNTs at or below 0.2wt% with concentrations as low as 0.025wt% [30] providing beneficial properties. Research with concentrations above 0.5wt% CNFs or CNTs often, but not always [39], result in decreased mechanical properties because of excess fiber clumping [6, 23, 28]. The most accepted explanation for clump of CNFs above 0.5wt%, despite the dispersion of fibers

in the mix water, is that CNFs tend to re-agglomerate in the mix water when the pH rises above 10 [40].

One of the most interesting properties gained from adding CNFs to cement is shown in crack mouth opening displacement (CMOD) tests—see Figure 8. CMOD tests are flexural specimens with a notch cut in the bottom of the specimen directly beneath the load application position. The width of the crack mouth is measured and total displacement recorded to provide insight on the ductility and post-crack behavior of the material. The most recent literature shows a post-peak behavior that resembles strain hardening in common steels.

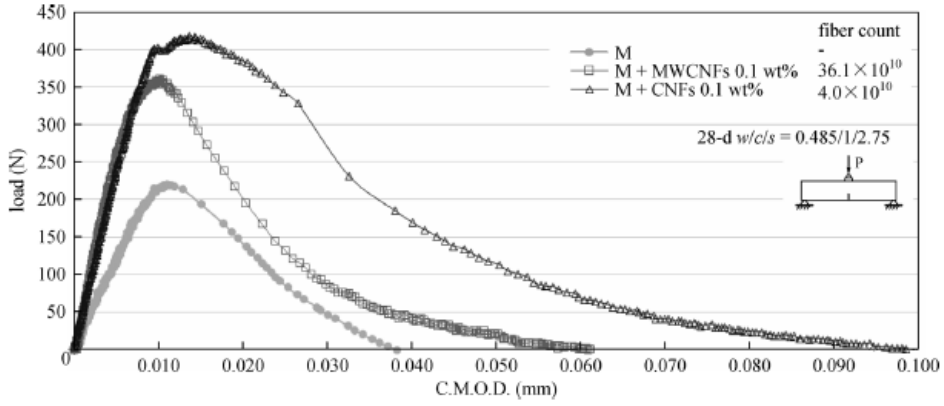

Figure 8: Load vs crack mouth opening displacement of mortar with and without nanofibers. Adding 0.1wt% CNFs significantly increased post-peak behavior until failure and created a resemblance of strain hardening. [24]

2.1.4 SEM Imaging of CNFs and CNTs in PCBMs

Many researchers have used SEM imaging to study the efficacy of their efforts on creating CNF/CNT PCBMs. Some of their images are presented in this section for the readers' benefit to provide examples of what others have done in the field.

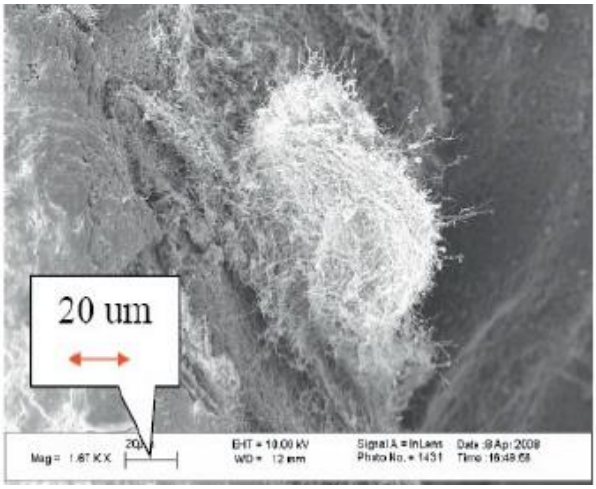

Figure 9: SEM image of CNF clump in OPC. The CNFs shown here were not properly separated prior to inclusion into the paste. [41]

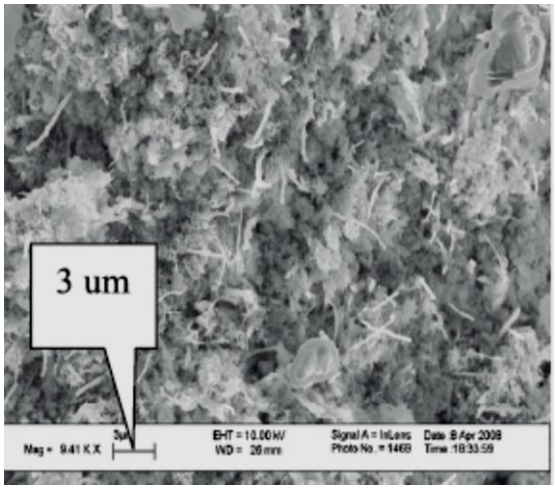

Figure 10: SEM image of well-dispersed CNFs in cement. [41]

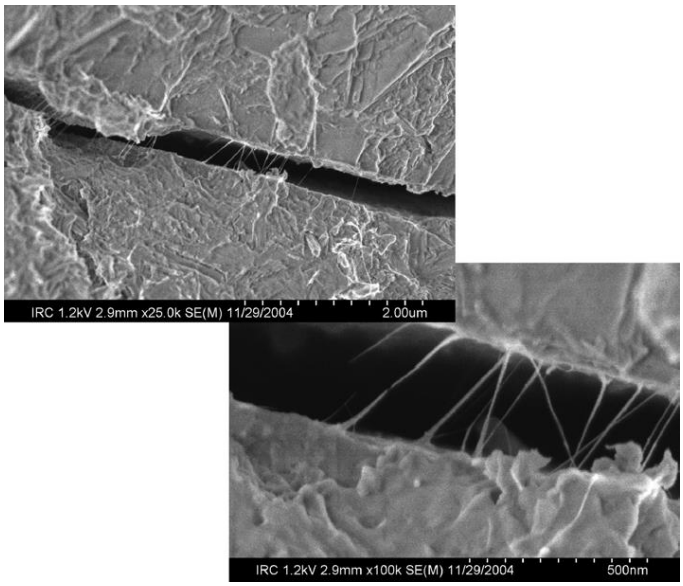

Figure 11: SEM image of CNT crack bridging in cement. [42]

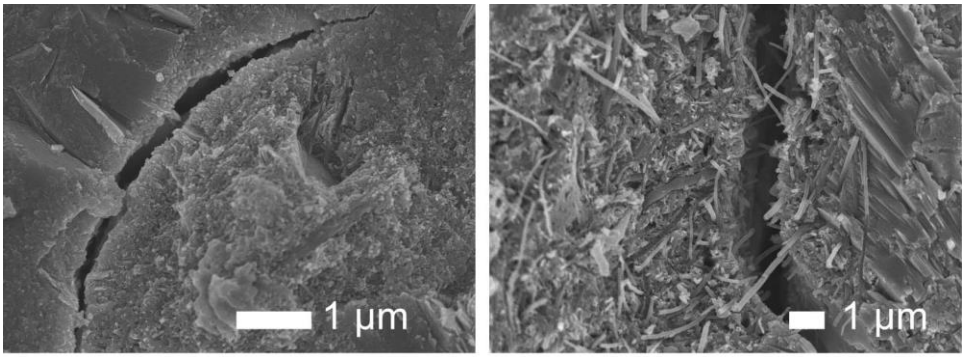

Figure 12: SEM images of (a) the fractured surface with no CNFs and (b) CNFs bundled in a small area. [33]

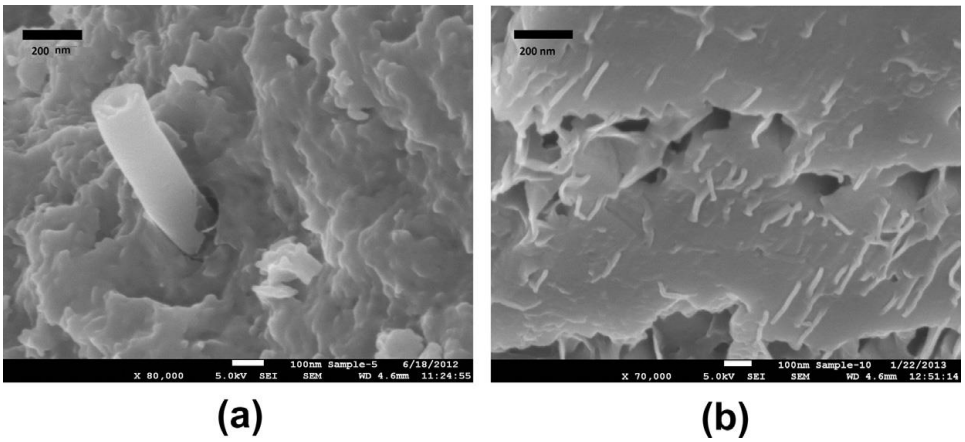

Figure 13: (a) High-magnification image of CNF at fractured surface of cement and (b) SEM image of cementitious paste depicting pull-out of dispersed CNFs. [43]

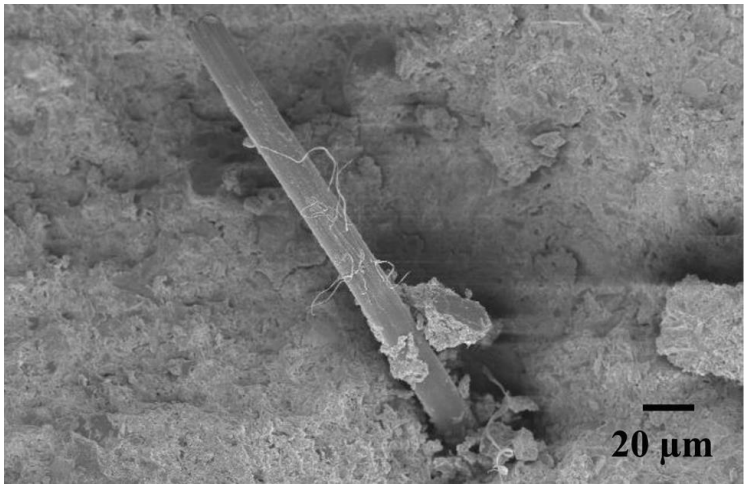

Figure 14: SEM image of cement matrix showing a PVA microfiber covered with CNFs. [44]

2.2 Nanofiber Uses in Other Materials

The first recorded application of carbon fibers was in light bulbs by Joseph Swan in the 1860s and then by Thomas Edison in 1879 [45]. In 1958, Roger Bacon began producing high-performance carbon fibers at the Union Carbide Parma Technical Center, setting the framework for modern carbon fibers and their applications [46]. Since their development, CNFs have become one of the most prominent members of the carbon fiber family with applications in fields such as energy conversion and storage, reinforcement of composites, and self-sensing devices. CNFs have tensile strengths and elastic moduli at least as strong or stronger than high-strength steels as shown in Table 1. In addition to high-strength mechanical properties, CNFs have excellent electrical and thermal conductivities (~10^3 Siemens/cm and ~1900 W m^{-1} K^{-1}, respectively) [47]. One

sensor developed as a CNF/elastomer composite was able to reversibly change its electrical conductivity by factors of 10^2-10^3 upon stretching to 120% strain and recovery to 40% strain [48]. Modifications of CNFs by making them porous or by creating complex structures of CNFs have allowed for multiple improvements to battery performance and energy storage [49, 50]. CNF/polymer composites can show increases in fracture resistance and flexural modulus by up to 78% and 98%, respectively, with additions of 1.0wt% CNFs as shown in Figure 15 [47, 51]. However, higher doses of CNFs in polymers have shown to decrease the tensile strength of the composite due to an increase in air voids and material defects that cause stress concentrations and, ultimately, premature failure.

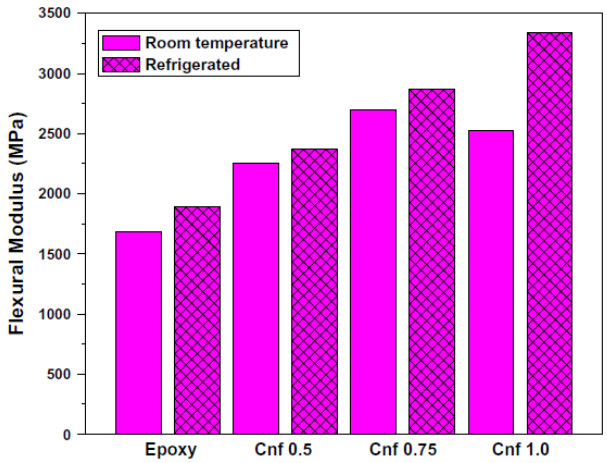

Figure 15: Flexural modulus of resin and CNF/epoxy nanocomposite samples showing the increasing flexural modulus with the addition of CNFs. Lower temperatures seem to increase the efficacy of the CNFs. [47]

CNFs and CNTs in ceramics show benefits in some regards but detrimental in others. As concluded in *Nanofibers—Production, Properties, and Functional Applications* [52],

> "The results show that introduction of CNTs/CNFs [into ceramics] usually results in finer microstructures. It also invariably leads to a drop in hardness. As for the fracture toughness, up to now the results are ambiguous. In most cases, the fracture toughness decreases, particularly for higher fractions of carbon phases. Yet, the potential for improving in this area by toughening mechanisms such as fiber pull-out, crack bridging, and deflection has been recognized. In this respect, future work is necessary to optimize the interface between the matrix and the fibers, which will ensure good bonding of the two phases, yet allowing the toughening mechanisms to be active."

In addition, adding CNFs to ceramics decreases the coefficient of friction by acting as a lubrication layer, and the wear resistance generally decreases with the same trend as hardness and fracture toughness. The electrical resistance can drop significantly with the addition of CNFs.

2.3 Dispersion Techniques for Nanofibers

2.3.1 In Cements

CNFs used in PCBM research are typically purchased in bulk and are delivered as a dry powder of tangled 'hairball' structures as shown in Figure 16. There are several methods currently used in literature to disentangle and disperse CNFs throughout the cement matrix. The least used and least effective method is to place the CNFs as-received into a

standard shear mixer to disentangle and disperse the CNFs as best as possible [25, 34, 53]. This method often weakens the macroscopic properties since the CNFs remain tangled together in the hairball structures and act as voids in the final material.

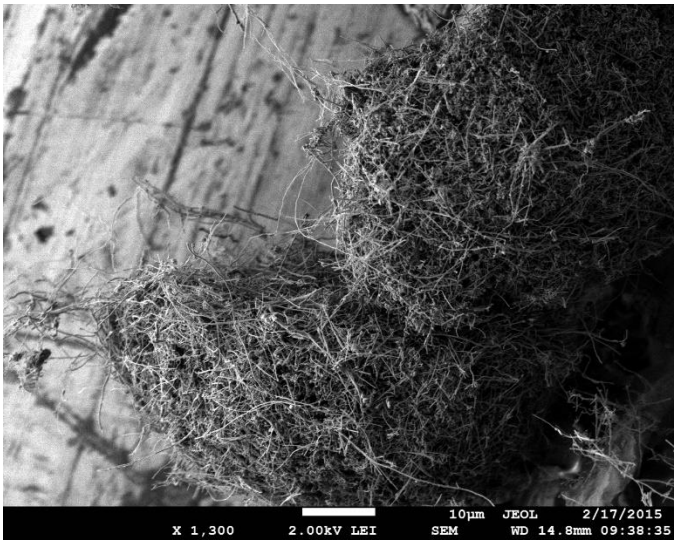

Figure 16: CNF tangled hairball structure as received from Pyrograf Products. This tangled structure is why sonication (or other effective means of dispersion) is required.

The susceptibility of nanoparticles and nanofibers to thermal effects and van der Waals' forces, especially in water where CNFs and CNTs display hydrophobic tendencies, creates a ubiquitous hindrance to successfully incorporating CNFs and CNTs into PCBMs. The nanoparticles readily agglomerate together to form clumps on the order of micrometers or millimeters that lead to inconsistent material properties and potentially diminished material strength and stiffness [6, 20, 27, 34, 54, 55]. Sonicating the CNFs in

an aqueous solution of the PCBM mix water with a surfactant such as superplasticizer is the most common procedure to attempt to create a uniform distribution of CNFs in cement paste; the surfactant decreases or eliminates the hydrophobic tendencies of CNFs, and the sonication disentangles and disperses the CNFs [56-59]. Other surfactants have been tried, including air entrainer and other superficial active agents that are not commonly found in PCBM research [36, 60], but superplasticizer is the most common choice due to its ubiquity in the field. In addition, some surfactants are used to enhance the bond strength between the fibers and the cement matrix by adding functional groups, and the fibers are then washed to remove the surfactant (e.g. sulfuric acid) before mixing with cement [61]. One drawback of using surfactants to modify the surface of the fibers is that the chemicals can affect the cement hydration if the fibers are not properly washed.

However, evidence of CNF and CNT clumps in hydrated cement paste samples suggests that a uniform dispersion of CNFs in the mix water does not guarantee a uniform dispersion of CNFs in the hydrated cement paste [40]. One mechanism of the CNF agglomeration is the free movement of CNFs between cement grains before the cement hydrates [62]; another mechanism is the apparent agglomeration of CNFs in aqueous solutions with a pH in excess of 10 (such as cement pore water) [28]; a third mechanism is compaction efforts (such as vibration) in conjunction with the previous two mechanisms further encourages the agglomeration of CNFs in the fresh cement paste.

These mechanisms cause CNFs to bundle together and form weak spots in the material or even float to the top of the mixture as a foam that can be up to 4 mm thick [20].

One of the rarest methods of achieving a uniform distribution of CNFs throughout the cement matrix is to use carbon-vapor deposition (CVD) and grow CNFs and CNTs directly onto cement grains [6, 21, 37, 63]. Portland cement and cementitious materials such as silica fume provide an excellent substrate on which CNTs and CNFs can grow, and having CNFs on the surface of each grain guarantees an excellent distribution of CNFs throughout the matrix. This technique has mixed results depending on the purity of the fibers that are grown.

There are currently two primary methods identified in the literature to discourage CNF agglomeration and the movement of CNF bundles through the fresh paste. The first method is to use concentrations of nanofibers as low as 0.048% by mass of cement or 0.10% by volume of cement in the mixture, discouraging re-agglomeration by drastically lowering the probability that CNFs will be in close proximity [22, 24, 29]. The second method is to use nanoparticles such as silica fume to mechanically impede the transport of CNFs through the fresh paste. Yazdanbakhsh showed that CNFs in a cement paste solution without silica fume moved freely, but the addition of silica fume to the mixture allows the CNFs to oscillate in place while preventing translation [28, 40, 62].

While silica fume does inhibit CNF transport in fresh cement paste, it is a pozzolan and usually added in mass fractions of ~10% or less by mass of cement (14% by volume of cement). Thus, the bulk of the particles present in the fresh paste are OPC and are 1-100μm in diameter [8]. Larger OPC particles induce a geometric clustering effect that force CNFs to clump together if used in high concentrations.

There are two seldom-used dispersion techniques that have shown promise but have had little progress. The first is a tedious method that involves sonicating CNTs or CNFs in pure alcohol, and then allowing the alcohol to evaporate [64]. This leaves behind a hybrid 'cake' of pre-mixed fibers and cement that can be broken apart and added to a standard mixer. The second technique was designed to encourage the use of a pre-sonicated CNT or CNF solution that has been extremely concentrated and can be added to mix water as a standard additive without further need of sonication [65].

2.3.2 In Other Materials

The dispersion of CNFs in materials other than PCBMs is primarily divided into two approaches: the melt mixing process and the sonication process in low viscosity solutions. The most widely used mixing process in polymers is melt mixing [66] which includes roll mill [67], Haake torque rheometer [68], and mini-max molding [69]. In these methods, CNFs are added to a liquified polymer, and mixing is performed generally with continuous massaging (roll-mill and mini-max) or with high-shear (Haake torque rheometer). A schematic of a roll-mill mixer is shown in Figure 17.

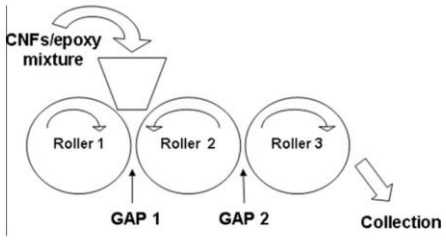

Stage	GAP 1 (μm)	GAP 2 (μm)
1	120	40
2	75	25
3	45	15
4 (four times)	15	5

Figure 17: A schematic of a typical roll-mill mixer. An epoxy mixture is rolled through the mixer several times to achieve a uniform mixture.

The sonication process is used both in polymers and ceramics. In ceramics, powder clinker nodules are sonicated with CNFs in a non-reactant fluid (often water) to disperse the CNFs throughout the powder; the same method was used in Section 2.3.1. The fluid is then driven off, and the mixed clinker/CNF powder is then heated and compressed to form the final ceramic. CNF-reinforced polymers are often epoxy with at least two separate fluids. The CNFs are sonicated in the solution with a lower viscosity; if both solutions are high-viscosity, one is altered with a solvent (such as alcohol) to lower the viscosity and allow sonication, and the solvent is later driven off. The hardening agent is then added to the sonicated CNF solution with mechanical stirring, resulting in the hardened CNF-reinforced epoxy.

2.4 Geometric Clustering

2.4.1 General Theory

A major hindrance to obtaining a PCBM with thoroughly dispersed CNFs is the effect of geometric clustering as introduced briefly in Section 1.1. As shown in Figure 18a, geometric clustering occurs when the host particles (e.g. cement grains) are much larger than the spacing between the particles (wherein lie the CNFs) [70]. At complete hydration of the cement matrix, the CNFs will lie only in the regions that were not originally occupied by cement grains, leaving large swaths of matrix that are not reinforced with CNFs. Figure 18b shows that even though there are statistically fewer large cement grains in the mixture by number of grains, those few grains occupy most of the volume of the cement. Approximately 95.5% of a typical OPC volume is occupied by grains that are larger than 20 μm.

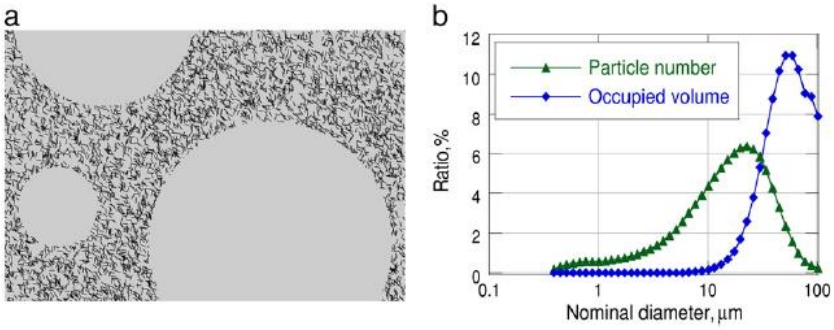

Figure 18: (a) Schematic illustration of geometric clustering of CNTs in cement paste. (b) Particle size distribution of typical OPC and the volume occupied by the particles of each size. Though there are relatively few particles with diameters above 50 µm, the larger particles occupy the majority of the volume. [70]

Geometric clustering does not play a major role with low concentrations of CNFs in the cement matrix as shown in Figure 19 [71]. Figure 19a is a schematic representation of a CNTs in a ceramic nano-composite. The area between ceramic particles in which CNTs can be distributed are shown with lighter color. Figure 19b is a schematic of a low dosage of CNTs dispersed between particles in Figure 19a, showing little to no evidence of geometric clustering. Figure 19c is similar to Figure 19b but with a high concentration of CNTs, clearly showing the effect of geometric clustering between particles.

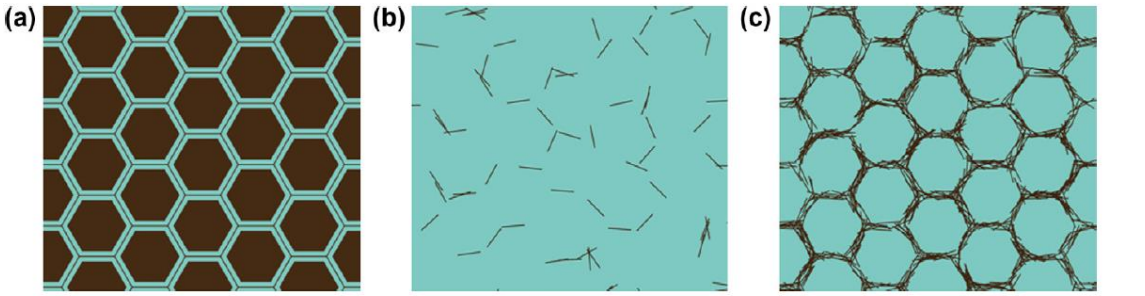

Figure 19: Schematic presentation of low and high concentrations of CNTs around hexagonal particles. (b) Low concentrations of CNTs do not show significant clumping. (c) High concentrations of CNTs clearly show geometric clustering. [71]

2.4.2 Dispersion Quantification

A unique, non-biased method was utilized to quantitatively analyze the dispersion of the CNFs in the cementitious matrices [70, 71]. In this method, the dispersion parameter is defined based on where a distribution of interest stands between two extrema: fully uniform and fully non-uniform dispersions. The fully uniform dispersion is defined as

one in which the mean distance from one particle to its nearest neighbors has a maximum value and the standard deviation of such distances a minimum value. The fully non-uniform dispersion is defined as one in which the mean distance from one particle to its nearest neighbors and the related standard deviation have minimum values, and the particles form a close-packed agglomeration as far as possible from the centroid of the domain to maximize the total distance required to move particles to the fully uniform dispersion. This definition of the fully non-uniform dispersion ensures a dispersion parameter between 0-1 for any analyzed domain of partially dispersed discrete particles. The dispersion of a given set of bodies within a given domain of interest (e.g., CNFs in an SEM micrograph) is quantified based on the minimal amount of work required to move the bodies from their current positions in the domain to the fully uniform state, in comparison to the work required to move the bodies from the fully non-uniform state to the fully uniform state. That is, the amount of work required to move the bodies/particles in the domain of interest to the fully uniform dispersion (S_i) is calculated and normalized by the amount of work required to move the particles in the fully non-uniform dispersion to the fully uniform dispersion (W_i)—see Figure 20. In Figure 20, the red circles represent a uniform distribution. The blue circles in Figure 20a represent a random dispersion. The blue circles in Figure 20b represent a fully non-uniform dispersion. The dispersion parameter (D) is then calculated such that a dispersion parameter close to 1 represents a well-dispersed distribution while a dispersion parameter close to 0 represents a poorly dispersed distribution, i.e.

Equation 4: Dispersion parameter

$$D = 1 - \frac{\sum S_i}{\sum W_i} \ni 0 \leq D \leq 1$$

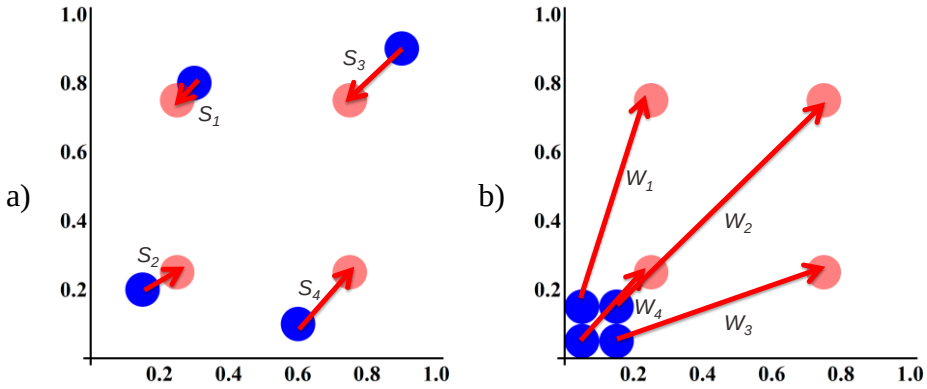

Figure 20: A schematic showing the work vectors to be used in Equation 4.

The scalar sum of the distances has an equivalent magnitude to the sum of the work to move the particles since one may assume a force vector with the magnitude of 1 without loss of generality in the calculated dispersion. One may solve for the minimum sum of distances to move the particles by tracking the motion of each individual particle, or, in a system of many particles, by tracking the flux of particles in a finite element meshed domain. Note that the absolute length scale of analyzed images is normalized in the dispersion parameter (owing to the ratio); thus, the dispersion parameter used in this research is independent of image scale. A more detailed discussion of the dispersion quantification method and the supporting theory may be found in [70-72]. The

dispersion parameter algorithm in this analysis does not account for rotational uniformity and calculates a dispersion parameter based solely on translational uniformity.

2.5 Restrained Ring Drying Shrinkage Testing

2.5.1 Restrained Ring Drying Shrinkage Test

The primary goal of the incorporation of fibers into PCBMs is to mitigate cracking. Hence, a simple, passive experiment for characterizing cracking time and development is a restrained ring test [73-78]. In this test, a steel ring is surrounded with concrete or mortar. After the mortar has cured for a specific amount of time, the temporary mold on the outermost edge of the mortar is then removed, and the outer radial face of the mortar is exposed to a dry environment. Since PCBMs are inherently porous, the dry environment removes water from the pores and induces capillary suction within the material, creating drying and stress gradients across the material as shown in Figure 21. Figure 21a shows the total stress developed in the PCBM ring. Figure 21b shows the internal stresses that develop in the PCBM ring due to material self-restraint; the outer layer of the PCBM is shrinking due to drying shrinkage while the inner layer of the PCBM is still saturated and resists deformation, creating a stress gradient through the material. Figure 21c shows the stress profile as determined from linear elasticity due to the resistance from the steel ring on the innermost surface of the PCBM.

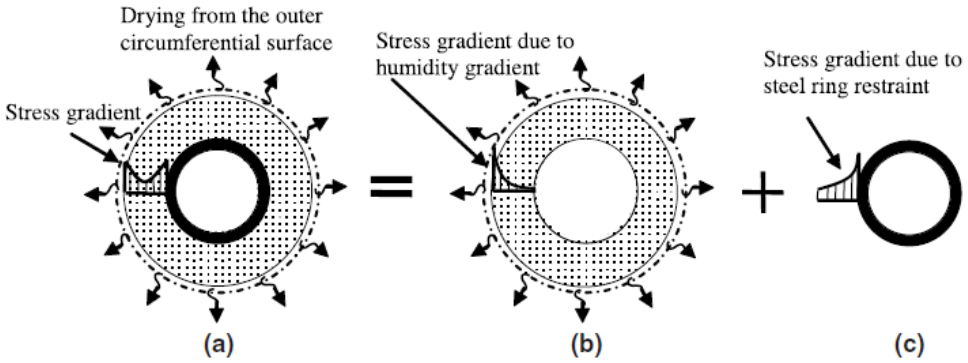

Figure 21: Conceptual illustration of the restraint components and a sample of stress gradient in the concrete ring. [77]

The top and bottom faces of the ring are sealed to prevent drying. Alternative, atypical ring test drying profiles have also been used such as 1) a sealed outer radial face with the top and bottom ring surfaces exposed to the drying environment [78, 79] or 2) elliptical rings with varying PCBM ring thickness [80, 81]. The mortar develops a free shrinkage gradient in the radial direction as it dries creating self-restraint tensile stresses, but the steel ring partially resists the free deformation creating tension in the mortar at the ring as well. The tensile stresses associated with self-restraint from the radial shrinkage gradient and the restraint from the steel ring increase with time as shrinkage increases and, eventually, the mortar cracks since the steel ring can sustain much greater stresses than the mortar [82]. The circumferential strain in the steel ring is recorded by mounting strain gages to the inner radial surface of the steel, and a crack in the mortar is evident in a sudden, drastic reduction in the strain in the steel. Data is presented as microstrain in the steel vs time as shown in Figure 22 [73]. In Figure 22, a crack in the concrete is

shown as a sudden drop in strain (around 10 days in this figure). Two mixtures 'S-1.0-XX' included steel fibers. One mixture, S-1.0-0.50, sustained stress (and strain) after cracking.

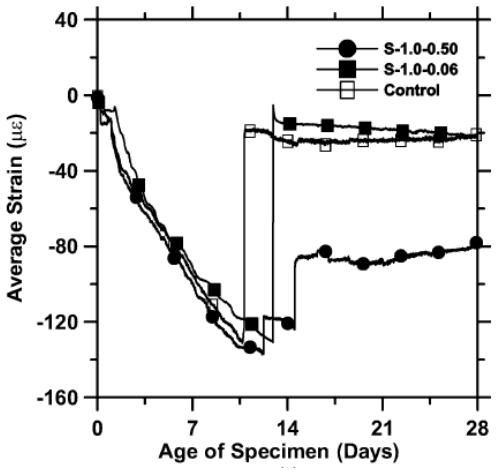

Figure 22: Average microstrain in the steel ring vs time exposed to drying in days. Two mixtures 'S-1.0-XX' included steel fibers with mixture S-1.0-0.50 sustaining strain after the formation of a macrocrack. [73]

2.5.2 ASTM Standard Ring and Experimental Ring

ASTM C1581 dictates the standard dimensions and test setup for a concrete restrained ring drying shrinkage test as shown in Figure 23 [75]. The standard dimensions of the test are given in Table 2. The inner surface of the outer ring, the outer surface on the inner ring, and the base are coated with a release agent. The test specimens are to be placed in two lifts, rodded 75 times per lift, and vibrated with each lift to consolidate the mixture. The specimen is to be kept at 23°C ± 2°C for 24 hours, and the outer mold is to

be removed at 24 hours. If specimen curing is to last longer than 24 hours, curing must continue with the mold removed. During testing, the top of the specimen is to be sealed with either paraffin wax or adhesive aluminum-foil tape. Strain gages mounted on the inside of the steel ring are to be read in intervals no greater than 30 minutes per measurement.

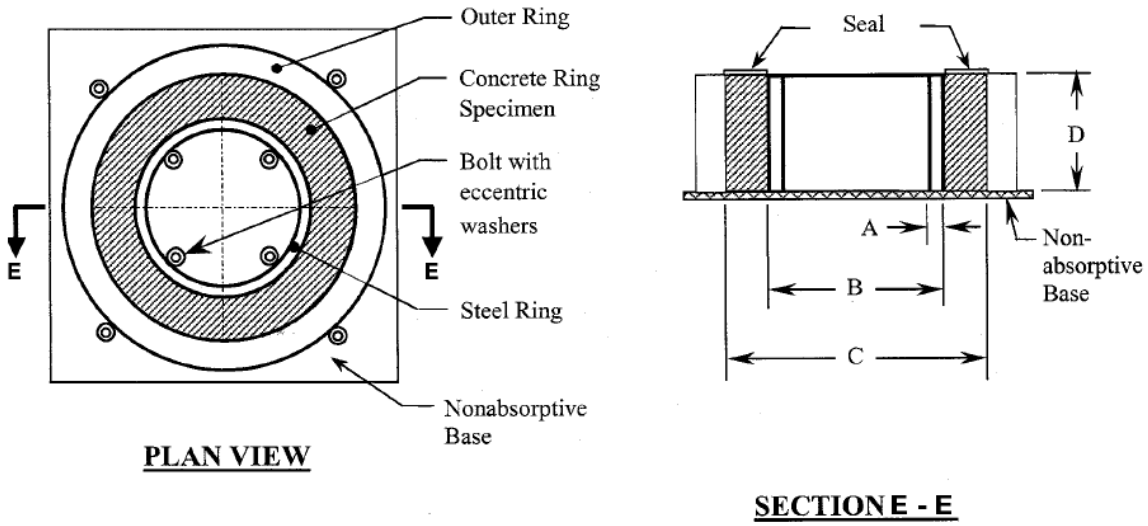

Figure 23: ASTM C1581 restrained ring drying shrinkage test.

Table 2: ASTM C1581 Restrained drying shrinkage test dimensions.

Figure Dimensions	SI Units	Inch-Pound Units
A	13 ± 1 mm	0.50 ± 0.05 in
B	330 ± 3 mm	13.0 ± 0.12 in
C	405 ± 3 mm	16.0 ± 0.12 in
D	150 ± 6 mm	6.0 ± 0.25 in

2.5.3 Linear Elastic Solution and Degree of Restraint

Linear elasticity dictates an equation for the stresses that develop in the mortar due to the pressure of the steel ring as shown in Equation 5 wherein ε_{steel} is the strain in the steel ring, E_s is Young's modulus of the steel ring, and R_{OS}, R_{OC}, and R_{IS} are the radii of the outer steel surface, the outer concrete surface, and the inner steel surface, respectively.

Equation 5: Restrained ring shrinkage test linear elastic solution

$$\sigma_{Actual-max} = -\varepsilon_{steel}(t) \cdot E_s \cdot \frac{R_{OS}^2 + R_{OC}^2}{R_{OC}^2 - R_{OS}^2} \cdot \frac{R_{OS}^2 - R_{IS}^2}{2R_{OS}^2}$$

However, this equation does not fully encompass the stress field induced by self-restraint during drying due to PCBM creep effects, specimen aging, and viscoelastic responses. Other researchers have successfully modeled the full stress field using material data related to pore size distribution, ring thickness, and other material inputs [74, 77], but this analysis was not conducted in this research.

The degree of restraint γ_r for the restrained ring drying shrinkage tests can be calculated based on Equation 6 wherein σ is the actual stress and σ_{fixed} is the theoretical stress at maximum restraint [83].

Equation 6: Degree of restraint

$$\gamma_r = \frac{\sigma}{\sigma_{fixed}}$$

γ_r varies between a value of 0 for no restraint and a value of 1 for maximum restraint. For the restrained ring drying shrinkage test, a fully restrained specimen would be modeled using Equation 5 with R_{IS} = 0 to simulate a solid steel disc instead of a hollow steel ring.

3. DIPSERSION OF CARBON NANOFIBERS*

3.1 Mechanical Dispersion Experiments

As mentioned in Section 2.3, the most important aspect of successfully incorporating CNFs into PCBMs is dispersion. A good dispersion of CNFs can improve the mechanical properties of the composite while a poor dispersion of CNFs can prove a detriment. CNFs that are purchased en masse are typically tangled in hairball structures as shown in Figure 16. The following sections document both failed and effective efforts from this research in dispersing CNFs into PCBMs. The PR-24-XT-PS CNFs from Pyrograf Products, Inc, used in this research had diameters of 50-150nm and lengths of 50-200μm as purchased. Scanning electron microscopy (SEM) imaging was conducted on a Jeol-7700 SEM. The OPC used in this study was a standard Type I/II cement that can be purchased from any construction store; detailed chemical and grain size analyses of the specific OPC used in this study can be found in later sections. Sonication procedures utilized a Sonics VCX750 probe-tipped sonicator with a CV33 probe at 20 kHz and 40% amplitude. Mechanical stirring was constantly employed using a Corning PC-353 magnetic stirring plate to encourage an even dispersion.

*Part of this chapter is reprinted with permission from "Dispersion of High Concentrations of Nanofibers in Portland Cement Mortars" by Joshua Hogancamp and Zachary Grasley, 2017. *Journal of Nanomaterials,* Volume 2017, 11 pages, Copyright 2017 by Joshua Hogancamp and Zachary Grasley. [84]

3.1.1 Improper CNF Dispersion Techniques

The first attempt in this research to disperse CNFs in PCBMs was by adding the CNFs into the mixture as received, similar to the addition of sand or silica fume into a regular mortar mixture. This technique invariably resulted in a final composite with diminished mechanical properties. Often the CNFs could be seen in the mixture as black streaks as shown in Figure 24. Given the actual size of CNFs, the fact that 1) there were black streaks and 2) the black streaks were obviously visible to the unaided eye both prove that the CNFs were not disentangling from the hairball structures nor dispersing evenly through the material. While superplasticizer has been shown to increase the efficacy of CNFs in PCBMs [29], it provided no benefit in these mixtures.

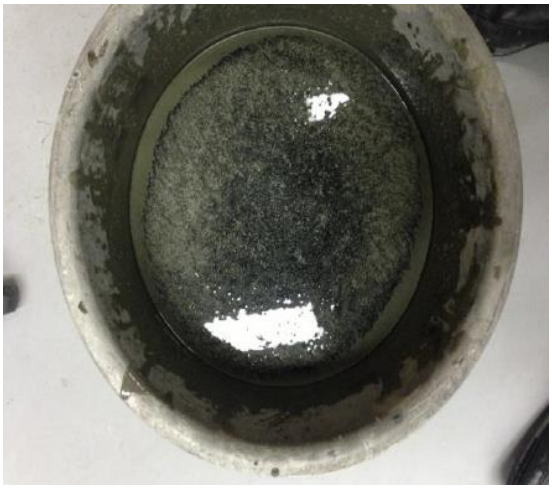

Figure 24: CNFs in fresh cement paste showing that uniform dispersion was not achieved. The black specs in the paste are agglomerations of CNFs.

The next attempt to disperse the CNFs was in mechanical mixing using a magnetic stirring plate. The CNFs were added to the mixture water with varying doses of superplasticizer (up to a 4:1 superplasticizer/CNF mass ratio [29]), and the solution was stirred for increasing lengthened time durations and with increasingly vigorous stirring. Even mechanical stirring at the 'optimum' superplasticizer/CNF mass ratio at the most vigorous stirring possible for 48 hours did not break apart the CNF agglomerations as shown in Figure 25. These results indicate that standard shear mixing and mechanical stirring are not sufficient to fully disperse CNFs into aqueous solution.

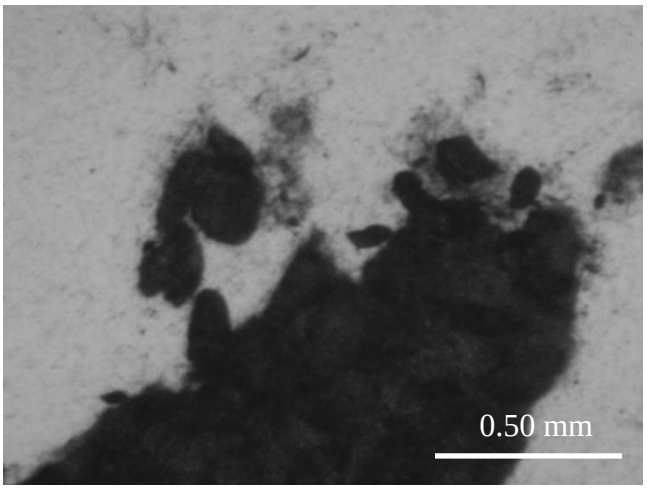

Figure 25: Optical microscope image of CNF agglomeration in superplasticizer-imbued mixture water after 48 hours of vigorous stirring.

3.1.2 Sonication in Aqueous Solution

Per literature reviews, the most common practice for disentangling and dispersing CNFs into aqueous solution is to sonicate the CNFs into the mixture water with a surfactant. A 4:1 superplasticizer/CNF mass ratio was chosen based on [29], and SEM imaging qualitatively revealed that ~30 minutes of sonication was adequate to disentangle the CNFs as shown in Figure 26.

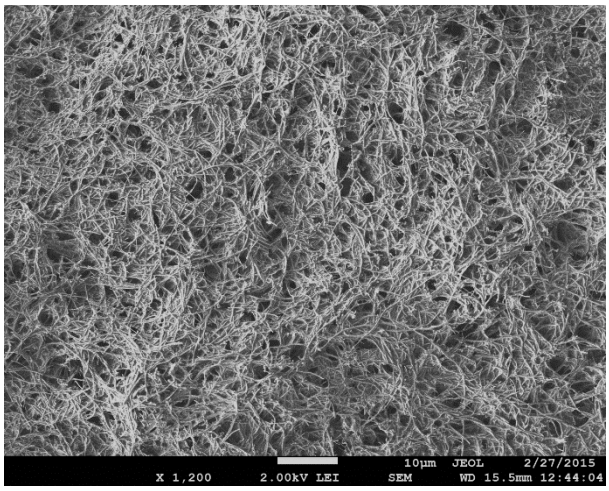

Figure 26: CNFs disentangled after 30 minutes' sonication in aqueous solution with superplasticizer.

Experiments of mortars with water-to-cement mass ratios (w/c) of 0.5 and sand-to-cement mass ratios of 2.75 were conducted with plain OPC and with OPC mixed with 0.1% CNFs by mass of cement (wt%) as recommended in much of the literature. The results of these preliminary experiments showed either no change or diminished

mechanical properties. SEM imaging of the broken samples was conducted to better understand why the samples were not behaving as well as others' tests in literature, and it was found that the CNFs were sparse in the hydrated specimens as shown in Figure 27. The hydrated specimens were found to have clumps of CNFs in some areas while large (and small) fractures had few, if any, CNFs bridging across the cracks.

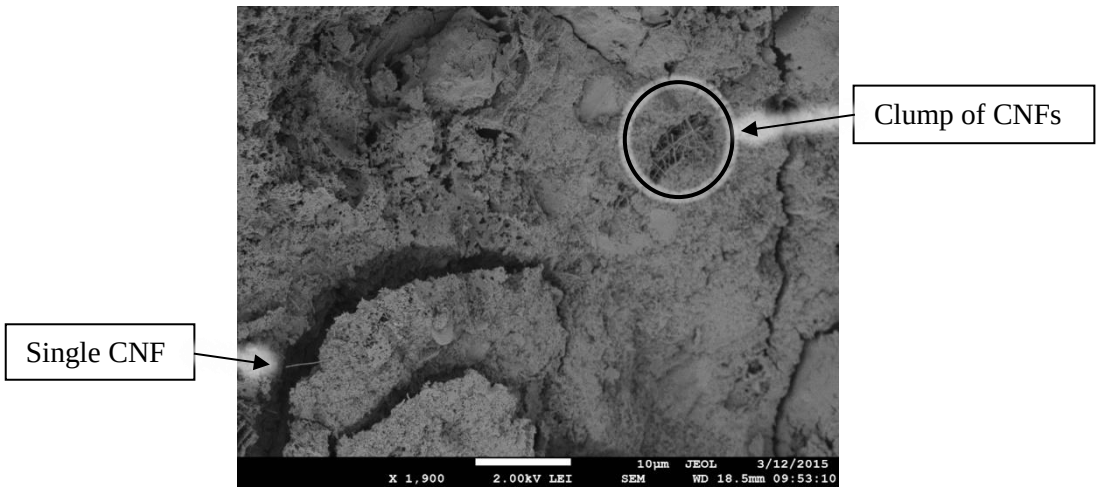

Figure 27: 0.1wt% CNFs sonicated in mixture water as seen in hydrated specimen. Clumps of CNFs were found in some places while large cracks were present in others with few or no CNFs protruding from the crack faces.

SEM imaging was conducted on unhydrated OPC powder with 0.1wt% CNFs dispersed by sonicating the CNFs with the cement in pure alcohol, and fibers were more difficult to find than was expected. The CNFs were few and relatively far between as shown in Figure 28.

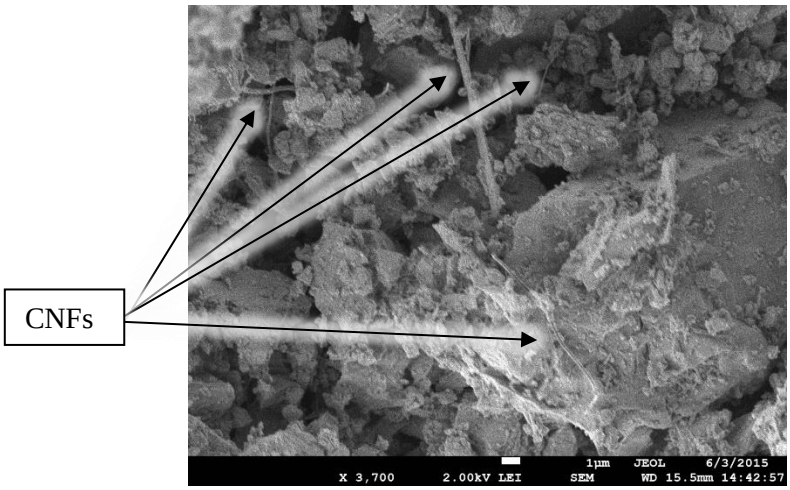

Figure 28: 0.1wt% CNFs dispersed in unhydrated OPC powder showing relatively few CNFs.

The concentration of CNFs was steadily increased up to 1.0wt% counteract the sparsity of CNFs in the OPC mortars, but a new issue was discovered in the process. CNFs as received are in tangled hairball structures, and the purpose of sonication is to disentangle the CNFs. As the CNFs disentangle, they take up more room in the aqueous solution. Note that the *actual* volume of the CNFs in aqueous solution does not change; rather, the CNFs disentangle and expand to fill the volume in the aqueous solution by spreading out. This apparent expansion is not an issue in CNF mixtures with low concentrations, e.g. 0.1wt% CNFs. However, as the concentration increased to 1wt% CNFs, the apparent expansion eventually filled the entire volume in the aqueous solution, rendering further sonication superfluous since there was no more room into which the CNFs could expand during disentanglement. The disentangled CNFs formed a weak skeletal structure in the

aqueous solution, and sonication efforts would only affect the CNFs immediately near the probe tip—see Figure 29.

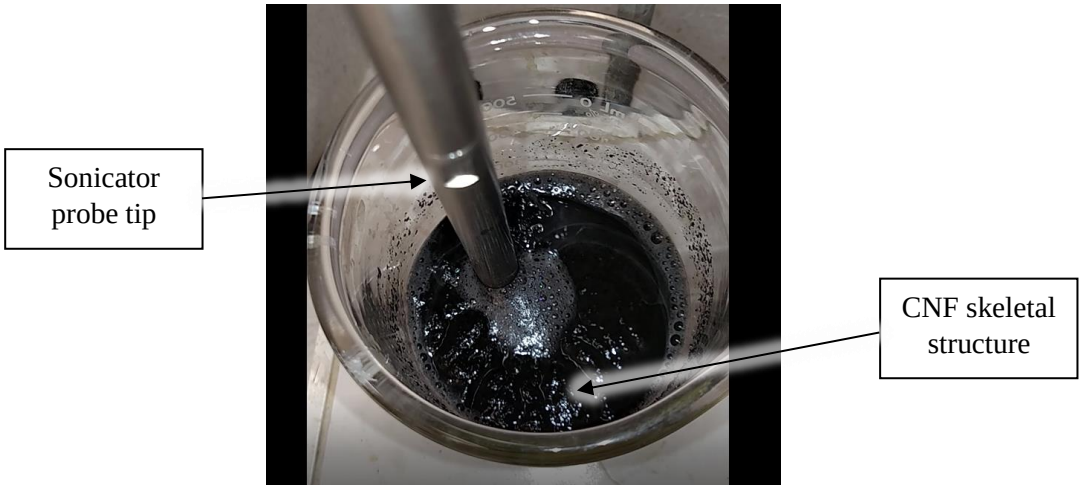

Figure 29: Weak skeletal structure formation of CNFs in aqueous solution. The portion of CNF slurry labeled 'CNF skeletal structure' is a massive solid-like agglomeration of CNFs protruding from the surface of the slurry.

Experiments with 1.0wt% CNFs in OPC mortars still showed either no change in or detriments to the composite's mechanical properties, and large cracks were found in the hydrated material with few CNFs bridging across as shown in Figure 30. The formation of this skeletal structure with high concentrations of CNFs in the mixture water posed a serious issue in further increasing the concentration of CNFs in PCBMs. The upper limit found in this research was 1.0wt% CNFs in a mixture with a w/c ratio of 0.5. Increasing the w/c ratio would allow for a higher concentration of CNFs by increasing the volume ratio of water in the mixture, but decreasing the w/c ratio would further limit the

concentration of CNFs by decreasing the volume ratio of water in the mixture. A new method for increasing the concentration of CNFs into PCBM was needed to increase the concentration beyond 1.0wt%.

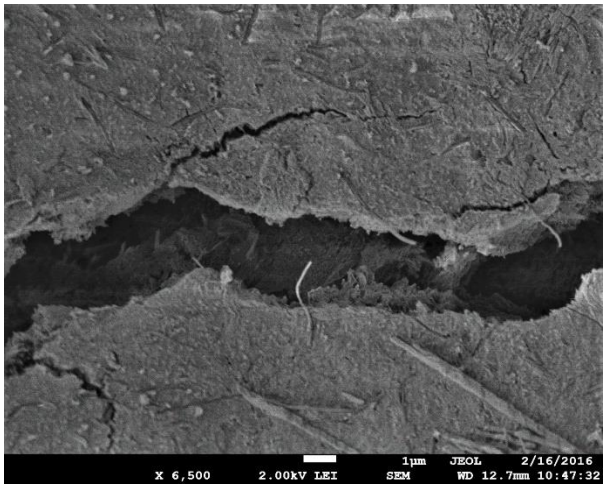

Figure 30: Hydrated 1wt% CNF hybrid CNF mortar showing few CNFs bridging across a crack.

3.1.3 Sonication in Alcohol

A method of dispersion CNFs among cement grains was utilized based on the work of Makar et al [64] and the information presented in Section 2.3.1. The CNFs were sonicated in pure ethyl alcohol with the cement in relatively low solids-to-alcohol concentrations to allow the CNFs to fully disentangle and disperse among the cement grains, and then the alcohol was evaporated using a distillation column to leave behind a pre-mixed hybrid CNF/cement powder. Using a low solids-to-alcohol concentration

allowed for any concentration of CNFs in cement to be created by limiting the CNFs in the alcohol and adding a proportional amount of cement. The CNFs were initially sonicated in pure ethyl alcohol for 15 minutes, and then cement was added to the alcohol/CNF suspension and further sonicated for an additional 30 minutes. CNFs and cement were added in exact proportions to maintain mass ratios, e.g. 2.00 grams of CNFs with 100.0 grams of cement for 2wt% CNFs. Mechanical stirring was constantly employed using a magnetic stirring plate to encourage an even dispersion throughout the slurry. The complete sonication setup is shown in Figure 31. After sonication, the slurry was poured into a distillation column to remove and recapture the bulk of the alcohol. The material remaining in the distillation column was then transferred to a well-ventilated oven for 24 hours at 105°C to ensure that all alcohol was removed. A hybrid cement/CNF ‘cake’ was produced in this process that was easily powdered using a metal utensil or a mortar and pestle.

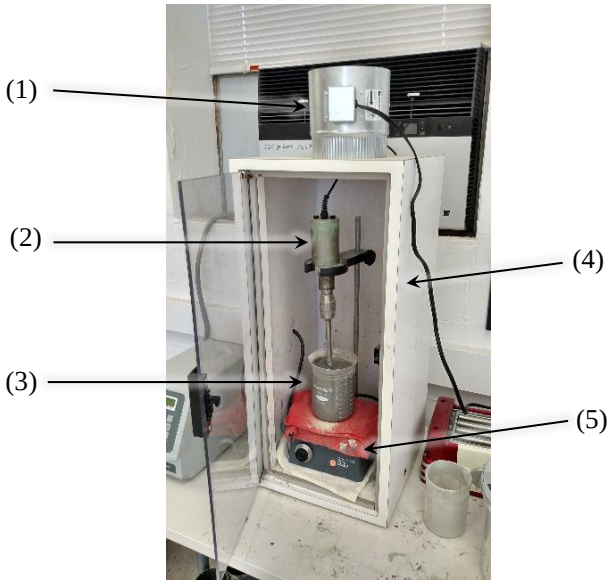

Figure 31: Sonication setup showing 1) ventilation fans, 2) sonicator, 3) CNF/alcohol/cement slurry, 4) acoustic noise-reducing cabinet, and 5) magnetic stirring plate.

The addition of high concentrations of CNFs to the cement changed the color of the material as shown in Figure 32. As a trial experiment, up to 10wt% CNFs were added to a microfine cement, and the cement became increasingly black. Adding microfibers did not change the color; only adding CNFs changed the color of the composite.

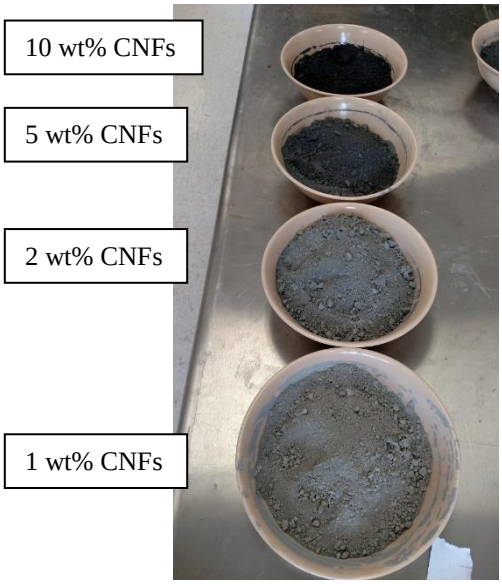

Figure 32: Hybrid microfine cement with 1wt% (bottom), 2wt% (middle-bottom), 5wt% (middle-top), and 10wt% (top) CNFs showing the color difference due to CNFs.

3.2 Cement Types and SEM Imaging of Dispersion

3.2.1 Cement Types

One of the issues of using CNFs in PCBMs is CNF transport through fresh cement paste. As mentioned in Section 2.3.1, CNFs in OPC freely translate through the fresh material, and a foam layer of CNFs can form on top of the cement during consolidation. It has been seen in literature that incorporating silica fume into the mixture stabilizes the system and inhibits CNF transport. Therefore, it was hypothesized that using a microfine Portland cement with a grain size distribution similar to silica fume would have the same stabilization effects of silica fume while simultaneously allowing higher dispersed concentrations of CNFs than an OPC mixture with 10% silica fume by mass of cement.

The two cements used were a common Type I/II Portland cement and a microfine Portland cement manufactured by Capitol Cement in San Antonio, TX. The cement grain size distributions are shown in Figure 33 along with that of a typical silica fume for comparison purposes as determined by a Horiba LA-910 particle size analyzer. The microfine cement has a mostly uniform grain size distribution in the same range as silica fume, and all grains are smaller than those in the OPC. The Blaine fineness of the OPC and the microfine cement are ~350 m^2/kg and >12,000 m^2/kg, respectively. Table 3 shows no notable difference in oxide composition of the two cements as determined using a Rigaku Supermini 200 X-ray fluorescence device.

Table 3: Oxide composition of microfine cement and Type I/II cement (OPC) by percent of total weight indicating similar oxide compositions between the two cements.

	SiO_2	Al_2O_3	Fe_2O_3	CaO	MgO	SO_3	Na_2O	K_2O
Microfine	20.5	5.3	1.7	63.2	1.2	4.7	0.1	0.6
OPC	20.0	4.9	3.8	62.7	1.0	3.4	0.1	0.5

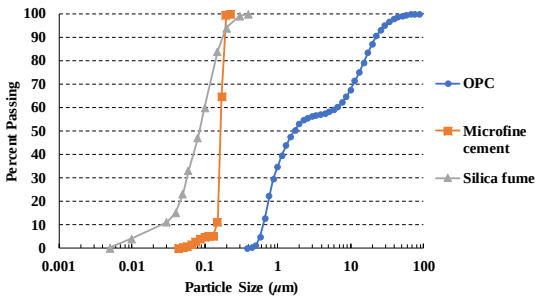

Figure 33: Percent passing graph showing the grain size distributions for OPC, microfine cement, and silica fume. Microfine cement and silica fume are similar sizes while OPC has larger grain sizes.

3.2.2 SEM Imaging of Dispersion

Initial SEM imaging of the hybrid cement powders revealed that the microfine cement with CNFs had far fewer clumps of CNFs than did the OPC with the same concentrations of CNFs as shown in Figure 34. Figure 34a is OPC with 1wt% CNFs. Figure 34b is microfine cement with 1wt% CNFs. Figure 34c is OPC with 2wt% CNF showing some CNF clumping. Figure 34d is microfine cement with 2wt% CNFs showing no CNF clumps. Figure 34e is OPC with 3wt% CNFs showing severe CNF clumping between the larger cement grains; the regions between the large OPC grains are filled with CNF clumps mixed with the smaller cement grains. Figure 34f is microfine cement with 5wt% showing no CNF clumping. The cement grain size difference between OPC and microfine is clear. As the concentration of CNFs increases in OPC, the CNF clumping between the larger cement grains becomes more obvious, whereas increasing the concentration of CNFs in the microfine cement does not necessarily lead to CNF clumping. More SEM images of CNFs in OPC and microfine cement can be found in Appendix B.

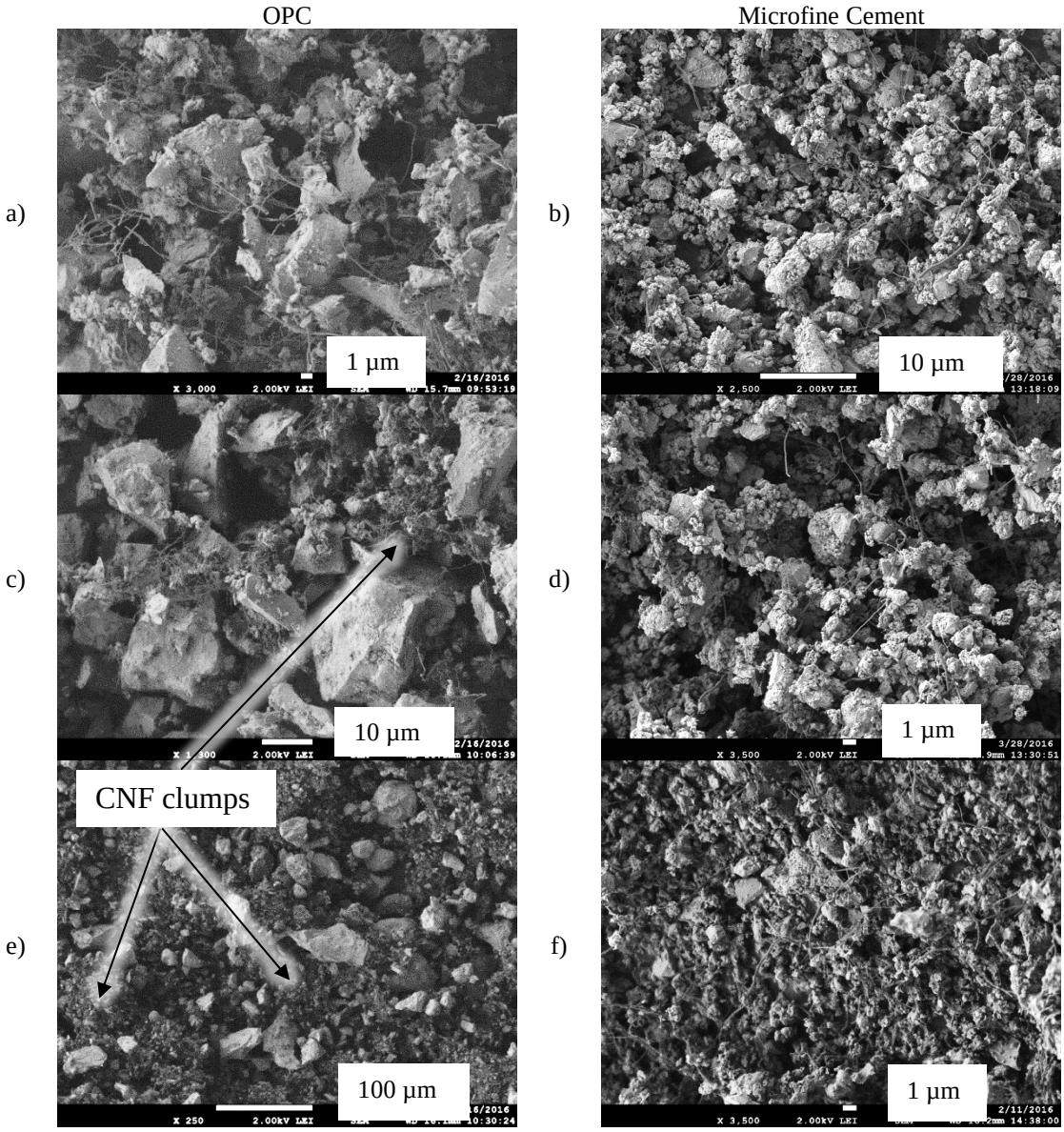

Figure 34: SEM images of hybrid cement powders. (a) OPC with 1wt% CNFs. (b) Microfine cement with 1wt% CNFs. (c) OPC with 2wt% CNF showing some CNF clumping. (d) Microfine cement with 2wt% CNFs showing no CNF clumps. (e) OPC with 3wt% CNFs showing severe CNF clumping between the larger cement grains; the regions between the large OPC grains are filled with CNF clumps mixed with the smaller cement grains. (f) Microfine cement with 5wt% showing no CNF clumping.

3.2.3 Issues with High CNF Concentrations

CNFs floated to the top of the hybrid OPC mortar specimens in a layer of foam during vibration as shown in Figure 35 and Figure 36. The foam was ~1mm and increased up to ~3mm in 1wt% CNFs and 3wt% CNFs hybrid OPC mortar mixtures, respectively. The foam layer appeared in hybrid OPC mortar specimens but not in the microfine cement mortar specimens, highlighting the instability of the hybrid OPC mixture and the effectiveness of utilizing small particles (in this case the small cement grains) to stabilize dispersions of CNFs. This observed foam layer has also been seen in other CNF-cement composite research [20]. Figure 36a is a low-magnification SEM image of the foam layer in a 3wt% CNF OPC mortar showing the vast amount of air bubbles, and Figure 36b is a more magnified SEM image of the foam showing that it is composed of CNFs loosely held together with hydration products.

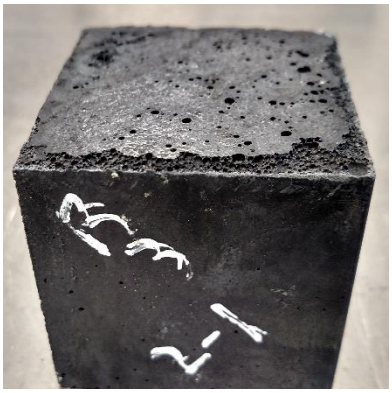

Figure 35: Foam layer of CNFs on the surface of a 50mm 2wt% CNF OPC hybrid mortar cube showing that CNFs did not form a stable mixture in OPC.

a) 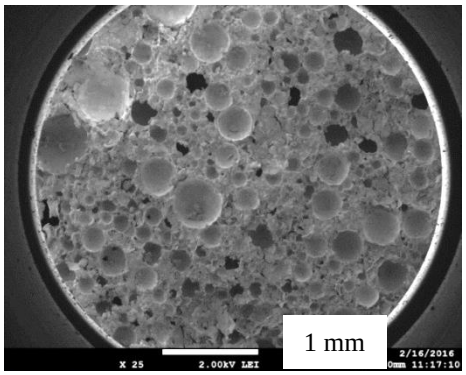

b) 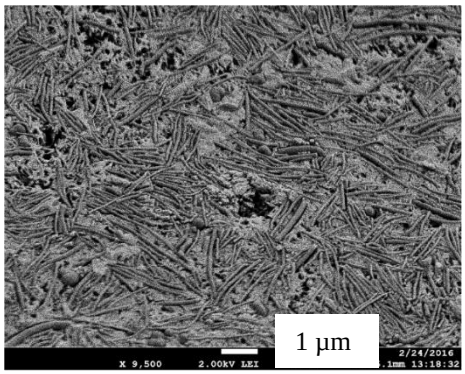

Figure 36: a) Low-magnification SEM image and b) magnified SEM image of the hardened foam layer in OPC hybrid mortar proving that the foam layer is formed from CNFs loosely connected by hydration products.

A separate issue occurred in microfine cement with the addition of 10wt% CNFs as shown in Figure 37. The CNFs were still well dispersed among the cement grains, but the resulting hybrid cement powder had such a high water demand that the powder could not be used to make an actual mortar. The mortar would not become liquid-like at a w/c ratio of up to 0.8 with any amount of superplasticizer; the mixture became liquid-like at a w/c ratio above 2.0, but the final hydrated mortar was not solid after 28 days at 98% RH. The specimens were oven dried, and a soft solid made primarily of CNFs wrapped around hydrated cement grains was formed after the water evaporated. The resulting solid was easily broken apart by hand and could absorb water as quickly as a common household sponge, though it should be said that this CNF sponge was much more expensive, difficult to make, and one-time-use only when soaking up water.

a) b)

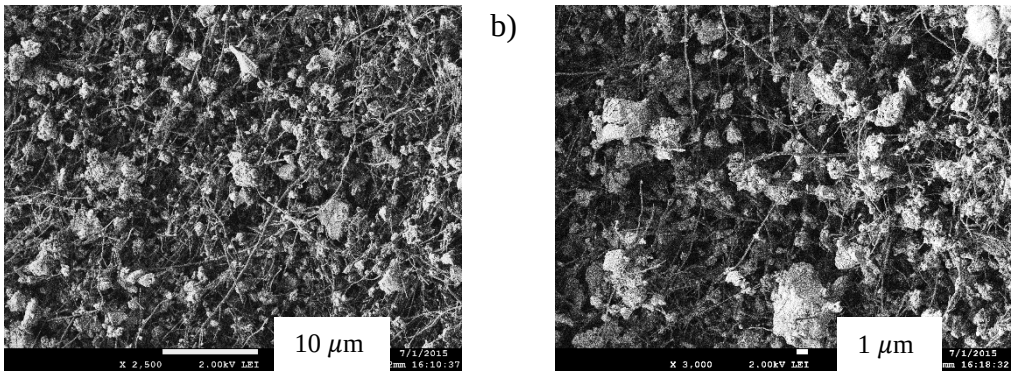

Figure 37: SEM images of 10wt% CNFs in microfine cement. There were so many CNFs that the cement grains could not touch each other after hydration (with typical mixing methods).

3.3 Computational Dispersion Simulations and Experiments

3.3.1 2-Dimensional Geometric Clustering Simulation

One of the goals of this research is to analyze the effect of grain particle size on the dispersion one might obtain for high concentrations of CNFs or other nanoparticles. Since dispersion quantification of the CNFs based on SEM images can be biased depending on the level of magnification, location of image capture, and image clarity, an unbiased computational simulation was conducted to determine the effect on dispersion of a concept called 'geometric clustering.' The work of Yazdanbakhsh et al. demonstrates that there is a maximum achievable dispersion of small filaments throughout a matrix composed of discrete particles—e.g., CNF filaments and cement particles [70, 72]. Geometric clustering occurs due to the fact that CNFs and an

unhydrated cement grain cannot co-occupy the same space, and this effect is intensified if the particle size distribution spans several orders of magnitude.

3.3.1.1 2-D Simulation Setup

Figure 38 displays the effect of geometric clustering on the dispersion of nanoparticles due to the particle size distribution of cement grains as determined by the distributions presented in Figure 33. An image of filled circles representing cement grains was generated based on a given circle area fraction of 0.6 with circle radii determined using the particle size distributions presented in Figure 33 and subject to the constraint that no circle could touch or overlap the edge of the image or another circle. The sizes of the images were based on the size of the largest circle, e.g. the OPC image frame length shown in Figure 38a-c was 3x larger than the diameter of the largest circle. A brute-force algorithm placed the largest circle first utilizing a random-number generator, followed by the second-largest circle, and so on until all circles were placed subject to the aforementioned constraints (Figure 38a and Figure 38d). Points representing nanoparticle 'centroids' were then placed in the open space around the circles subject to the constraint that no point centroid could be placed inside of a circle (Figure 38b and Figure 38e). Since a defined 'centroid' size would create an upper limit to the number of points that could be placed in an image without overlapping the existing cement-grain circles, the nanoparticles were graphed as small, filled circles, but mathematically treated as points such that they had no effective size to more clearly accentuate the geometric clustering effect (i.e., the plotted, filled nanoparticle circles could overlap so

long as their centroids did not coincide). A distribution of only the nanoparticles without the cement grain circles (Figure 38c and Figure 38f) was compared to two other distributions: one in which the same number of points are placed in a hexagonal distribution (fully uniform), and another in which the same number of points are placed in one spot in the corner of the image (fully non-uniform). In this latter case, since the points had no size, they were all placed at the (0,0) coordinate of the image where (0,0) is the bottom left corner. The dispersion of the points was calculated using Equation 4, shown here again for convenience:

$$D = 1 - \frac{\sum S_i}{\sum W_i} \ni 0 \leq D \leq 1$$

Figure 38a shows a cement grain particle size distribution based on the OPC with a cement grain area fraction of 0.6. Figure 38b shows the particle size distribution from Figure 38a with 2107 nanoparticle centroids randomly dispersed among the grains. Figure 38c shows the nanoparticle centroids in Figure 38b without the cement grains from Figure 38a showing the unreinforced regions left from the cement grains. Figure 38d shows a cement grain particle size distribution based on the microfine cement with a cement grain area fraction of 0.6; a sample size element is placed in Figure 38a that shows the relative size of the images. Figure 38e shows the particle size distribution from Figure 38d with the same number of nanoparticle centroids in Figure 38b randomly dispersed among the grains. Figure 38f shows the nanoparticle centroids dispersed in Figure 38e without the cement grains from Figure 38d showing unreinforced regions left

by the cement grains, but overall potential dispersion is improved with the use of microfine cement when compared to Figure 38c.

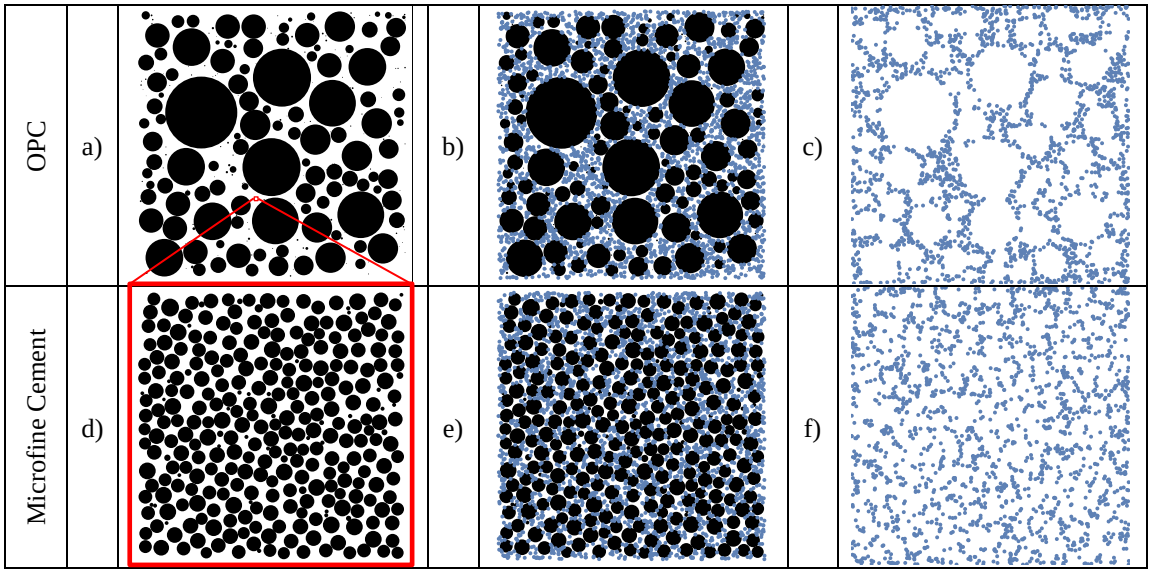

Figure 38: Examples of the geometric clustering of nanoparticles due to the particle size dispersion of cement grains. a) A cement grain particle size distribution based on the OPC with a cement grain area fraction of 0.6. b) The particle size distribution from (a) with 2107 nanoparticle centroids randomly dispersed among the grains. c) The nanoparticle centroids in (b) without the cement grains from (a) showing the unreinforced regions left from the cement grains. d) A cement grain particle size distribution based on the microfine cement with a cement grain area fraction of 0.6; a sample size element is placed in (a) that shows the relative size of the images. e) The particle size distribution from (d) with the same number of nanoparticle centroids in (b) randomly dispersed among the grains. f) The nanoparticle centroids dispersed in (e) without the cement grains from (d) showing unreinforced regions left by the cement grains, but overall potential dispersion is improved with the use of microfine cement when compared to (c).

3.3.1.2 2-D Simulation Results

The dispersion of centroids around 2D cement grains is presented in Figure 39 for three simulated powder mixtures: nanoparticles with OPC, microfine cement, and pure random nanoparticles with no cement grains. Five images were analyzed per data point. The OPC and microfine cement dispersion parameters are calculated using images similar to those in Figure 38. A drawback of using images similar to those in Figure 38 is that the image scale is not the same for both images—Figure 38a has a length scale 80x larger than that of Figure 38d. A comparison of images with the same scale could not be conducted due to computational limitations. Therefore, a 'pure random' simulation was created to represent the comparison of OPC and microfine mixtures at the same length scale. The pure random simulation was an image of nanoparticle 'centroids' placed without constraint which is what would have been seen in an image of microfine cement grains with the same length scale as an image of OPC grains. Figure 39 shows that the maximum achievable dispersion parameter for nanoparticles in OPC grains is definitively lower than that for nanoparticles in microfine cement: 0.98, 0.96, and 0.94 for pure random, microfine, and OPC, respectively. The dispersion parameter continued to increase for all microstructures, but the dispersion parameter reached closer to 1 in the pure random case since the OPC case was limited by geometric clustering.

A product of geometric clustering is that the range of the analyses decreased as the number of centroids in the image increased, where range is defined as the difference between the minimum and maximum values. The geometric clustering effect may not be

apparent in images with few centroids (in the cases presented herein, less than 100) since the dispersion parameters for each case fall within the others' ranges. In other words, each successive image with new randomly-placed centroids can seem to be an image without constraints, resulting in a large range. As the number of centroids increases, each successive image of new randomly-placed centroids forms a pattern due to geometric clustering, and the ranges decrease with increasing numbers of centroids in each set of dispersion parameters.

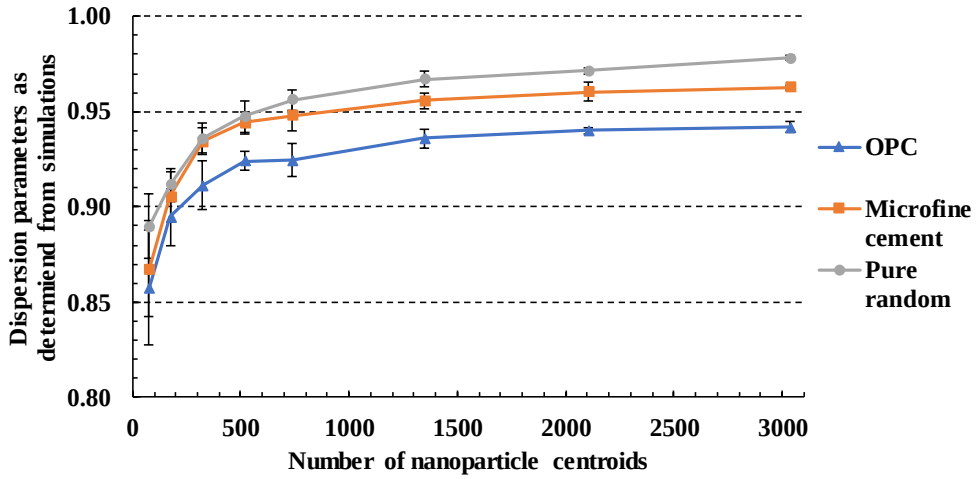

*Figure 39: Dispersion parameters of computational simulations. The dispersion parameter continued to increase for all microstructures, but the dispersion parameter reached closer to 1 in the pure random case since the OPC case was limited by geometric clustering. Error bars are 0.5*range.*

3.3.1.3 2-D Simulation Conclusions

Geometric clustering of nanoparticles due to the size of the cement grains creates a definitive difference in dispersion parameters between 2D OPC and microfine cement simulations, with microfine cement having a higher achievable level of dispersion. The range in 2D geometric clustering simulations substantially decreased with the addition of more nanoparticles, proving that geometric clustering has more impact as the concentration of nanoparticles increases.

3.3.2 Scanning Electron Microscopy Analysis

3.3.2.1 SEM Analysis Setup

The dispersion quantification method described in Section 2.4.2 can be applied to systems either of discrete particles or of particle concentrations, the latter being especially applicable in images where it is impractical or impossible to identify individual particles. Here, the aforementioned dispersion quantification method was applied to SEM images of the hybrid materials. The SEM images were analyzed to isolate the CNFs and create secondary images of only CNFs as shown in Figure 40; the secondary images provided concentration maps of CNFs that were used as initial condition inputs for a finite element (FE) implementation of the aforementioned dispersion analysis. The concentration maps of CNFs may be seen as analogous to concentrations of gas released in specific locations inside a closed container. The gas inside the container will progressively diffuse throughout the container until a uniform

concentration is reached across the domain. In addition, continuum thermodynamics dictates that the gas will expend the minimum possible amount of energy (work) to achieve the uniform concentration [72]. The governing expression describing the diffusion of a gas inside a closed container from initial regions of high and low concentration to a uniform concentration may thus be applied to quantify dispersion according to the aforementioned approach. The initial condition in such a problem is the initial, partially distributed concentration map of CNFs by using an algorithm that relies on FE analysis of the aforementioned diffusion problem. In images of particle concentrations, the FE analysis calculates the flux of CNFs across each element as a function of time as the initial CNF concentration map flows to a uniform concentration, from which the distance traveled by CNFs through each element was calculated. By summing the distances traveled by CNFs in each element over the entire model duration and assuming a unity force vector for each element, the total work performed in dispersing the CNFs was determined (S_i). All edges of the FE model domain are assigned to be insulated to represent the closed container in the gaseous analogy. S_i is normalized as shown in Equation 4 by computationally rearranging the concentration map and placing all particles into a single agglomeration in one corner as far from the centroid of the domain as possible, and then calculating the total work performed in dispersing the fully non-uniform CNF concentration map to uniform concentration (W_i).

a) b)

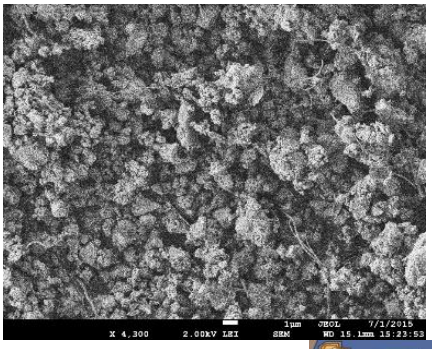

c)

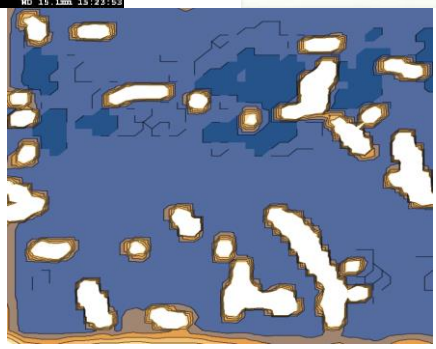

Figure 40: (a) SEM image of 1wt% CNFs dispersed in microfine cement. (b) Image of highlighted CNFs from (a). (c) Contour map of CNFs from (b) to be used in the finite element analysis.

3.3.2.2 SEM Analysis Results

The 2D FE-implemented dispersion analysis of multiple SEM images of each dry hybrid materials resulted in the dispersion parameters shown in Figure 41. Five images were analyzed per data point. The dispersion parameters for both microfine cement and OPC had similar dispersion parameters at 1wt% CNFs. At 2wt% CNFs, the dispersion parameter of the microfine cement increased more than for OPC since the OPC dispersion was limited by geometric clustering. At 3wt% CNFs, the microfine cement dispersion parameter continued to increase (similar to the trend seen in the computational simulations in Section 3.2) while the OPC dispersion parameter decreased due to excessive CNF clumping. SEM imaging in Figure 34 shows that the CNFs can

disperse between the smaller OPC grains, but they cannot entangle (wrap around) the larger cement grains. Since the CNFs can only disperse among the smaller cement grains, the apparent CNF concentration is increased in the grains that surround the large OPC grains while remaining at zero in the grains themselves. In addition, the dispersion parameter decreased in this FE analysis due to a limited image size. The image size has a limit since individual CNFs must be able to be seen and traced, and therefore the larger cement grains in the OPC took large portions of the image as seen in Figure 34c. 5wt% CNFs were not attempted in OPC since the CNFs were subject to excessive clumping at 3wt% CNFs. The dispersion parameter of hybrid microfine cement continued to increase with 5wt% CNFs, quantitatively supporting the hypothesis that the use of microfine cement reduces the geometric clustering effect on CNFs.

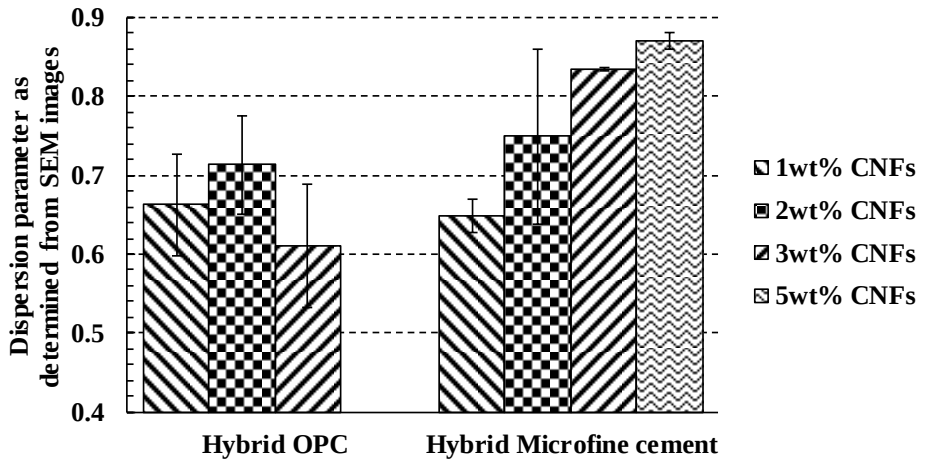

*Figure 41: 2D FEA results of SEM images. The dispersion parameter for the hybrid microfine cement continued to increase with higher concentrations of CNFs while that of the hybrid OPC eventually reduced due to excessive CNF clumping. Error bars are 0.5*range.*

The ranges in Figure 41 shed light on the risk of inherent bias and unreliability of using SEM imaging to quantitatively determine dispersion of CNFs in cement grains. The hybrid OPC results have a range of ± 0.14; this range is a product of the difficulty in finding images without excessively large cement grains. The ranges of the hybrid microfine cement show that the SEM images of the microfine cement can be as biased as the hybrid OPC images; generally, the hybrid microfine dispersion parameter ranges are smaller than those of the hybrid OPC, but the hybrid microfine 1wt% dispersion parameter has the largest range in the analysis. This shows the unreliability of using only SEM images without supporting experiments to quantitatively define dispersion in mixtures whose constituents' sizes range over several orders of magnitude.

3.3.2.3 SEM Analysis Conclusions

Hybrid OPC is susceptible to excessive clumping of CNFs between large cement grains at concentrations above 1wt% CNFs, while CNFs showed only sporadic clumping in hybrid microfine cement at concentrations up to 5wt% CNFs. Dispersion analysis of SEM imaging utilizing an FEA algorithm revealed that the excessive CNF clumping in OPC can hinder dispersion. The large ranges of the dispersion parameters determined from the SEM images suggested that SEM imaging is susceptible to bias when calculating quantitative information.

4. MECHANICAL PROPERTIES*

The mechanical properties of low concentrations (up to 1wt%) of CNFs and CNTs in PCBMs have been documented in other literature, but this research focuses on concentrations at or above 1wt% CNFs in both OPC and in microfine cement. While the primary focus of the research was on cracking resistance via the restrained ring drying shrinkage test, the data from the ring test requires additional material properties to be correctly interpreted. Those additional material properties for both OPC and microfine cement are presented in this section since a discussion of the ring test results requires this information.

4.1 Mortar Mixing Techniques

CNFs were added to the cement as described in Section 3.1.3. Other fiber types that were added to some restrained ring shrinkage tests include milled carbon microfibers (MCMFs), chopped carbon microfibers (CCMFs), and polyvinyl alcohol (PVA) microfibers. The properties of these particular fibers are listed in Table 4. The CNFs used were PR-24-XT-PS purchased from Pyrograf Products, Inc. The PX35MF0150

*Part of this chapter is reprinted with permission from "Dispersion of High Concentrations of Nanofibers in Portland Cement Mortars" by Joshua Hogancamp and Zachary Grasley, 2017. *Journal of Nanomaterials,* Volume 2017, 11 pages, Copyright 2017 by Joshua Hogancamp and Zachary Grasley. [84]

MCMFs and PX35CF0125-13 CCMFs were purchased from Zoltek. The PVA RECS15 microfibers were purchased from Nycon. CCMFs were added to the hybrid cement mixtures using the same sonication process described in Section 3.1.3. If the hybrid mixture had CNFs and MCMFs, the MCMFs were added to the sonication slurry at the same time as the cement. If the microfine cement hybrid mixture had only MCMFs, the MCMFs and cement were sonicated for 10 minutes with mechanical stirring. If the OPC mortars included only MCMFs, the MCMFs were mixed with the OPC by placing both in a rotary tumbler for 12 hours at a speed of 1 rotation per second. Optical microscope observations confirmed that the MCMFs were adequately dispersed in the OPC as shown in Figure 42.

Table 4: Fiber properties pertinent to this research.

Fiber Type	**Diameter**	**Length**	**Tensile Strength (MPa)**	**Elastic Modulus (GPa)**	**Elongation at Break (%)**
CNF	70-200 nm	50-200 μm	2920	240	--
MCMF	7.2 μm	~100 μm*	4137	242	1.5
CCMF	7.2 μm	13 mm	4137	242	1.5
PVA	38 μm	8 mm	1600	41	13
*Length varies due to ball-milling process					

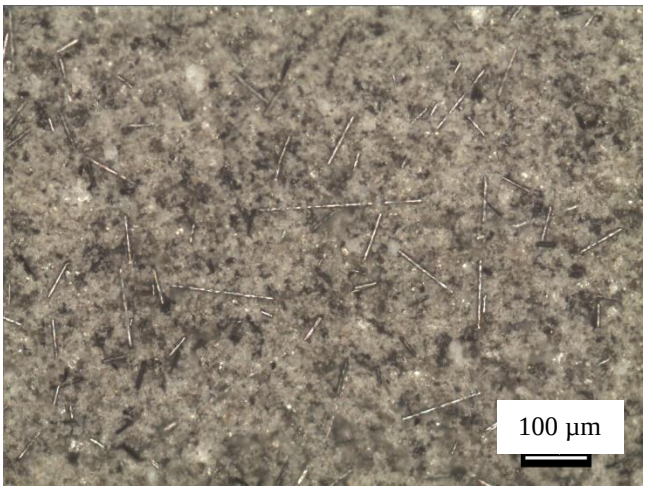

Figure 42: OPC with 4wt% MCMFs pre-mixed. MCMFs are white in this image due to light reflecting off the fibers. The MCMFs were well dispersed throughout the material, and no clumps of MCMFs were found.

The mortar was proportioned with a water/cement mass ratio of 0.4-0.6 and a sand/cement mass ratio of 1.75. An ASTM 20-30 Ottawa silica sand was chosen because of its minimal fines content and its minimal absorption capacity; a primary motivation for the inclusion of sand in the test mixtures was to aid in breaking apart any cement clumps during mixing. The sand passes through a No. 20 sieve and is retained on a No. 30 sieve (roughly 600-850 μm in diameter). This is considered a fine aggregate but is mid-sized for sand; a No. 200 sieve, the finest sand sieve, has a 74 μm spacing. The admixtures used were a polycarboxylate high-range water reducer (HRWR) and a sucrose-based retarder. The HRWR was needed in OPC mixtures with CNFs and in all microfine mixtures. The retarder was needed in the microfine mixtures since this cement sets in less than 5 minutes in ambient conditions as shown in Figure 43; all microfine mixtures used 3wt% retarder to delay set to approximately 40 minutes. It should be

noted that the OPC mixture with 1wt% CNFs was, for reasons unclear, susceptible to flash set, so 3-4 drops (~0.2 milliliters) of retarder were added to each kilogram of mortar.

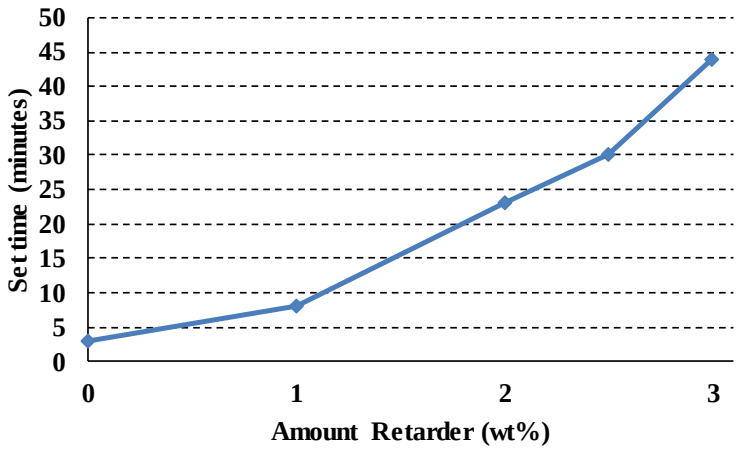

Figure 43: Set time of microfine cement with retarder and 0.8wt% HRWR. 3wt% retarder was chosen for this research to allow time for mixing, filling molds, and consolidation before set.

Each mortar mixture was mixed using a Hobart N50 mortar mixer. The incorporation of such high concentrations of CNFs and the use of microfine cement required a non-standard mixing procedure. The water was mixed with the liquid admixtures, and then the sand and liquids were placed into the bottom of the mixing bowl. The cement hybrid powder was added and mixed on low for 60 seconds. A metal spatula was used to scrape the sides of the bowl and the mixing paddle to remove any material that may have

become congealed. The material was mixed[*] for an additional 120 seconds, and then the sides of the mixing bowl and the mixing paddle were scraped again. The material was mixed for an additional 180 seconds, and then the consistency of the material was qualitatively examined. If the mixture was still solid-like, the process was repeated in 120 second mixing intervals until the mixture became fluid for at least 120 seconds. This process could require 15 minutes of mixing for microfine cement with 5wt% CNFs and 5wt% MCMFs. Mortar was placed in molds in 25 mm lifts and rodded 75 times per lift with a 6mm glass stirring rod, and each lift was vibrated for up to 120 seconds. The molds used in this research are listed in Table 5. Microfine cement mixtures required 120 seconds of vibration per lift due to the high water demand of the microfine cement and the CNFs; no bleeding occurred in any microfine cement mixture. OPC mixtures required as little as 5 seconds of vibration (for samples without CNFs) or up to 20 seconds of vibration (for samples with 3wt% CNFs); no bleeding occurred in OPC samples with no CNFs, and Section 3.2.3 discusses bleeding in OPC cement hybrid samples.

[*] Mixed on low if the material was still solid-like (resembling a powder or individual particles) or on medium/high if the material was liquid-like (a single, malleable mass or a liquid).

Table 5: Molds used in this research and their applications.

Mold	Reference	Dimensions	Application
Rectangular prisms	ASTM C490	25 mm x 25 mm x 279 mm	Flexure, Izod impact, free drying shrinkage, CMOD
Mortar cubes	ASTM C109	50 mm x 50 mm x 50 mm	Elastic modulus
Restrained ring	Modified ASTM C1581	Figure 5 / Table 8	Restrained ring drying shrinkage
Cylinders	--	22 mm x 50 mm	Compressive strength

4.2 Free Drying Shrinkage Prisms

The first property analyzed to supplement the restrained ring drying shrinkage test was unrestrained drying shrinkage. Free drying shrinkage prisms were fabricated using the molds specified in ASTM C490: 25 mm x 25 mm x 279 mm prisms with gage studs in the ends [85]. Three specimens were cast for each mixture that contained no CNFs and for each mixture that contained 3wt% CNFs. The specimens were cast and cured at 98% RH and 23°C for 24 ± 0.5 hours with the tops of the specimens exposed. They were demolded at 24 ± 0.5 hours, the tops and bottoms of the specimens were sealed with aluminum-backed foil tape, and their mass losses and length changes were recorded under exposure to constant 50% RH and 23°C. The data points were recorded every 2 hours for the first 14 hours and then at irregular intervals. The drying prisms had two opposing faces sealed with aluminum tape to mimic the 1-dimensional drying conditions of the rings.

Mass loss and axial shrinkage data for both cement types (with and without CNFs), presented in Figure 44 and Figure 45, shed light on the pore structure of the materials and provide beneficial information for interpreting the ring test results.

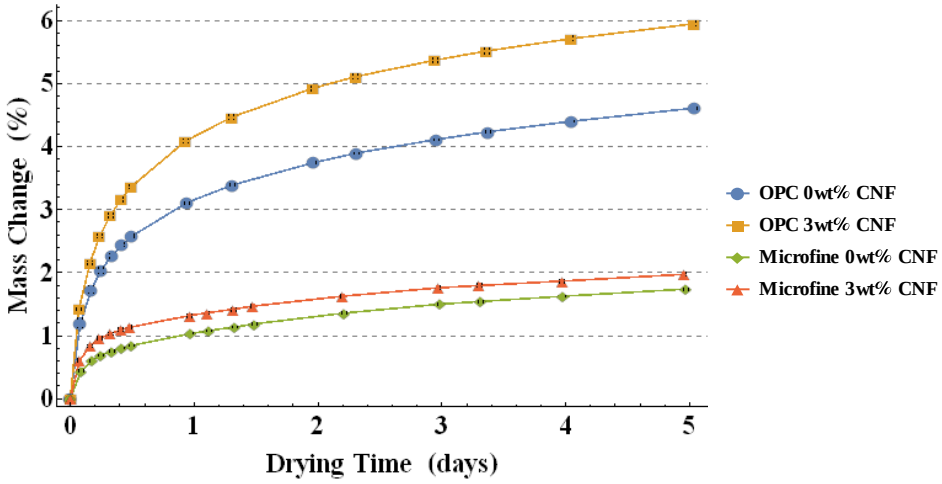

Figure 44: Percent change in mass of drying shrinkage mortar prisms. Error bars are one standard deviation from the mean but are almost too small to be seen in the image.

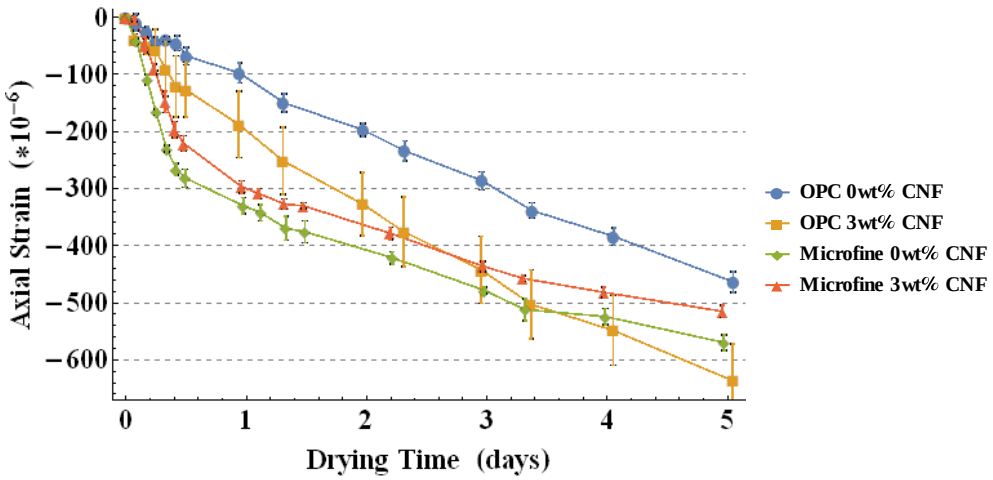

Figure 45: Unrestrained axial strain of drying shrinkage mortar bars. Error bars are one standard deviation from the mean.

Figure 44 shows that both cement types had a higher rate of mass loss with the addition of CNFs, though the difference between plain and CNF mortar is smaller in microfine cement mortar. The OPC mortars lose more mass than the microfine mortars after 1 day of curing. This is likely due to a finer pore structure developing early in the microfine mortar since the microfine cement hydrates much faster than the OPC. A fine pore structure will retain more water at a given RH than will a coarse pore structure due to osmotic suction effects. The water trapped inside coarse pores will readily evaporate at a given RH while the water trapped inside fine pores will not readily evaporate. Furthermore, the hypothesis that the microfine cement pore structure is refined at an earlier age is corroborated by the free axial shrinkage data shown in Figure 45. The microfine cement mortar had reduced axial shrinkage strain rate with the addition of CNFs, while OPC had an increased axial shrinkage strain rate with the addition of CNFs.

The microfine mortars initially had more axial drying shrinkage than did the OPC mortars; a finer pore structure can induce greater shrinkage at a given RH since a material with fine pores will have higher osmotic suction than a material with coarse pores [86-88].

The OPC mortar with 3wt% CNFs is shown in Figure 44 to have increased mass loss while having increased free axial shrinkage in Figure 45 (compared to the control). These effects are attributed to excessive CNF clumping in the cement due to geometric clustering. CNFs that are clumped together between the larger cement grains would increase the pore sizes in those zones. It is theorized that the clumped CNF zones created a network of larger pores in the composite material that allowed water inside the material to evaporate more quickly via the network. An increased rate of drying throughout the material would simultaneously increase the rates of mass loss and free axial shrinkage.

The microfine cement with 3wt% CNFs is shown in Figure 44 to have slightly increased mass loss while having decreased free axial shrinkage in Figure 45 (compared to the control). These effects are attributed to a slight pore coarsening through the material due to the CNFs. A coarser pore structure would increase mass loss while reducing free axial shrinkage at a given RH since the water would evaporate more readily due to decreased osmotic suction effects at that RH.

The pore coarsening in the hybrid microfine cement is not the same as the effect that CNFs have in OPC. In the hybrid microfine cement, the cement pore structure is *uniformly* coarsened (slightly) by the addition of CNFs. In the hybrid OPC, the cement pore structure is theorized to be minimally affected by the CNFs since most of the CNFs agglomerate between the larger cement grains; however, the agglomerations of CNFs create a network of voids (highways for moisture, of a sort) that link the hydrated OPC zones to the exterior.

4.3 Mortar Cube Elastic Modulus

Mortar samples were prepared for testing at 1 day, 3 days, 7 days, and 28 days. ASTM standards were followed for time of testing, e.g. 1-day testing occurred at 24 $\pm$ 0.5 hours. After 24 ± 0.5 hours, the samples were demolded and exposed to 98% relative humidity (RH) and 23°C until time of testing. Three 50 mm mortar cubes cast using molds described in ASTM C109 were uniaxially compressed for each mixture using a displacement-controlled load frame at a rate of 1 mm/min with data points recorded at 20 Hz [89]. An elastic modulus was approximated via the (roughly) linear portion of the slope of the mortar cube load vs loading head displacement curve as shown in Figure 46. Elastic stiffness results are normalized by the control mixture for each cement type rendering the units for elastic stiffness irrelevant.

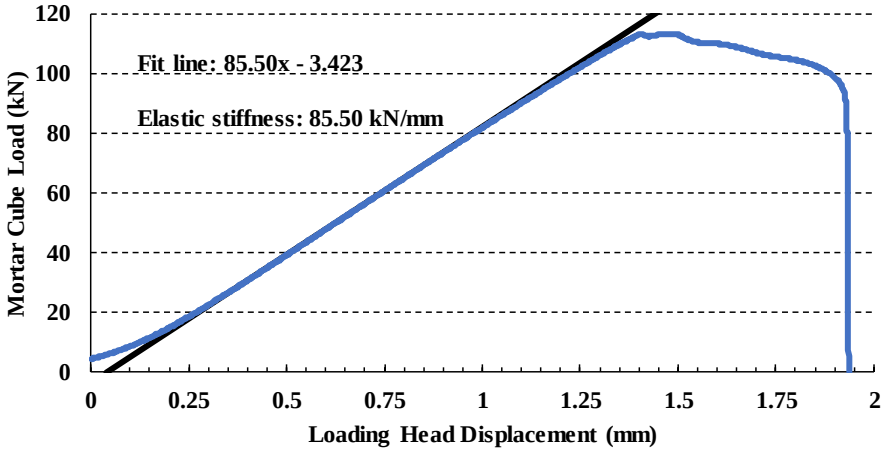

Figure 46: Load vs loading head displacement of a mortar cube compression test. Elastic stiffness of the mortar cube was approximated using a fit line through the roughly linear portion of the load vs displacement curve. Elastic stiffness results were presented normalized by the control mixtures, so the units for elastic stiffness were irrelevant.

The mortar cube elastic moduli for ages 1 day, 3 days, 7 days, and 28 days at various concentrations of CNFS are shown in Figure 47 and Figure 48 as normalized by the control; i.e. a value of 100% indicates that the specimen had the same stiffness/flexural strength as the specimen without CNFs. The elastic stiffness of the hybrid microfine mortar shown in Figure 48 was not significantly impacted and remained within 8% of the control specimens. The elastic stiffness of hybrid OPC mortar shown in Figure 47 revealed no specific trend, but 75% of specimens had a lower stiffness than the control mixture.

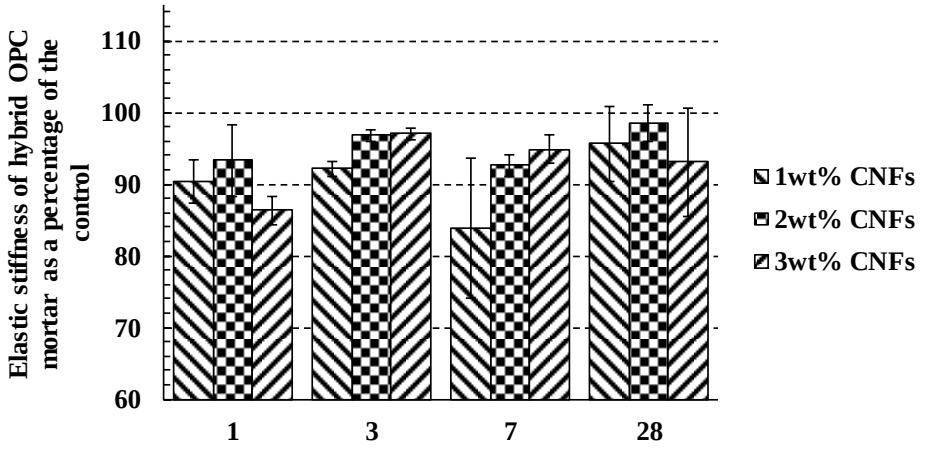

*Figure 47: Elastic stiffness of hybrid OPC mortars as a percentage of the control. 75% of mixtures were signficantly less stiff than the controls. Error bars are 0.5*range.*

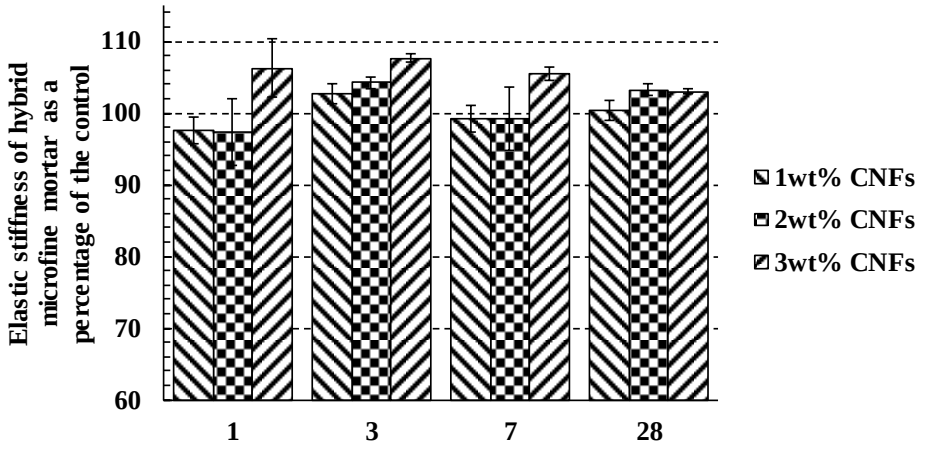

*Figure 48: Elastic stiffness of hybrid microfine cement mortars as a percentage of the control. All specimens were ±8% of the control suggesting that CNFs did not significantly effect stiffness. Error bars are 0.5*range.*

The compression cubes elastic moduli results reinforce the proposition that the dispersion of CNFs is improved in the hybrid microfine cement versus the hybrid OPC.

The hybrid OPC had CNF clumping issues, especially at concentrations above 1wt% CNFs, and the elastic moduli of the hybrid OPC mortar were often lower than the control specimens. CNFs in the microfine hybrid mortar had inconsistent but inconsequential effects on the elastic modulus, suggesting that the hybrid microfine cement mortar did not have clumping issues and had a more stable dispersion of CNFs.

4.4 Flexure Prisms

Two 25 mm x 25 mm x 279 mm mortar flexure prisms using the molds specified in ASTM C490 were tested for each mixture under a 4-point flexure test apparatus as described in Figure 49 using a compression-controlled load frame at a rate of 1 mm/min with data points recorded at 20 Hz [85]. Flexure specimens were placed in the 4-point flexure apparatus such that the top of the specimens were 90° to the force plane and the flexure apparatus contacted sides of the specimens that were in contact with the mold; this orientation minimized any error from material settling or bleeding effects that occurred during vibration.

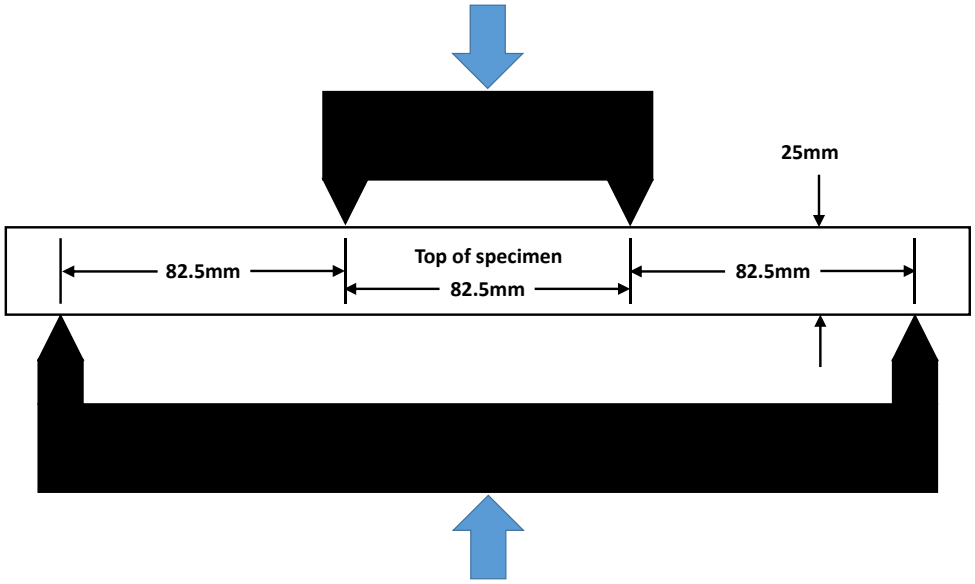

Figure 49: 4-point bending flexure testing schematic.

The flexure prism ultimate stress for ages 1 day, 3 days, 7 days, and 28 days at various concentrations of CNFS are shown in Figure 50 and Figure 51 as normalized by the control; i.e. a value of 100% indicates that the specimen had the same flexural strength as the specimen without CNFs. The hybrid microfine cement flexural prisms in Figure 51 showed a definitive trend that increasing the concentration of CNFs increases the ultimate flexural strength by up to 50%. The hybrid OPC flexural prism strengths shown in Figure 50 indicate a reduced strength versus the control for 1wt% CNFs addition while 2wt% and 3wt% additions of CNFs indicate a comparable strength to the control after 3 days age.

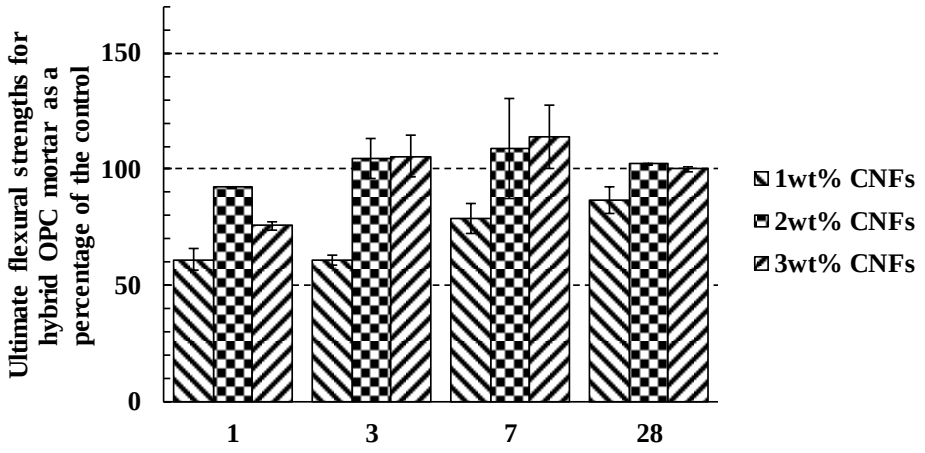

*Figure 50: Flexural strength results for hybrid OPC mortars as a percentage of the control. 50% of specimens were weaker than the controls while the other 50% were unaffected or regained strength up to the control. Error bars are 0.5*range.*

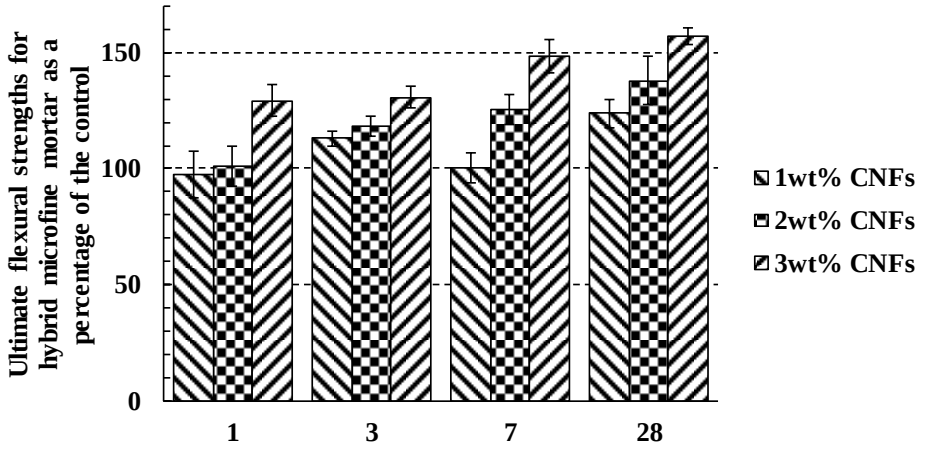

*Figure 51: Flexural strength results for hybrid microfine cement mortars as a percentage of the control. Increasing CNF concentrations increased flexural strength up to 50%. Error bars are 0.5*range.*

The mechanical tests of mortar flexure prisms reinforce the proposition that the dispersion of CNFs is improved in the hybrid microfine cement versus the hybrid OPC. The hybrid OPC had CNF clumping issues, especially at concentrations above 1wt% CNFs, and the flexural strengths of the hybrid OPC mortar were often lower than the control specimens. CNFs in the microfine hybrid mortar often increased flexural strengths, suggesting that the hybrid microfine cement mortar did not have clumping issues and had a more stable dispersion of CNFs.

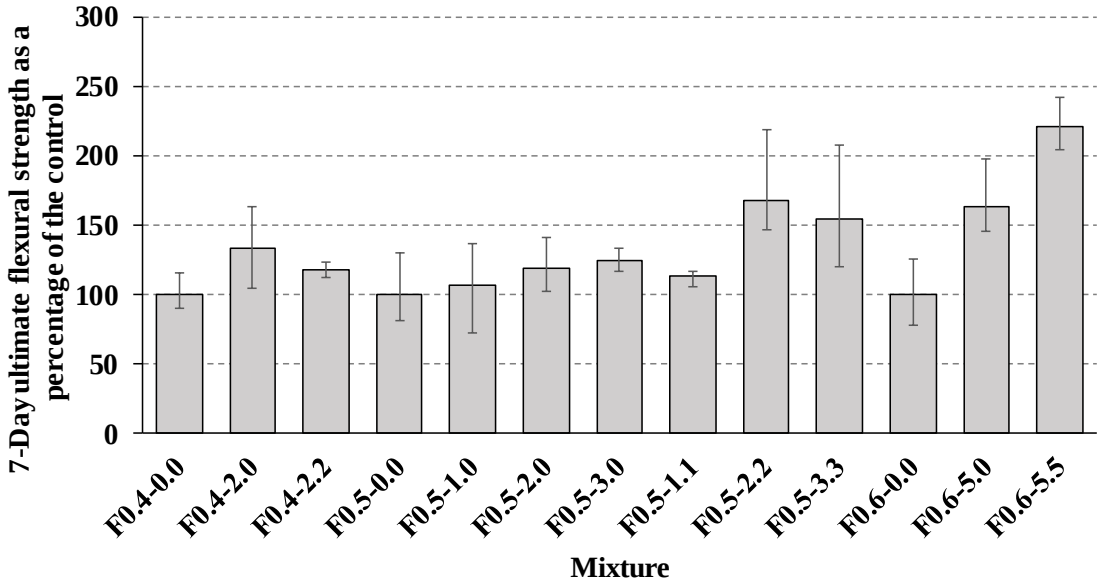

Figure 52: Ultimate flexural strength of microfine cement mortar prisms with CNFs and, where applicable, MCMFs as a percentage of the control. Increasing CNF and MCMF concentrations typically increased strength, but consolidation issues created large ranges in results. Error bars show the min and max values of the tests.

Figure 52 shows the results of 7-day flexural strength tests of microfine cement mortar prisms with CNFs and MCMFs. Four specimens were tested per mixture. Decreasing the w/c ratio from 0.6 to 0.4 (without fibers) increased the ultimate flexural strength from 2.80 MPa to 4.70 MPa. The strongest mixture was F0.4-2.0 with an ultimate strength of 6.26 MPa, follow by F0.6-5.5 with an ultimate strength of 6.18 MPa. The mixture with the highest gain compared to its control w/c ratio mixture was F0.6-5.5 with a 221% increase compared to F0.6-0.0, followed by F0.5-2.2 with a 168% increase compared to F0.5-0.0. The wide margins of error in Figure 52 are most likely due to consolidation issues. The microfine cement mortars were viscous, especially with the addition of high concentrations of fibers or a lower w/c ratio, and it was extremely difficult to remove air voids from the composite. The data in Figure 52 suggest that the addition of CNFs and MCMFs to microfine cement mortar can increase the flexural strength up to 221%, but workability issues and air voids cause uncertainty in any one particular specimen.

4.5 Compressive Strength Cylinders

Four cylinders with diameter 22 mm and height 50 mm were prepared for 7-day testing for several mixtures, primarily of microfine cement with various amounts of fibers. Specimens were left in the molds for 24 ± 0.5 hours at 23°C and 98% RH, and then they were soaked in lime water until time of testing. Specimens were uniaxially compressed for each mixture using a displacement-controlled load frame at a rate of 1 mm/min with

data points recorded at 20 Hz. The top and bottom of each specimen were cut with a concrete saw to make them smooth and level.

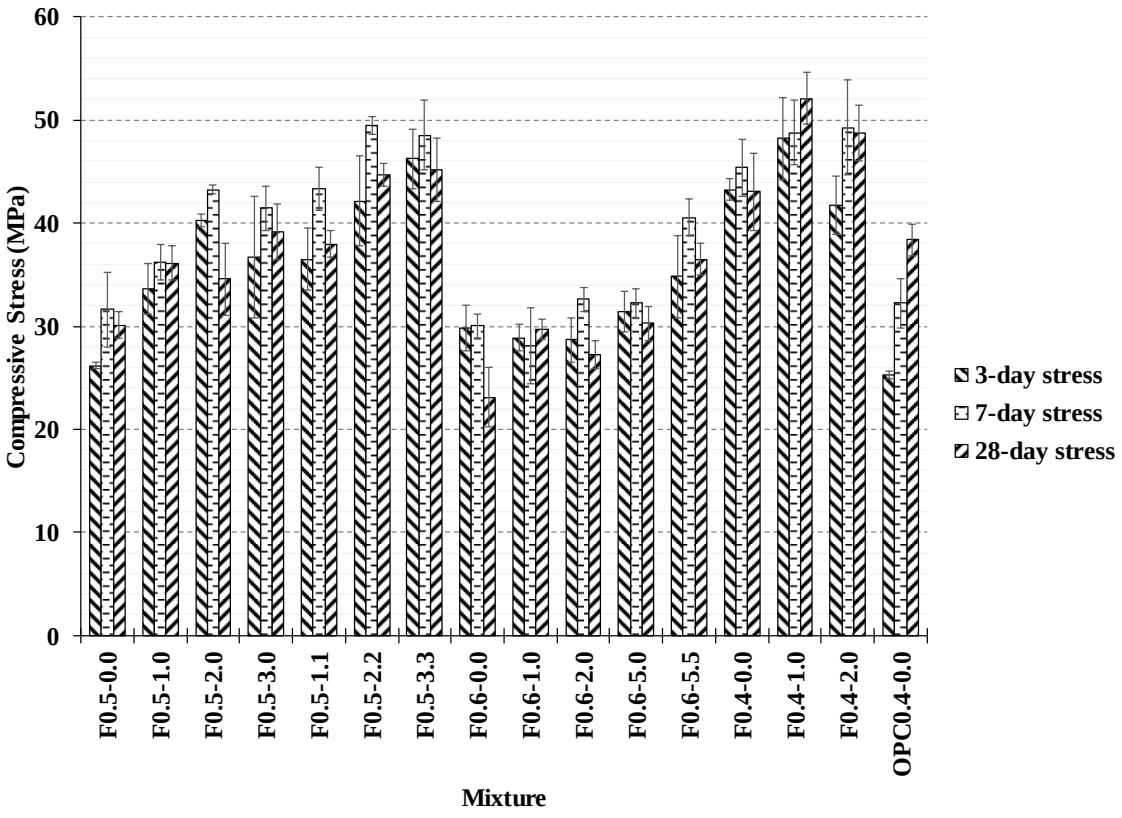

Figure 53: Compressive stress of various mixtures. 28-day strengths in microfine cements were lower than 7-day strengths for unknown reasons. Error bars are one standard deviation to each side.

The compressive strength results shown in Figure 53 have some interesting trends. Adding CNFs increased the compressive strength in mixtures with w/c ratios of 0.4 and 0.5, but mixtures with a w/c ratio of 0.6 had compressive strengths that remained more

or less constant with CNFs. Adding MCMFs to the hybrid microfine cement mortars increased the compressive strength in both w/c ratios tested (0.5 and 0.6). However, an uncommon effect occurred in this test: the 28-day strengths of the microfine cement mortar specimens were lower than the 7-day strengths in 13 out of 15 mixtures with or without fibers. One possible explanation could be the hydration process combined with the lime-water curing. The microfine cement hydrates much faster than OPC, and a 7-day specimen is almost fully hydrated while OPC is still hydrating up until and beyond 28 days. The microfine cement mortars being completely hydrated, the lime-water curing may have inadvertently introduced a chemical phase change in the specimens that had consequences on the microfine cement but not on the still-hydrating OPC. The 28-day strengths will therefore be ignored in data comparisons.

Since the 28-day strengths of the microfine cement mortars were uncharacteristic of PCBMs, the 7-day strengths will be used for comparison purposes as shown in Figure 54. Each mixture has been normalized by the control mixture for that specific w/c ratio, e.g. all F0.5-X.X mixtures are normalized by F0.5-0.0. The mixture with the highest gain is F0.5-2.2 with 56% increased compressive strength, a higher gain than dropping the w/c ratio from 0.5 to 0.4 (43% gain).

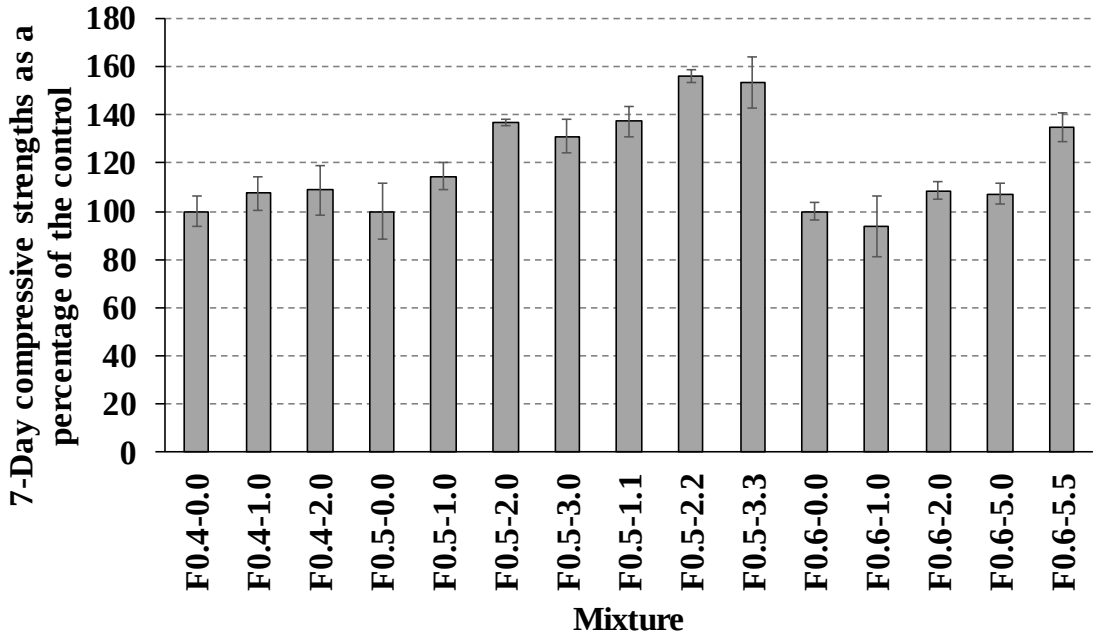

Figure 54: 7-day compressive strengths of hybrid microfine mortars as a percentage of the controls. Error bars are one standard deviation to each side.

A statistical analysis was completed on the 7-day compressive strengths using Tukey's method. There were 16 mixtures (OPC0.4-0.0 was included) compared with 4 specimens per mixture, resulting in 48 degrees of freedom. Using a significance value of $\alpha = 0.05$, the Tukey's *q* value is 4.67. For each comparison, Equation 7 was used to calculate the Tukey's score where μ is the sample mean, *MSE* is the mean square error of the data set, and *n* is the number of samples tester per mixture.

Equation 7: Tukey's score

$$Tukey's\ Score = \frac{\mu_1 - \mu_2}{\sqrt{\frac{MSE}{n}}}$$

Table 6: Tukey's Method comparison of compressive strengths

Mixture	**OPC0.4-0.0**	**F0.4-2.0**	**F0.4-1.0**	**F0.4-0.0**	**F0.6-5.5**	**F0.6-5.0**	**F0.6-2.0**
F0.5-0.0	0.49	13.85	13.44	10.77	6.98	0.47	0.76
F0.5-1.0	3.12	10.24	9.83	7.17	3.37	3.14	2.84
F0.5-2.0	8.62	4.74	4.33	1.67	2.13	8.64	8.35
F0.5-3.0	7.23	6.12	5.72	3.05	0.74	7.25	6.96
F0.5-1.1	8.72	4.63	4.23	1.56	2.23	8.74	8.45
F0.5-2.2	13.47	0.12	0.53	3.19	6.98	13.49	13.20
F0.5-3.3	12.77	0.59	0.18	2.48	6.28	12.79	12.49
F0.6-0.0	1.73	15.09	14.68	12.02	8.23	1.72	2.01
F0.6-1.0	3.23	16.58	16.18	13.51	9.72	3.21	3.50
F0.6-2.0	0.27	13.08	12.67	10.01	6.22	0.29	
F0.6-5.0	0.02	13.38	12.97	10.31	6.51		
F0.6-5.5	6.49	6.87	6.46	3.80			
F0.4-0.0	10.29	3.07	2.66				
F0.4-1.0	12.95	0.41					
F0.4-2.0	13.36						
Mixture	**F0.6-1.0**	**F0.6-0.0**	**F0.5-3.3**	**F0.5-2.2**	**F0.5-1.1**	**F0.5-3.0**	**F0.5-2.0**
F0.5-0.0	2.74	1.25	13.25	13.96	9.21	7.72	9.11
F0.5-1.0	6.35	4.85	9.65	10.36	5.60	4.11	5.50
F0.5-2.0	11.85	10.36	4.15	4.85	0.10	1.39	
F0.5-3.0	10.46	8.97	5.53	6.24	1.49		
F0.5-1.1	11.95	10.46	4.04	4.75			
F0.5-2.2	16.70	15.21	0.71				
F0.5-3.3	15.99	14.50					
F0.6-0.0	1.49						
Mixture	**F0.5-1.0**						
F0.5-0.0	3.61						

Table 6 tabulates a comparison of the compressive strengths of all mixtures. If a Tukey score between two mixtures is above the *q*-value of 4.67, the two mixtures are statistically different with 95% confidence (designated by a highlighted cell). For

example, the value in the table is the comparison between mixtures OPC0.4-0.0 and F0.5-0.0; with a value of $0.49 < 4.67$, there is not a significant difference between the compressive strengths of the two mixtures. Comparing the mixtures F0.5-3.3 with F0.5-3.0 has a value of $5.53 > 4.67$, so there is a significant difference between the compressive strengths of the two mixtures. Some interesting aspects of Table 6 are summarized below:

- At a w/c ratio of 0.6, the addition of CNFs does not significantly change the compressive strength, but adding MCMFs does significantly increase the compressive strength.
- At a w/c ratio of 0.5, the addition of 1wt% CNFs does not significantly change the compressive strength, but the addition of 2wt% CNFs with or without MCMFs does increase the compressive strength.
- At a w/c ratio of 0.5, F0.5-2.2 and F0.5-3.3 (the strongest mixtures) are significantly stronger compared to mixtures without MCMFs and F0.5-1.1, but the two mixtures are not significantly different from each other.
- The mixture OPC0.4-0.0 is not significantly different from the F0.5-0.0 and F0.6-0.0 mixtures, but the F0.4-0.0 mixture is significantly stronger than the OPC0.4-0.0.

4.6 Izod Impact Strength

Izod impact testing was performed on prisms fabricated using the molds specified in ASTM C490 and cut to a shorter length: 25 mm x 25 mm x 57 mm. The Izod impact test is originally designed for plastics as described in ASTM D256, but the test is similar to the Charpy impact test and can be performed on many different materials [90]. Figure 55 shows the Izod testing equipment used in this research. A pendulum hammer drops from a specified height and impacts the sample. The sample is clamped in a cantilever fashion at the base of the machine, and the hammer impacts and fractures the specimen as shown in Figure 56. The initial height of the hammer has a potential energy; at the base of the pendulum swing, all the potential energy has transferred to kinetic energy. The pendulum fractures the sample and rises on the other side of the swing; the height of the pendulum on the up-swing is less than the initial height due to energy loss fracturing the sample. The energy loss fracturing the sample is equivalent to the difference in potential energies of the hammer from initial height to final height in the up-swing. While ASTM D256 calls for a notched sample, an unnotched sample can also be used in the test.

Figure 55: Izod impact test equipment.

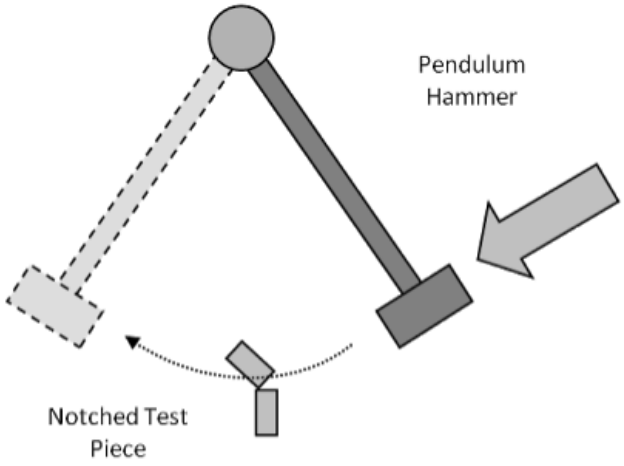

Figure 56: Schematic of Izod hammer impact on sample.

Four 25 mm x 25 mm x 57 mm microfine cement mortar specimens were tested per mixture, and the results are presented in Figure 57. The control mixtures with no fibers (0.4-0.0, 0.5-0.0, and 0.6-0.0) have decreasing facture energy with increasing w/c ratio as expected, but the mixtures with fibers showed no specific trend. Some mixtures had

low fracture energy values compared to the control; the probable cause is excess air in the specimens due to consolidation issues. Other mixtures had higher fracture energy values but with higher ranges as well. For example, mixture 0.6-5.0 had the highest average fracture energy and the largest range; this set of specimens were subject to multiple fractures during the test instead of a single clean break. Multiple fractures in a break can double or triple the fracture energy reported in the Izod test. In conclusion, there is no significant effect of CNFs and MCMFs on fracture energy. Consolidation could have a much larger effect on fracture energy than CNFs or MCMFs.

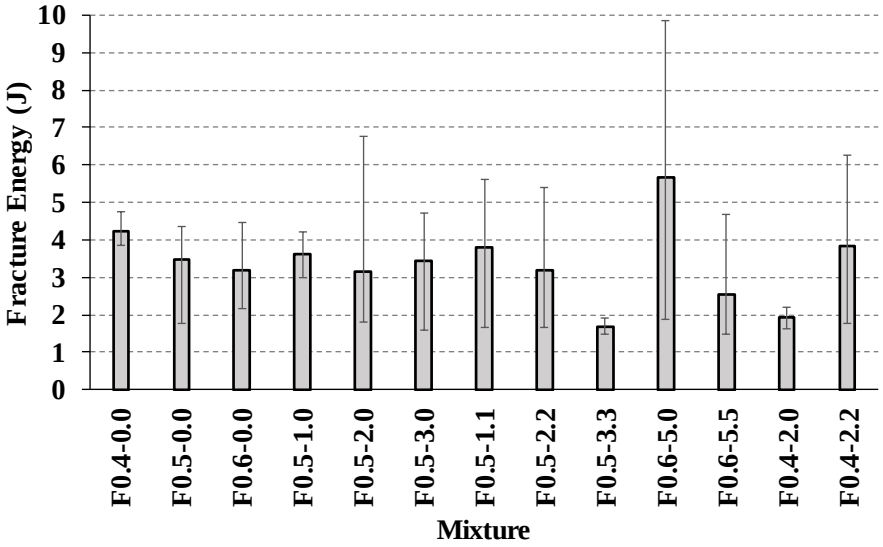

Figure 57: Izod fracture energy absorbed per mixture. All mixtures are microfine cement mortar. No significant trends were observed. Error bars show the maximum and minimum values.

4.7 Crack Mouth Opening Displacement Prisms

CMOD tests were performed on microfine cement mortar mixtures with various amounts of CNFs and MCMFs. 25 mm x 25 mm specimens were tested in 3-point bending with a gage length of 102 mm and with a 3 mm (deep) x 4 mm (wide) notch cut in the middle of the bottom of the specimen as shown in Figure 58. The load applicator was displacement-controlled at a rate of 0.05mm/min with data recorded at 100 Hz to ensure proper monitoring of peak and post-peak behavior. The CMOD gauge was attached to knife edges glued to the bottom of the specimen. The CMOD gauge was not calibrated by the manufacturer at the displacements measured, but it could not be compressed to the calibration range since doing so required enough force to alter test results or possibly break the sample before testing; therefore, all values recorded during these tests are qualitative, and the values recorded could be a slight misrepresentation of the actual values. Each test was continued until specimen complete specimen fracture. The mixtures tested were F0.4-0.0, F0.5-0.0, F0.6-0.0, F0.5-1.0, F0.5-2.0, F0.5-3.0, F0.5-1.1, F0.5-2.2, F0.5-3.3, F0.6-5.0, F0.6-5.5, F0.4-2.0, and F0.4-2.2.

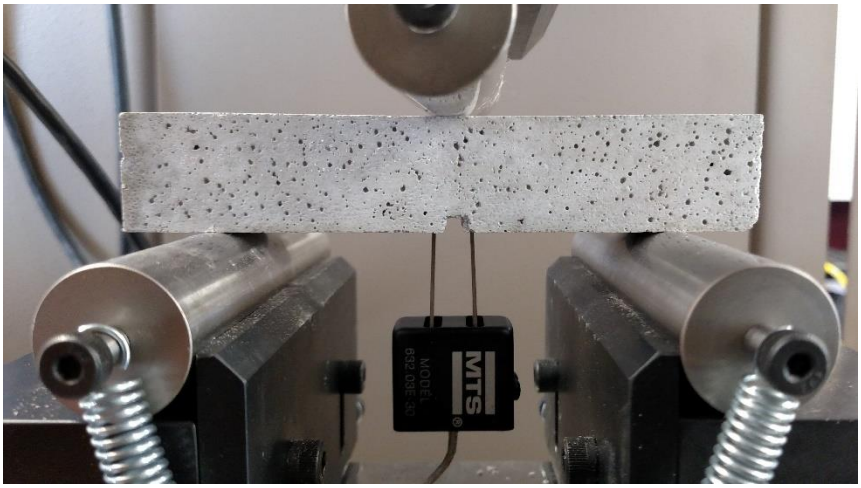

Figure 58: Example of CMOD specimen during testing.

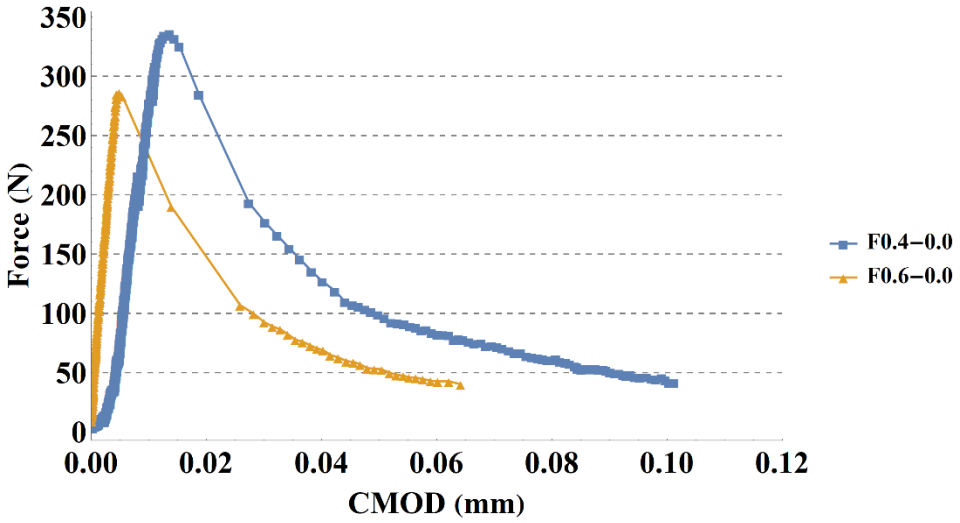

Figure 59: Control CMOD mixtures with w/c ratios of 0.4 and 0.6. Lowering the w/c ratio increased peak load and ultimate CMOD.

The behaviors of the control mixtures at each w/c ratio are shown in Figure 59. Each mixture showed a rapid reduction in applied force after the peak load, and the specimens

failed at ~50 N applied force. A 'rapid failure' is seen in the CMOD results by a lack of data points on specific parts of the curve; for example, the immediate post-peak behaviors of the specimens in Figure 59 have only a few data points on the falling edge of the curve, indicating the rapid change in Load vs CMOD.

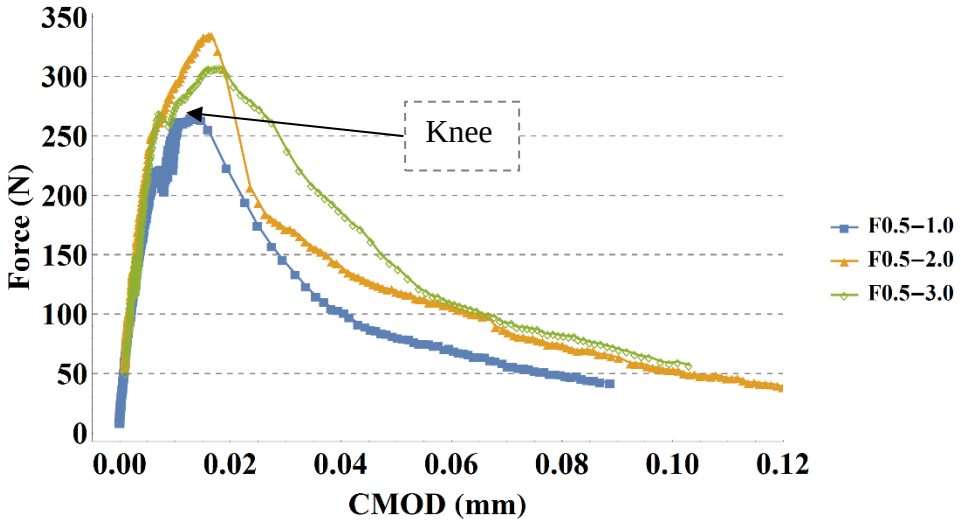

Figure 60: CMOD mixtures with only CNFs and w/c ratios of 0.5. A 'knee' seemed to form in the mixtures that resembles a switch from 'undamaged' material to 'damaged' material. The knee behavior is explained in the restrained ring drying test section.

Figure 60 shows CMOD test results for mixtures with a w/c ratio of 0.5 and CNFs (without any other fibers). Each curve had a segment of rapid change in Load vs CMOD during specimen failure similar to the curves in Figure 59, but the behavior immediately before and after the peak load is significantly different in the mixtures with 2wt% and 3wt% CNFs. In mixtures F0.5-2.0 and F0.5-3.0, there is a bend in the curves resembling

the knee shown in the restrained ring drying shrinkage tests shown in Section 5.3. This bend could be the effect of crack-bridging by CNFs during initial composite failure; the cement matrix begins to crack and fail, but the CNFs bridge the cracks and retain the composite's strength though with a lower stiffness (manifesting as a gentler slope in the Load vs CMOD curve). While behavior immediately before and after the peak force is affected by CNF crack bridging, it should be noted that the specimens failed at a CMOD only slightly larger than specimens without CNFs. The post-peak behavior of F0.5-3.0 showed some material difference insofar as the force did not drop as quickly after the peak, suggesting that 3wt% CNFs did contribute to holding the material together for a narrow crack.

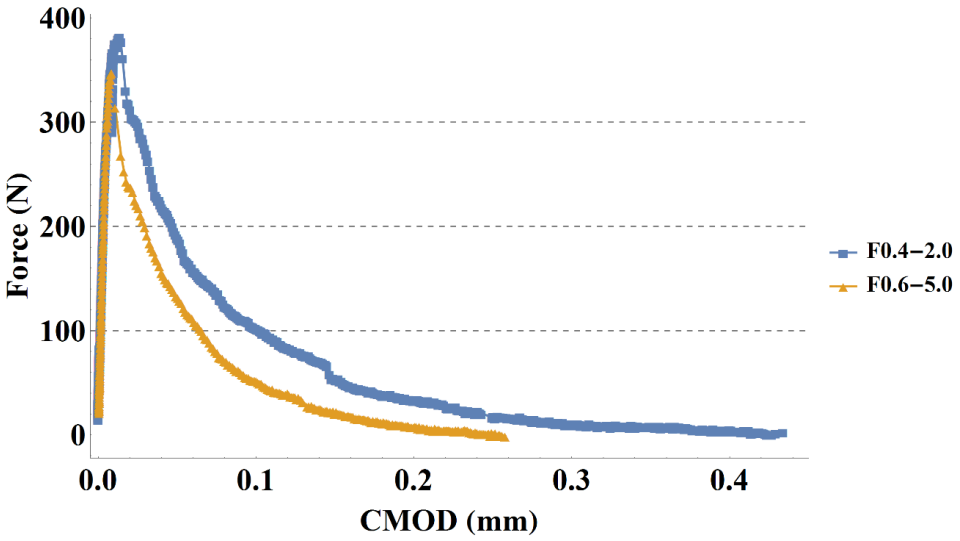

Figure 61: CMOD mixtures with only CNFs and w/c ratios of 0.4 and 0.6. These results suggest that lowering the w/c ratio could be more beneficial than higher concentrations of CNFs in hybrid mortars with only CNFs (no MCMFs).

Figure 61 shows the results of mixtures with w/c ratios of 0.4 and 0.6 with only CNFs. Mixture F0.6-5.0 reached a higher peak strain that its control mixture in Figure 59 (~350N and ~290N for F0.6-5.0 and F0.6-0.0, respectively). More importantly, the specimen held together until a CMOD of ~0.26mm while the control mixture failed at ~0.064mm. The result that 1wt%, 2wt%, and 3wt% CNFs did not significantly increase the ultimate CMOD while 5wt% CNFs did increase the ultimate CMOD suggests that there can be an addition of CNFs high enough to bridge cracks throughout composite failure. Similarly, lowering the w/c ratio to 0.4 increased the load carried post-peak and increased the ultimate CMOD reached before material failure from ~0.11mm (control mixture) to ~0.45mm. This result suggests that lowering the w/c ratio could increase the efficacy of the CNFs in the composite in tension.

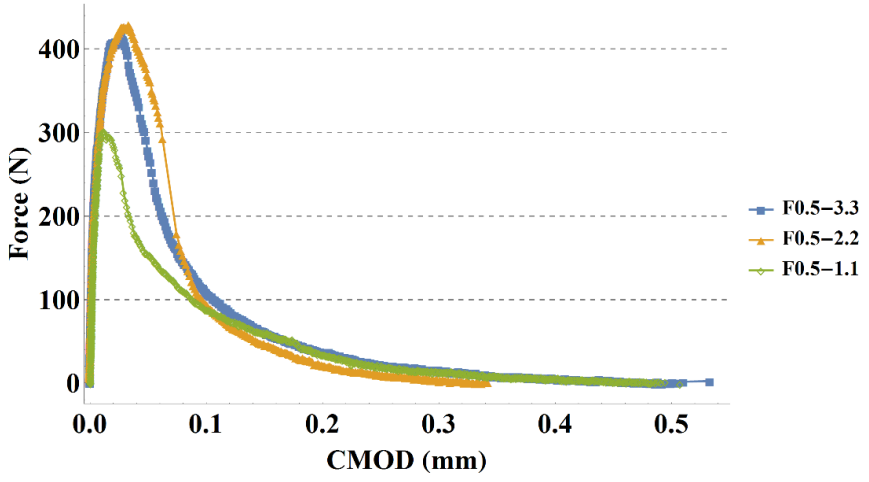

Figure 62: CMOD mixtures with CNFs and MCMFs and w/c ratios of 0.5. F0.5-2.2 and F0.5-3.3 performed better than F0.5-1.1, suggesting that increasing the fiber concentrations beyond 1wt% is beneficial, but further concentrations from 2wt% to 3wt% are not.

Figure 62 shows the results of mixtures with CNFs and MCMFs at a w/c ratio of 0.5. The peak load reached up to ~430N for two of the three specimens shown, though other specimens tested for mixtures with 2wt% and 3wt% MCMFs reached the same peak load as the specimens with the same concentration of CNFs but no MCMFs. These results suggest that adding MCMFs in high concentrations (above 1wt%) can increase the peak load, but the MCMFs do not guarantee that possibility. Increasing the concentration of MCMFs higher than 3wt% could give more consistent results, but more testing is required for definite conclusions on composite behavior consistency. One conclusion that can be deduced from Figure 62 is that adding MCMFs to the hybrid CNF mortars does increase the ultimate CMOD and improves post-peak behavior by sustaining load for a longer duration.

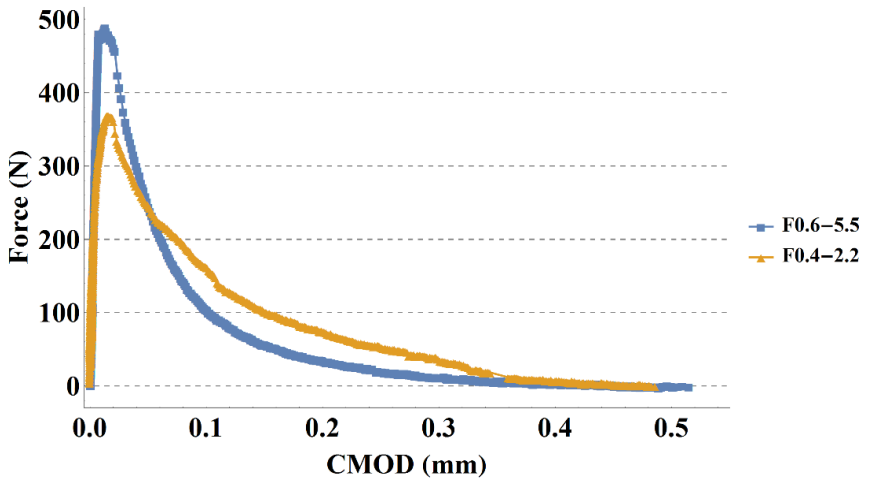

Figure 63: CMOD mixtures with CNFs and MCMFs and w/c ratios of 0.4 and 0.6. The mixture with more fibers (F0.6-5.5) reached a higher peak load, but the lower w/c ratio mixture (F0.4-2.2) sustained higher loads at larger CMOD.

Figure 63 shows mixtures of hybrid CNF mortar with MCMFs at w/c ratios of 0.4 and 0.6. Mixture F0.4-2.2 reached approximately the same ultimate force as mixture F0.4-2.0 (~360N and ~350N, respectively), but the mixture with MCMFs sustained higher loads as the CMOD increased and reached a higher ultimate CMOD than the mixture without MCMFs. Mixture F0.6-5.5 reached the highest peak load out of all mixtures (~500N) and an ultimate CMOD of ~0.51mm, but its load capacity vs CMOD fell off more rapidly than did mixture F0.4-2.2. The fact that mixture F0.4-2.2 sustained a higher load (relative to peak load) at larger CMOD suggests that a lower w/c ratio can increase the efficacy of CNF-MCMF hybrid mortars.

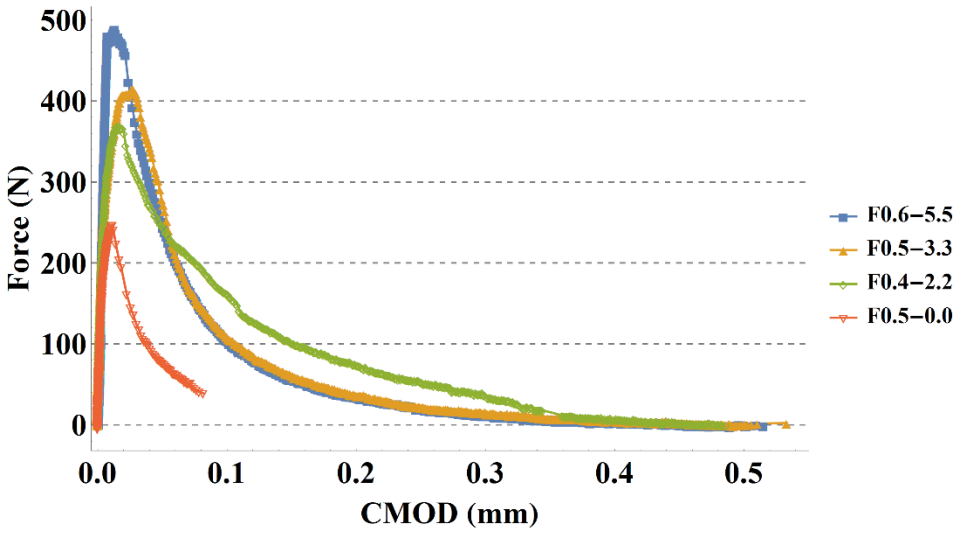

Figure 64: Comparing the best CMOD mixtures with the standard mixture F0.5-0.0. Adding higher concentrations of CNFs and MCMFs increased the ultimate force, but it seems that lowering the w/c ratio increases the toughness and the efficacy of the fibers.

Figure 64 compares the standard mixture in this research (F0.5-0.0) with three of the best mixtures. The highest peak load was achieved with mixture F0.6-5.5. Mixture F0.5-3.3 had similar post-peak behavior to mixture F0.6-5.5 but a lower ultimate load. Mixture F0.4-2.2 sustained higher loads than mixtures F0.6-5.5 and F0.5-3.3 at CMOD greater than ~0.07mm. The results of the CMOD tests are summarized in Table 7. The toughness of the material in N-mm was calculated by integrating the Force vs CMOD curves. From Table 7, lowing the w/c ratio increases the toughness of the mortar as expected. Adding more than 1wt% CNF (without MCMFs) also increases toughness. Adding CNFs while lowering the w/c ratio increases toughness in a superposition manner, i.e. the difference in toughness between F0.4-2.0 and F0.4-0.0 is the same as the sum of the differences between 1) F0.4-0.0 and F0.5-0.0 and 2) F0.5-2.0 and F0.5-0.0. Adding MCMFs increased the toughness of all mixtures, though adding more MCMFs did not necessarily increase the toughness in incremental amounts; for example, F0.5-2.2 and F0.5-3.3 had approximately the same toughness and peak load.

Table 7: CMOD test results summary

Mixture	Average peak load (N)	Average ultimate CMOD (MM)	Average toughness (N-mm)
F0.4-0.0	342	0.108	17.1
F0.5-0.0	255	0.097	11.6
F0.6-0.0	310	0.073	9.4
F0.5-1.0	265	0.079	11.6
F0.5-2.0	340	0.130	18.6
F0.5-3.0	288	0.134	17.6
F0.5-1.1	297	0.533	27.6
F0.5-2.2	371	0.379	31.2
F0.5-3.3	368	0.446	30.7
F0.6-5.0	358	0.306	18.6
F0.6-5.5	477	0.501	36.6
F0.4-2.0	398	0.429	29.7
F0.4-2.2	362	0.512	43.1

4.8 Conclusions

Free drying shrinkage prisms show that OPC and microfine cement with and without CNFs behave in similar fashions but do so at different rates due to the faster hydration of microfine cement. 3wt% CNFs OPC specimens lose mass and shrink faster than the control. Since hybrid OPC specimens are subject to geometric clustering, the faster mass loss and shrinkage are attributed to a network of interconnected zones containing agglomerations of CNFs that allow water to travel through the specimen to the surface. 3wt% CNFs microfine cement specimens lose slightly more mass and shrink less than the control. This is attributed to a slight pore coarsening throughout the hybrid specimen,

but the pore coarsening is uniform throughout the material and is not due to CNF agglomerations as in hybrid OPC.

Mortar cube elastic moduli results reinforce the proposition that the dispersion of CNFs is improved in the hybrid microfine cement versus the hybrid OPC. The hybrid OPC had CNF clumping issues, especially at concentrations above 1wt% CNFs, and the elastic moduli of the hybrid OPC mortar were often lower than the control specimens. CNFs in the microfine hybrid mortar had inconsistent but inconsequential effects on the elastic modulus, suggesting that the hybrid microfine cement mortar did not have clumping issues and had a more stable dispersion of CNFs.

The hybrid OPC had CNF clumping issues, especially at concentrations above 1wt% CNFs, and the flexural strengths of the hybrid OPC mortar were often lower than the control specimens. CNFs in the microfine hybrid mortar often increased flexural strengths, suggesting that the hybrid microfine cement mortar did not have clumping issues and had a more stable dispersion of CNFs. Flexure prisms with both CNFs and MCMFs suggest that their addition to microfine cement mortar can increase the flexural strength by up to 221%, but workability issues and air voids cause uncertainty in any one particular specimen.

Compressive strength cylinders had several interesting aspects. At a w/c ratio of 0.6, the addition of CNFs does not significantly change the compressive strength, but adding

MCMFs does significantly increase the compressive strength by up to 56%; however, dropping the w/c ratio from 0.5 to 0.4 can increase the compressive strength by up to 45%. At a w/c ratio of 0.5, the addition of 1wt% CNFs does not significantly change the compressive strength, but the addition of 2wt% CNFs with or without MCMFs does increase the compressive strength. At a w/c ratio of 0.5, F0.5-2.2 and F0.5-3.3 (the strongest mixtures) are significantly stronger compared to mixtures without MCMFs and F0.5-1.1, but the two mixtures are not significantly different from each other. The mixture OPC0.4-0.0 is not significantly different from the F0.5-0.0 and F0.6-0.0 mixtures, but the F0.4-0.0 mixture is significantly stronger than the OPC0.4-0.0.

Izod impact strength tests show that there is no significant effect of CNFs and MCMFs on fracture energy. Consolidation could have a much larger effect on fracture energy than CNFs or MCMFs.

Further testing is required for definite trends, but the data presented for CMOD suggest that:

- Lowering the w/c ratio increases the efficacy of both CNFs and MCMFs.
- The addition of CNFs up to 2wt% increased peak load and ultimate CMOD, but furtherance to 3wt% CNFs did not provide much more benefit.
- The mixture with the highest peak load was F0.6-5.5, but the mixture with the highest toughness was F0.4-2.2. These two data imply that high concentrations of CNFs and/or MCMFs in combination with a low w/c ratio could provide

compounded benefits that are better than either technique alone. Current mixing procedures do not permit a low w/c ratio mixture with 5wt% CNFs, so a new mixing method for needs development to test this theory.

- CMOD tests show that adding more than 1wt% CNF (without MCMFs) increases flexural toughness. Adding CNFs while lowering the w/c ratio increases toughness in a superposition manner. Adding MCMFs increased the toughness of all mixtures, though adding more MCMFs did not necessarily increase the toughness in incremental amounts.

5. RESTRAINED RING DRYING SHRINKAGE TESTS

The foremost property that was explored in this research is the resistance of cement hybrid mortar against cracking due to restrained drying shrinkage. A simple, passive experiment for characterizing cracking time and development is a restrained ring test [73-78]. In this test, a steel ring is surrounded with concrete or, in this report, mortar. After the mortar has cured for a specific amount of time, the temporary mold on the outermost edge of the mortar is then removed, and the outer radial face of the mortar is exposed to a dry environment to induce shrinkage. The top and bottom faces of the ring are sealed to prevent drying. The mortar develops a free shrinkage gradient in the radial direction as it dries, but the steel ring partially resists the free deformation, inducing tension in the mortar. The tensile stresses associated with self-restraint from the radial shrinkage gradient and the restraint from the steel ring increase with time as shrinkage increases and, eventually, the mortar cracks since the steel ring can sustain much greater stresses than the mortar [82]. The circumferential strain in the steel ring is recorded by mounting strain gages to the inner radial surface of the steel, and a crack in the mortar is evident in a sudden, drastic reduction in the strain in the steel.

5.1 Experimental Setup

The restrained ring test geometry used in this research was a modified version of that described in ASTM C1581, with the setup shown in Figure 65. The only dimension that is not to scale of the ASTM C1581 ring is that of the thickness of the steel. The thickness of the steel required was back-calculated from the expected strengths of the material and Lame's solution for the stress in the outer (mortar) ring as shown in Equation 5 [73]. The steel ring had an outer diameter of 114 ± 0.5 mm, a thickness of 3.0 ± 0.1 mm, and a height of 57 ± 1 mm. The removable, outer radial mold had an inner diameter of 152 mm and a height of 57 ± 1 mm. Table 8 compares dimensions between ASTM C1581 and this experimental setup. The waterproof seal applied to the top of the ring was aluminum-backed tape, which has shown good performance as a drying barrier [91, 92]. The inner base of the steel ring and the outer base of the removable mold were sealed with caulk to prevent leaks and to keep the rings in place during vibration.

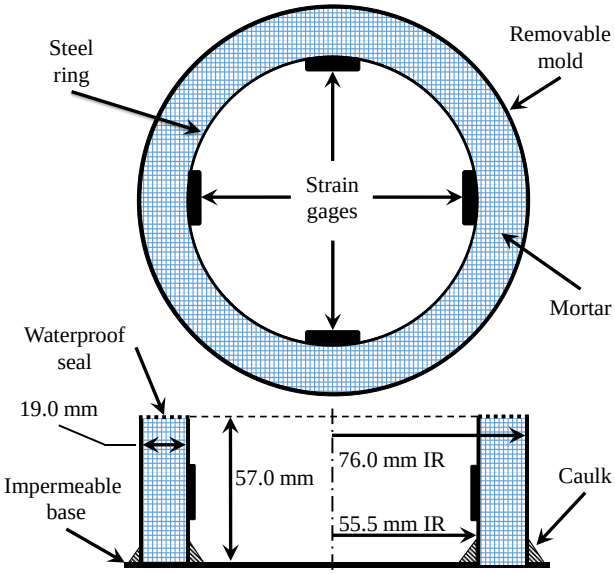

Figure 65: Ring test setup. 'IR' is an abbreviation for 'inner radius'. A non-stick sheet is placed between the mortar and the impermeable base.

Table 8: Comparison of ASTM C1581 and experimental setup.

Dimension	**ASTM C1581**	**Experimental**
Steel thickness	13 ± 1 mm	3.0 ± 0.1 mm
IR Steel	158.5 ± 1.5 mm	55.5 ± 0.25 mm
IR outer mold	202.5 ± 1.5 mm	76.0* mm
Height	150 ± 6 mm	57 ± 1 mm
Degree of Restraint γ_r	0.146	0.100
*No error given by the manufacturer		

The degree of restraint in Table 8 is calculated using Equation 5 and Equation 6. The numerator of Equation 6 is calculated using actual ring geometry values in Equation 5; the denominator is calculated in a similar fashion but with $R_{IS} = 0$ to simulate maximum restraint. The material for both rings is assumed to be the same, hence the Young's

moduli of the expressions cancel and the degree of restraint is wholly based on ring geometry. The strain in the steel is inconsequential in this calculation since that variable is measured in real time using strain gages.

Each ring was equipped with four 6.2 mm, 350 Ohm strain gages patterned in a full Wheatstone bridge with two Poisson gages and two linear gages. This pattern automatically compensates for temperature and lead-wire resistance, and it largely compensates for manufacturing tolerances or alignment error in mounting the strain gages. The strain was recorded at 5 minute intervals using a D4 Data Acquisition Unit from Vishay Precision Group.

As our interest was focused on early-age cracking resistance, ring tests were performed on young specimens. The mortar cured for 24 ± 0.5 hours after casting with its sides sealed and the top exposed to 98% relative humidity (RH) and 23°C in a Cincinnati Sub-Zero precision climate controlled chamber. After the curing period, the outer mold was removed, the top was sealed with aluminum-backed tape, and the specimen was subjected to a constant 50% RH and 23°C in the same climate chamber.

After calibration trials, only two specimens were made for each OPC mixture since all mixtures performed in a similar fashion without any significant changes. Excellent repeatability of tests for a specific mixture suggested that further tests were not necessary. Four specimens were made for microfine cement mixtures with CNFs up to

3wt%, and two specimens were made for microfine cement mixtures above 3wt% CNFs and for microfine cement mixtures with CNFs and other fibers.

Table 9 shows all of the restrained ring shrinkage test mixtures performed in this research.

Table 9: Fiber concentrations in restrained ring tests.

Cement Type	W/C Ratio	CNFs (wt%)	MCMFs (wt%)	Other Fiber Type	Other Fiber (wt%)	HRWR (wt%)
OPC	0.4	0	0	--	--	0
OPC	0.5	0	0	--	--	0
OPC	0.5	1	0	--	--	0.1
OPC	0.5	2	0	--	--	0.7
OPC	0.5	3	0	--	--	1.3
MF	0.5	0	0	--	--	0.9
MF	0.5	1	0	--	--	1.2
MF	0.5	2	0	--	--	1.5
MF	0.5	3	0	--	--	1.8
MF	0.6	5	0	--	--	4.0
MF	0.7	5	0	--	--	1.0
MF	0.5	2	2	--	--	1.2
MF	0.6	5	5	--	--	4.0
MF	0.5	0	2	--	--	0.9
MF	0.4	0	0			1.5
MF	0.4	2	0	--	--	4.0
MF	0.4	2	2	--	--	4.0
MF	0.6	5	5	CCMF	2	4.0
MF	0.6	5	5	PVA	3	4.0
MF	0.6	5	0	PVA	2	4.0

5.2 Ordinary Portland Cement

This section discusses the effects of adding CNFs and MCMFs to OPC on restrained drying shrinkage resistance.

5.2.1 OPC with CNFs

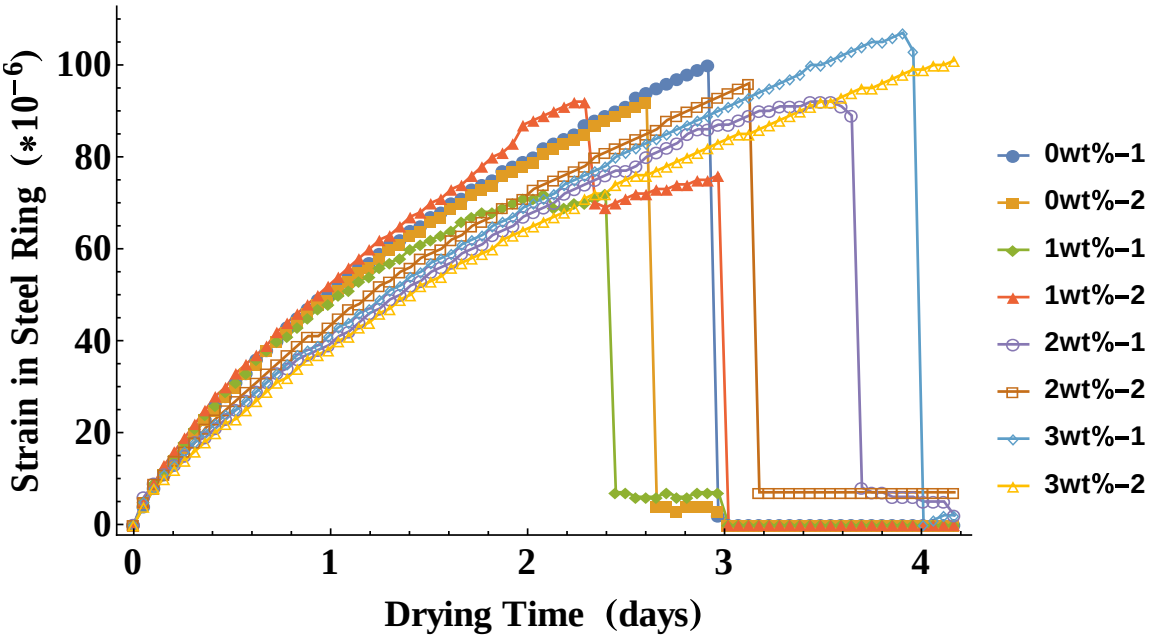

Figure 66: Circumferential strain of inner surface of steel ring vs time (days) for OPC mortars with 0wt% CNFs, 1wt% CNFs, 2wt% CNFs, and 3wt% CNFs. Sample 1 and Sample 2 for a given mixture are designated as '-1' and '-2'. No significant changes were seen between mixtures.

Ring test results for OPC mortar mixtures are shown in Figure 66. The OPC mortar rings exhibited the same general trend for all concentrations of CNFs with minor differences in cracking strain, cracking time, and slight variability in the shape of the curves suggesting that the CNFs did not significantly affect the response. The mixtures with 1wt% CNFs performed worst in terms of cracking time and peak strain, and the poor performance was attributed to the tendency of the mixture to flash set during placement as discussed in Section 4.1. The mixtures with 2wt% CNFs cracked at peak strain similar to the control mixtures but at a slightly later time. The time delay in cracking is theorized to be due to the lower stiffness of the material; elastic modulus data is presented in Section 4.3. The mixtures with 3wt% CNFs reached a slightly higher peak strain as well as delayed cracking time from the control. The average peak strain and time of cracking are shown in Table 10.

Table 10: Summary of OPC CNF restrained ring tests.

		Control	1wt% CNFs	2wt% CNFs	3wt% CNFs
OPC	Average peak strain (microstrain)	97.0	73.5	94.0	102.5
	Average time of cracking (days)	2.80	2.70	3.41	4.08

The time delay in cracking is again theorized to be primarily caused by the lower stiffness and reduced shrinkage (due to pore coarsening) of the material due to the CNFs and is not attributable to increased ductility. The culmination of these results suggests

that the addition of high concentrations of CNFs to OPC mortar does not significantly improve drying shrinkage crack resistance but does open more avenues for detrimental effects such as flash set, mixing difficulties, and possibly higher transport coefficients due to the pore coarsening. An example of a cracked OPC mortar ring with 0.1wt% CNFs is shown in Figure 67; all OPC mortar rings had cracks similar to the one shown in Figure 67.

Figure 67: OPC restrained mortar ring with 0.1wt% CNFs and a macrocrack.

One interesting aspect of the hybrid cements, both OPC and microfine cement, is the color of the final composite. Figure 68 shows the color difference between a plain OPC mortar and a hybrid 2wt% CNFs mortar. The CNFs caused the mortar, both OPC and microfine cement, to become black. Other fibers types, including high concentrations of MCMFs, did not change the color of the composite.

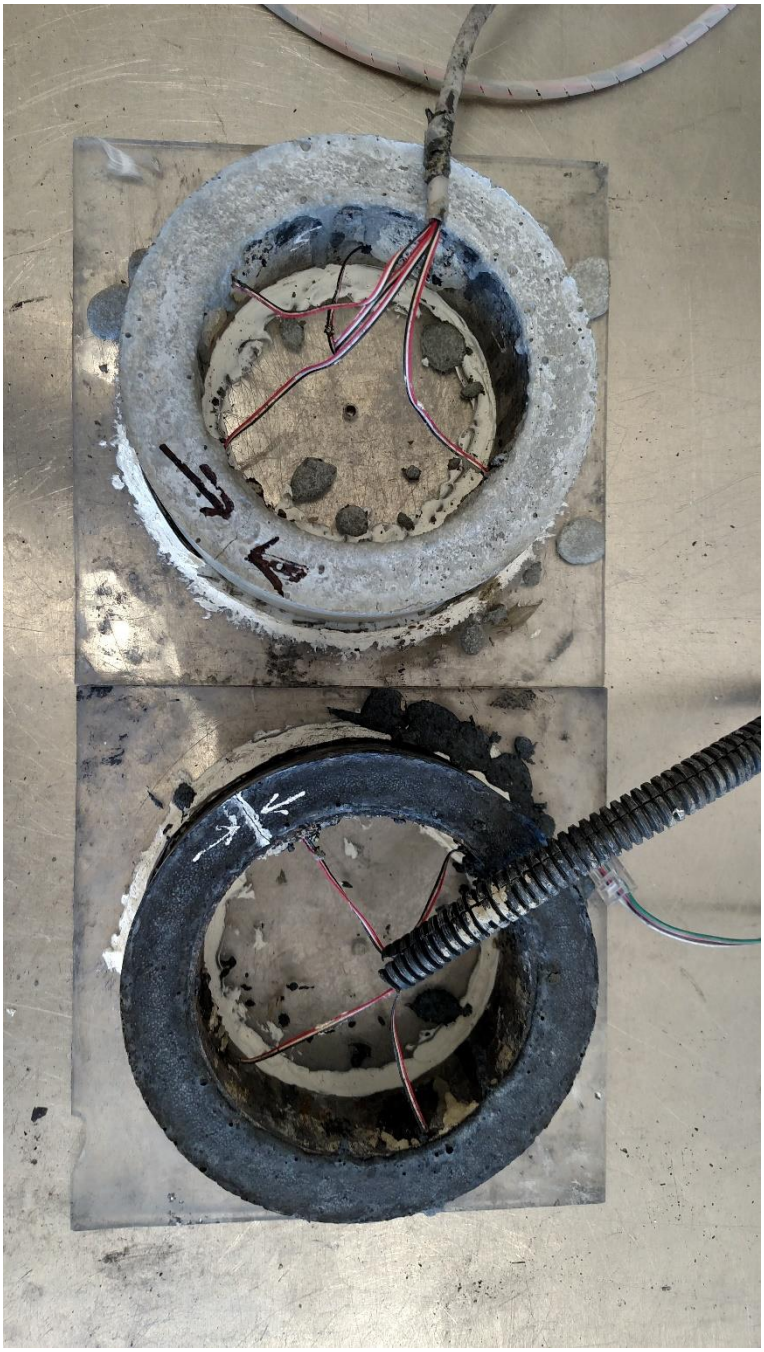

Figure 68: Plain OPC mortar ring (top) and 2wt% CNFs hybrid microfine cement mortar ring (bottom) showing the color difference.

5.2.2 OPC with MCMFs

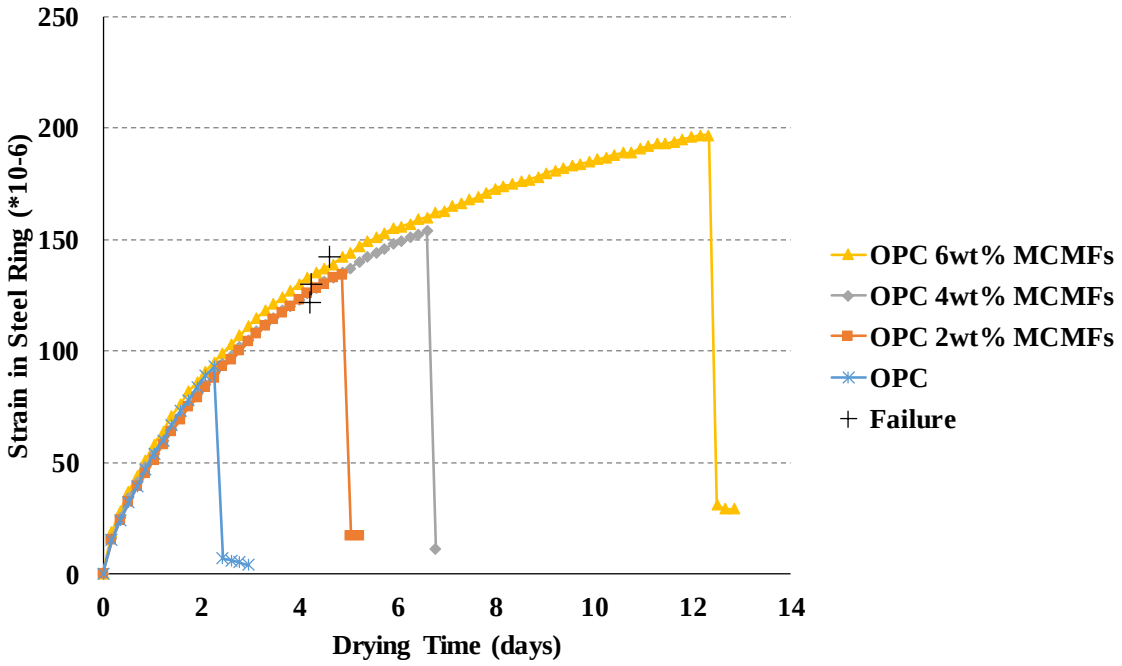

Figure 69: Circumferential strain of inner surface of steel ring vs time (days) for OPC mortars with pre-mixed MCMFs. Increasing MCMF concentration delayed the formation of a macrocrack. However, the markers labeled 'Failure' are time and strain of failure for specimens with 2wt%, 4wt%, and 6wt% MCMFs, suggesting that MCMFs do not guarantee improved performance at these concentrations.

Little testing has been completed for OPC with MCMFs that are pre-mixed with cement by rotary tumbling for 12 hours as described in Section 4.1, but some restrained ring shrinkage testing data is shown in Figure 69. Two specimens of OPC with 2wt%, 4wt%, and 6wt% MCMFs were made for each mixture with a w/c ratio of 0.4 and sand/cement ratio of 1.75. No HRWR was required; there was no obvious change in workability with

the addition of 6wt% MCMFs to the OPC mortar at a w/c ratio of 0.4. Figure 69 shows that adding 2wt%, 4wt%, and 6wt% MCMFs extended the cracking time from 2.32 days to 4.87 days, 6.69 days, and 12.48 days, respectively. The increase factors are 2.1, 2.9, and 5.4 for 2wt%, 4wt%, and 6wt% MCMFs, respectively. Also shown in Figure 69 are markers labeled ‘Failure’; these markers show that the cracking times and strain for the other 2wt%, 4wt%, and 6wt% specimens are roughly equivalent to the 2wt% MCMFs specimen. The fact that half of the specimens with MCMFs cracked at approximately the same time and microstrain suggests that the composite has consequential flaws that can negate the effect of high concentrations of fibers, but the nature of those flaws is not yet well understood.

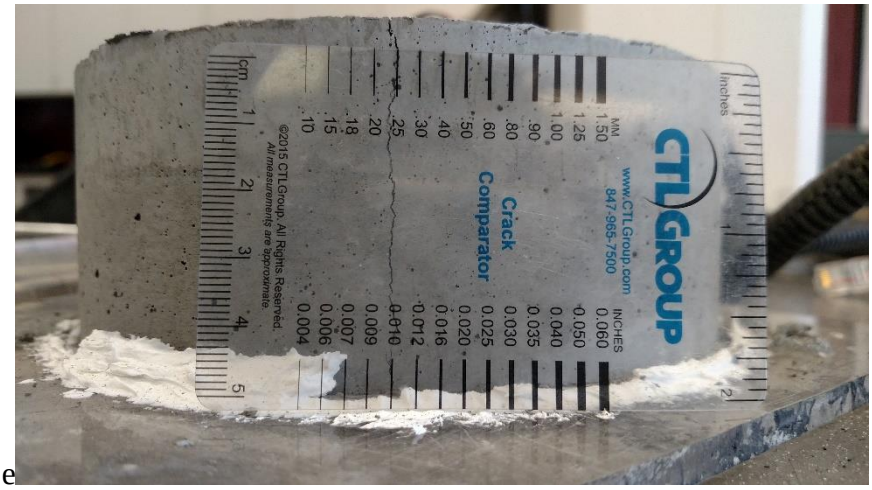

Figure 70: OPC restrained mortar ring with 2wt% MCMFs with ~0.25mm wide macrocrack. CTLGroup has no affiliation with this research.

An example of the cracked restrained mortar ring is shown in Figure 70. One significant point to be made about OPC mortar with MCMFs is the brittle nature of the composite. PVA and steel fibers are often used in PCBMs because of the significant post-crack ductility added to the composite. MCMFs do not add significant post-crack ductility at concentrations used in this research; the restrained rings cracked and no post-crack behavior was seen that was different from an unreinforced mortar. This behavior is most likely because carbon fibers are more brittle than PVA and steel fibers and do not strain/elongate as much as PVA and steel before fracture.

5.2.3 Conclusions

Restrained drying shrinkage ring tests revealed that the incorporation of CNFs into OPC mortar proved detrimental to the material at worst and marginally beneficial to the material at best. These effects are attributed to 1) the limit of achievable dispersion of CNFs through the matrix due to the size disparity between the CNFs and the OPC grains – i.e., the geometric clustering effect – and 2) to the apparent segregation of CNFs out of dispersion during vibration, which may also be induced by the size disparity of the cement grains and the CNFs. The data presented herein indicates that the effects of adding high concentrations CNFs to OPC mortars are inconsistent and vary from marginally beneficial to detrimental. Restrained drying shrinkage ring tests also revealed that the incorporation of MCMFs into OPC mortar have the potential to delay drying shrinkage cracking time by a factor of up to 5.4 at 6wt% MCMFs, but further research is needed to solidify the results and to determine the cause of flaws in the material.

5.3 Microfine Cement

5.3.1 Microfine Cement with CNFs

5.3.1.1 Restrained Ring Drying Shrinkage Test Results

Ring tests conducted with microfine cement mortar and 0wt% CNFs, 1wt% CNFs, 2wt% CNFS, and 3wt% CNFs revealed significant differences among the mixtures including peak strain reached, time until cracking, and general strain vs. time graph shape, as shown in Figure 71. In Figure 71, the term ‘Alt’ is used to show the strain in the steel ring at time of cracking for different specimens, and only one full example of strain vs drying time graph is shown per %wt CNFs.

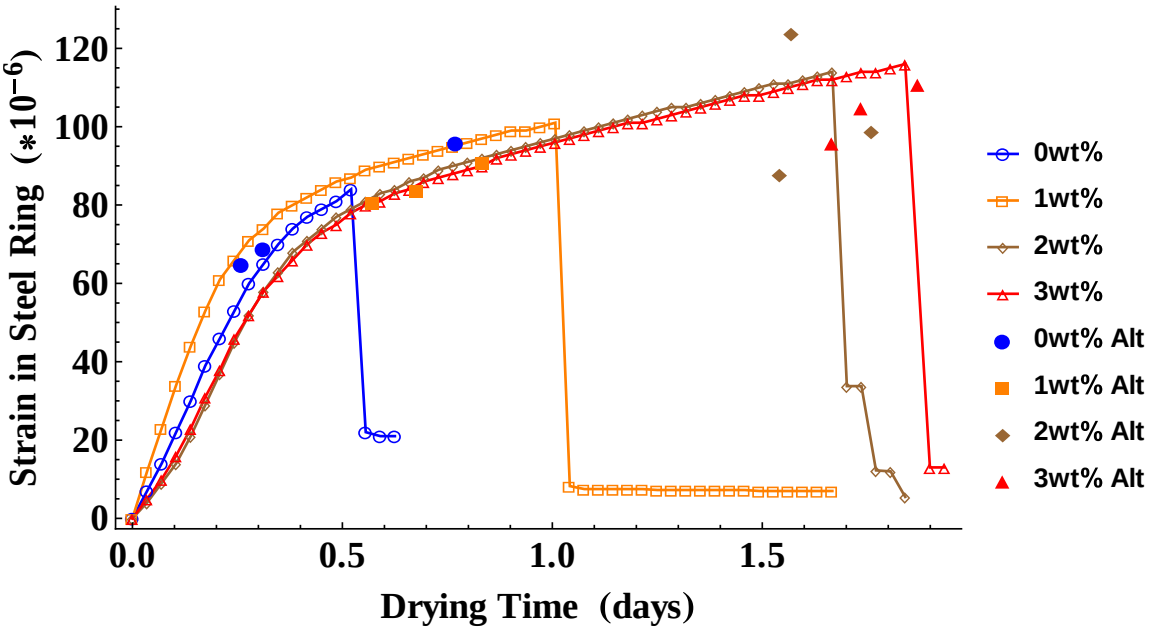

Figure 71: Typical circumferential strain of inner surface of steel ring vs time (days) for microfine cement mortars with 0wt% CNFs, 1wt% CNFs, 2wt% CNFs, and 3wt% CNFs. The term 'Alt' is applied to points that show the failure strain and time of cracking for other specimens. A 'knee' formed in the graph resembling a switch from an 'undamaged' material to a 'damaged' material.

Average peak strain and time of cracking for OPC and microfine cement mixtures are shown in Table 11. The control microfine cement mortar formed a macrocrack much sooner than the OPC mortar. In addition, the control microfine cement mortar only reached an average of 79 microstrain whereas the OPC mortar rings reached an average of 97 microstrain. The cause of the early macrocrack at a lower strain in the microfine cement mortar is twofold: 1) the microfine cement mortar was much stiffer than the OPC mortar due to faster early-age cement hydration, and 2) the microfine cement mortar had increased drying shrinkage compared to the OPC mortar as presented in Section 4.2;

both causes contribute to higher circumferential stresses at the outer radial surface of the mortar.

Table 11: Summary of OPC and microfine cement CNF restrained ring tests.

		Control	1wt% CNFs	2wt% CNFs	3wt% CNFs
OPC	Average peak strain (microstrain)	97.0	73.5	94.0	102.5
	Average time of cracking (days)	2.80	2.70	3.41	4.08
Microfine	Average peak strain (microstrain)	79.0	89.5	106.2	107.2
	Average time of cracking (days)	0.46	0.78	1.63	1.79

A prominent feature of Figure 71 is the difference in the general shape of the curves when compared to Figure 66. The control microfine cement mortar is roughly linear until ~60% of its peak strain, at which point its slope begins to drop. The mixtures with 1wt% CNFs reach an average of 90 microstrain before breaking while also reaching further into what will henceforth be called the 'knee' of the graph: a sudden shift of slope in strain vs. time. The remaining two mixtures—2wt% CNFs and 3wt% CNFs—passed well beyond the knee and sustained much higher strains than the control mixture. The OPC mortar graphs in Figure 66 show a gradual change in slope due to creep, changes in drying coefficients, etc.; the rather sudden change in slope of the measured strains observed in Figure 71 is, to the authors' knowledge, unique amongst ring tests to the hybrid microfine cement mortars tested in this research. This curve shape suggests

that the increased dispersion of CNFs in the microfine cement allowed more microcrack bridging by CNFs, delaying the formation of a macrocrack. Initially, all mixtures behaved the same in that the curves would start to bend at ~60% of peak microstrain; this bend is due to the initiation of microcracking in the cement matrix. Mixtures with and without CNFs had the same bend occur at approximately the same time and microstrain. However, curves of mixtures with CNFs would pass through the bend and sustain higher microstrains and delay the formation of a macrocrack. In theory, all mixtures behave the same before the bend in the curves since the undamaged cement matrix is the dominant material prior to the initiation of microcracking. As microcracks form in the cement matrix and before the formation of a macrocrack, the curves begin to bend. The microcracks quickly form a macrocrack in mixtures without CNFs, but CNFs bridge across the microcracks and sustain the composite material in mixtures with CNFs. Cracking times were delayed in hybrid microfine mortars by factors of 1.7, 3.5, and 3.9 for 1wt% CNFs, 2wt% CNFs, and 3wt% CNFs, respectively. Peak cracking strain was increased in hybrid microfine mortars by factors of 1.1, 1.3, and 1.4 for 1wt% CNFs, 2wt% CNFs, and 3wt% CNFs, respectively. Thus, the use of microfine cement significantly enhanced the efficacy of CNFs (in comparison to OPC) in extending the cracking time under restrained drying conditions.

An example of a cracked hybrid microfine cement mortar ring is shown in Figure 72 wherein the crack is highlighted in white paint. The hybrid microfine cement mortar

rings all had macrocracks similar to the one shown, but no other cracks were visible before the formation of the macrocrack.

Figure 72: Hybrid microfine cement mortar ring with 2wt% CNFs with a macrocrack (highlighted in white paint).

5.3.1.2 Further Data Analysis

Two primary possibilities are considered herein to explain the existence of the knee shown in Figure 71, and subsequently, to infer the delayed cracking time induced by the inclusion of CNFs in the microfine cement mortar. First, it is possible that there is a time-dependent property or behavior of the microfine cement mortar without CNFs that exhibits a similar, characteristic knee that then induces the presence of the knee in the ring strains. If the knee present in Figure 71 were a product of a rapid change in drying shrinkage rate, then a similar trend would be present in the drying shrinkage data; since

the maximum drying path distance is similar between the ring test (19mm) and the unrestrained drying shrinkage prism test (13mm), the drying shrinkage kinetics should likewise be similar. The drying shrinkage data for OPC mortar and microfine cement mortar without CNFs are shown in Figure 73. Each curve is fitted with a simple fit equation (of the form $Loss = C_1 t^{C_2}$ where C_1 and C_2 are fit parameters and t is time in days) to show that the two materials behave in a similar fashion but at different rates. The fit functions have R^2=0.99 and R^2=0.97 for OPC and microfine, respectively. For OPC mortar, C_1 = -112, C_2 = 0.882. For microfine cement mortar, C_1 = -317, C_2 = 0.386.

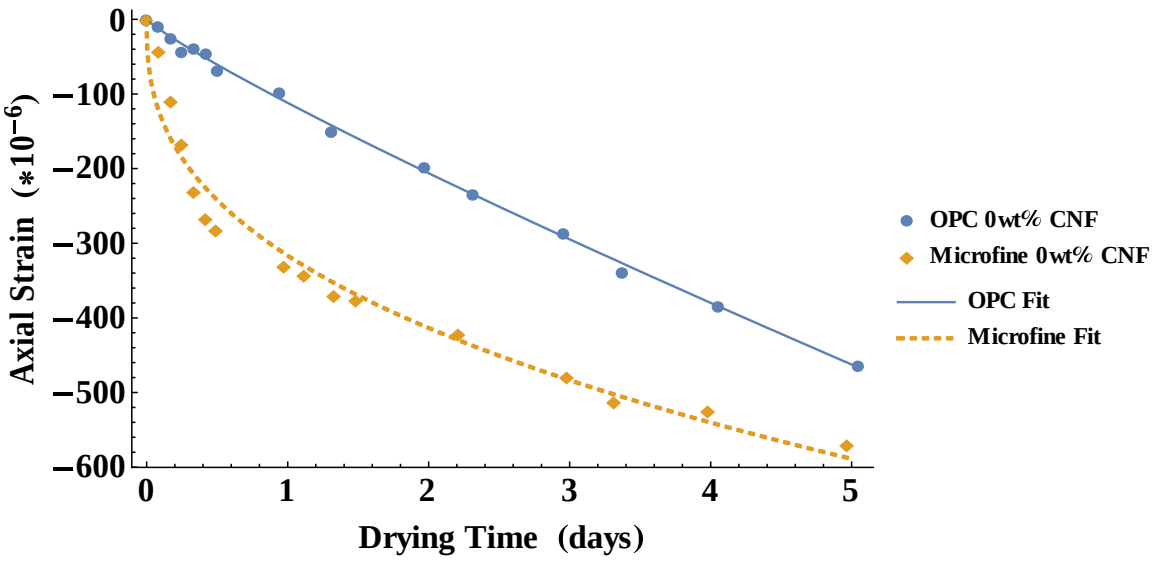

Figure 73: Axial free strain curves of OPC and microfine cement control mortars exposed to drying. Both data sets were fit with the same fit equation with different coefficients, suggesting that the drying behavior is the same for OPC and microfine cement but with different rates.

In Figure 73, the curves with OPC and microfine cement mortars have the same basic shape with different fit coefficients, yet the characteristic knee in the ring test data is only seen in the microfine mixtures with CNFs. This finding debunks the hypothesis that the knee in the ring test data is a material property of the microfine cement mortar. The second explanation for the observed ring test data for the microfine cements is that the sudden shift in slope at the knee is due to internal microcracking. In the control mixtures, the mortar begins to crack at the nanometer and micrometer scale, and the microcracks join and form a failure-inducing macrocrack. However, CNFs that are thoroughly dispersed throughout the microfine cement mortars bridge the cracks and hold the material together as shown in Figure 74 and Figure 75.

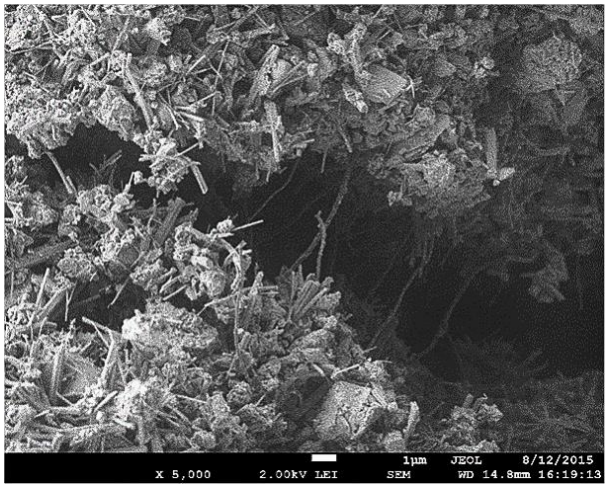

Figure 74: SEM image of hydrated microfine cement mortar showing CNFs bridging a microcrack.

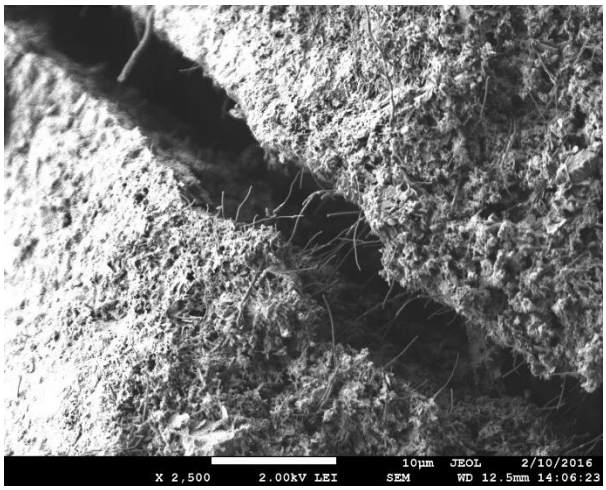

Figure 75: Another SEM image of hydrated microfine cement mortar showing CNFs bridging a microcrack.

5.3.1.3 Conclusions

The sudden shift in slopes in the strain vs. time curves in microfine mortar mixtures with CNFs in Figure 71 are thus theorized to be the result softening caused by the switch from an ‘undamaged’ material to a ‘damaged’ material. The strain behavior in the time period prior to the knee in each mixture was dominated by the properties of the mortar matrix of sand and hydrated cement since all microfine mortar mixtures behaved in a similar manner, though there was some difference in slope due to different stiffness, different drying rates, and possible creep or viscoelastic effects. During the knee, it is proposed that each mixture began developing microcracks that damaged the integrity of the mortar matrix, a theory reinforced by Figure 71 wherein the knee began forming at approximately the same strain for all mixtures regardless of maximum strain reached. This knee is independent of the presence of CNFs and is entirely dependent on the

material properties of the cement matrix in the mortar. Eventually, the proliferation of microcracks in the mortar matrix reached a damage threshold and subsequently resulted in the formation of a macrocrack in the control microfine cement mortar mixtures. The microfine cement hybrid mortar mixtures, however, were able to sustain the damage due to crack bridging by the well-dispersed CNFs, and the existing microcracks could not propagate to form a macrocrack until more damage was induced. This formation of microcracks bridged by CNFs changed the apparent macro-mechanical properties of the mortar during the knee of the graph, e.g. apparent stiffness and drying shrinkage rates, resulting in the observed sudden shift in slopes in the strain vs. time curves. The maximum strain reached and time of cracking, and therefore the amount of damage required to induce a macrocrack, in the microfine mortar mixtures had significant gains between the control mixture, 1wt% CNFs, and 2wt% CNFs, but the furtherance from 2wt% CNFs to 3wt% CNFs exhibited a diminishing return. Cracking times, measured from the initiation of drying, were delayed by factors of 2.0, 5.5, and 5.7 for 1wt% CNFs, 2wt% CNFs, and 3wt% CNFs, respectively.

5.3.2 Microfine Cement with CNFs and/or MCMFs

The previous section describes the success in attaining crack bridging by CNFs in microfine cement mortar. It was then theorized that the cracking resistance of the hybrid cement could be enhanced by incorporating microfibers in addition to CNFs. The general theory of multi-scale fiber reinforcement without the formation of a macrocrack is based on the idea that crack bridging by CNFs would cause an apparent macrostrain.

In essence, microcracks form in the cement matrix but are held together by the CNFs and do not propagate together; the formation of thousands of microcracks can manifest in the composite as an apparent macrostrain. It is well known that microfibers enhance mechanical properties in PCBMs by crack bridging, but the cracks that form in FRC are easily seen with the unaided eye; this is true because fibers (both CNFs and microfibers) need the material to strain before adding significant properties. CNFs add strength and cracking resistance much sooner than microfibers due to their size; CNFs are ~100x smaller than microfibers, and therefore they require less strain in the cement matrix to become effective. Since the hybrid microfine cement mortar has increased cracking resistance, it is possible that the apparent macrostrain given by CNF crack bridging may be enough to engage microfibers without the formation of a macrocrack.

Preliminary restrained rig drying shrinkage testing was conducted with PVA microfibers in the hybrid microfine cement mortars; the composite showed the same behavior as in Figure 71 with some post-crack behavior, but the macrocrack still formed before the PVA microfibers had any effect. Upon inspection of the cracked composite, it was found that the PVA fibers were not thoroughly distributed as shown in Figure 76. Since PVA fibers are too large to be included in the sonication/distillation technique used for CNF dispersion, a different type of fiber was used for the multi-scale fiber reinforcement testing.

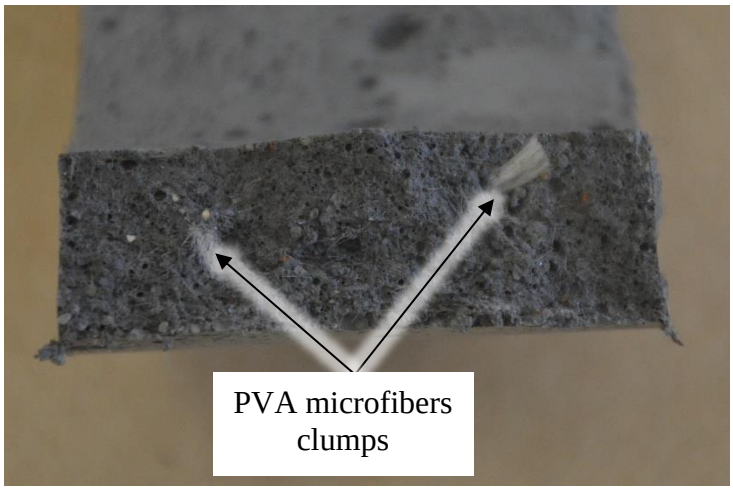

Figure 76: PVA microfiber clumps in the cracked surface of a mortar ring.

As shown in Table 4, MCMFs are ~5x smaller in diameter than PVA microfibers, but they are also ~80x shorter. While PVA microfibers resemble clumps of hair, MCMFs are so small that they are seen as a black powder. The MCMFs were added to the hybrid CNF microfine cement during sonication, and the addition of MCMFs did not have any significant effect on the workability of the mixtures.

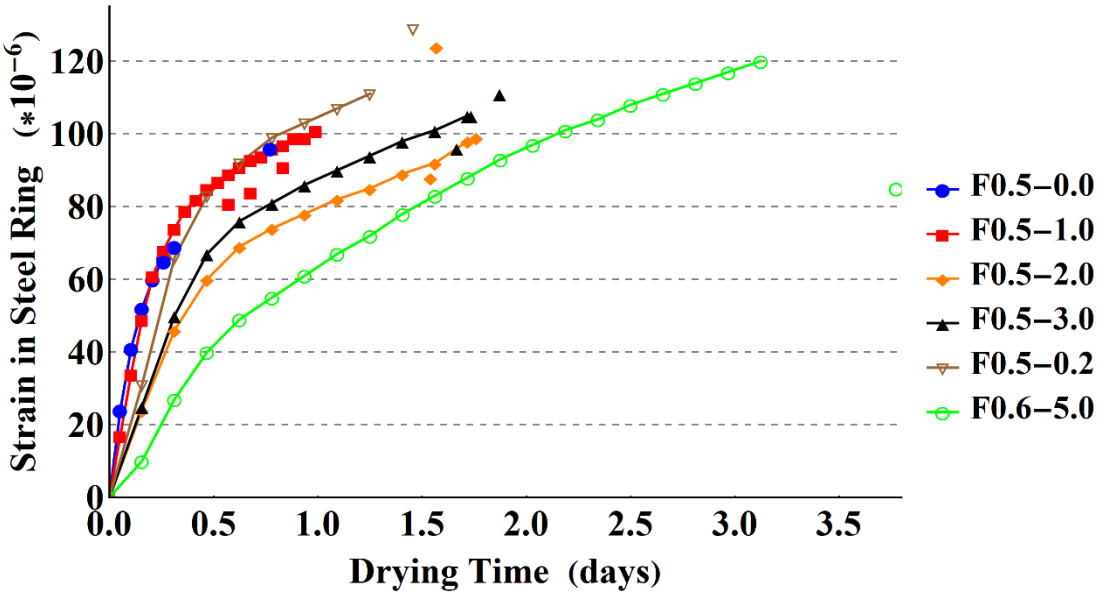

Figure 77: Control tests for microfine cement mortar with only CNFs or only MCMFs. The fiber type, fiber concentration, and w/c ratio are shown in the legend.

Before showing the results of adding both CNFs and MCMFs into a microfine cement mortar, the results of a few other control tests are shown in Figure 77. Plain microfine cement mortar, 1wt% CNFs, 2wt% CNFs, and 3wt% CNFs have been seen in a prior section. 5wt% CNFs microfine cement mortar required a w/c ratio of 0.6 to be mixed due to the extremely high water demand, and no amount of superplasticizer in a w/c ratio of 0.5 would make the mixture liquid-like. The knee in the 5wt% CNFs mixture occurs at a much lower strain than the 0.5 w/c ratio mixtures due to an inherently weaker cement matrix, but the high concentration of CNFs enables the composite material to delay the formation of a macrocrack and sustain a high microstrain than its 0.5 w/c ratio CNF companions. In addition to CNF hybrid composites, a mixture was made with only MCMFs in microfine cement mortar (dispersed using the same alcohol/sonication

technique). The material performed in a similar manner to mixtures with CNFs in that the curve had a knee; while this does seem promising, further work was not completed on microfine cement mortars with MCMFs because the results in Figure 77 are overshadowed by the combination of CNFs and MCMFs.

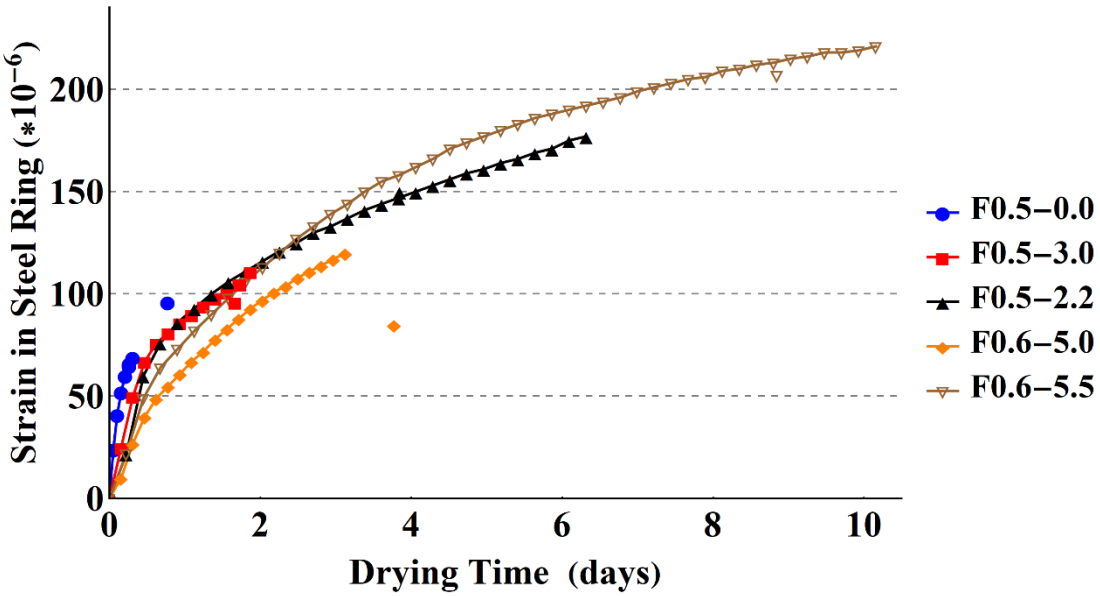

Figure 78: F0.5-2.2 and F0.6-5.5 compared to previous results.

The first test run with the combination of both CNFs and MCMFs in microfine cement mortar was 2wt% CNFs and 2wt% MCMFs as shown in Figure 78. The 2wt% CNFs 2wt% MCMFs mixture initially behaved the same as the 2wt% CNFs mixture, but the mixture remained intact (no macrocrack) for 6.48 days after exposure to 50% RH and reached 178 microstrain in the steel. The time delay in cracking of the 2wt% CNFs

2wt% MCMFs mixture is a factor of 14.1, 3.6, and 2.1 compared to plain microfine cement mortar, 3wt% CNFs, and 5wt% CNFs, respectively. The combination of CNFs with MCMFs in the material provided benefits that were greater than the sum of the individual benefits from CNFs or MCMFs alone. Another test using 5wt% CNFs 5wt% MCMFs proved even greater benefits with a peak microstrain of 222 and a macrocrack formation delay of 10.2 days (time delay factor of 22.2).

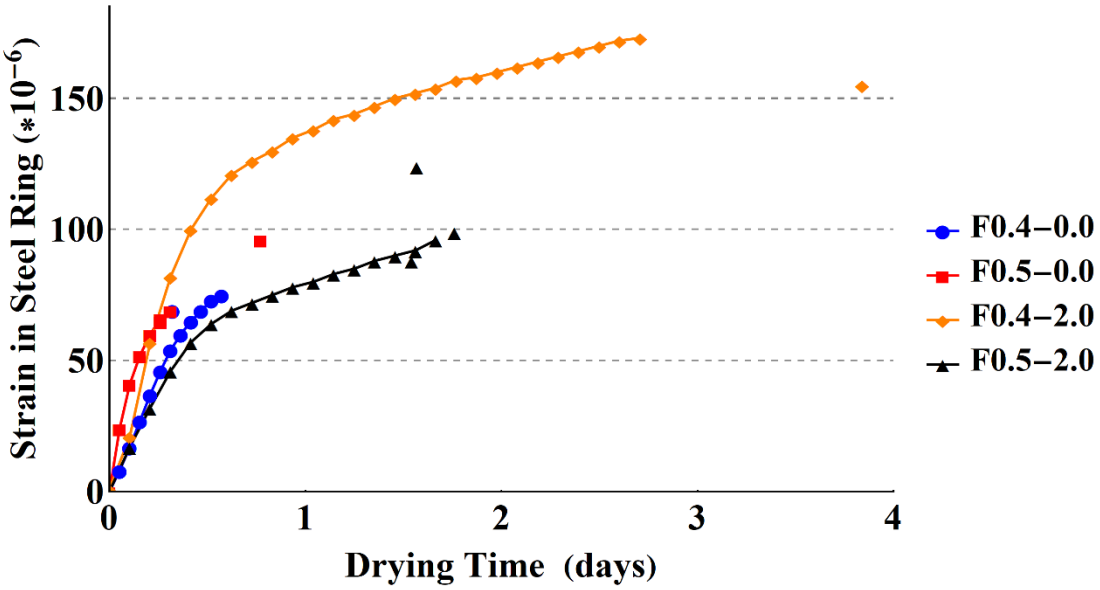

Figure 79: Restrained ring drying shrinkage tests with 0.4 w/c ratio

The next step in determining the effects of multi-scale fiber reinforcement on hybrid microfine cement mortars was to drop the w/c ratio to 0.4. A major setback in attempting to drop the w/c ratio is workability issues. The high water demand of the hybrid

microfine cement mortar required high doses of HRWR, and dropping the w/c ratio while incorporating CNFs severely inhibited workability. Figure 79 shows the effects of dropping the w/c ratio from 0.5 to 0.4 with plain microfine cement mortar and a 2wt% CNFs mixture. The plain mortar with a 0.4 w/c ratio had similar behavior compared to the plain mortar with a 0.5 w/c ratio. However, adding 2wt% CNFs to the 0.4 w/c ratio microfine cement mortar improved the cracking resistance both in terms of ultimate microstrain reached and time until cracking.

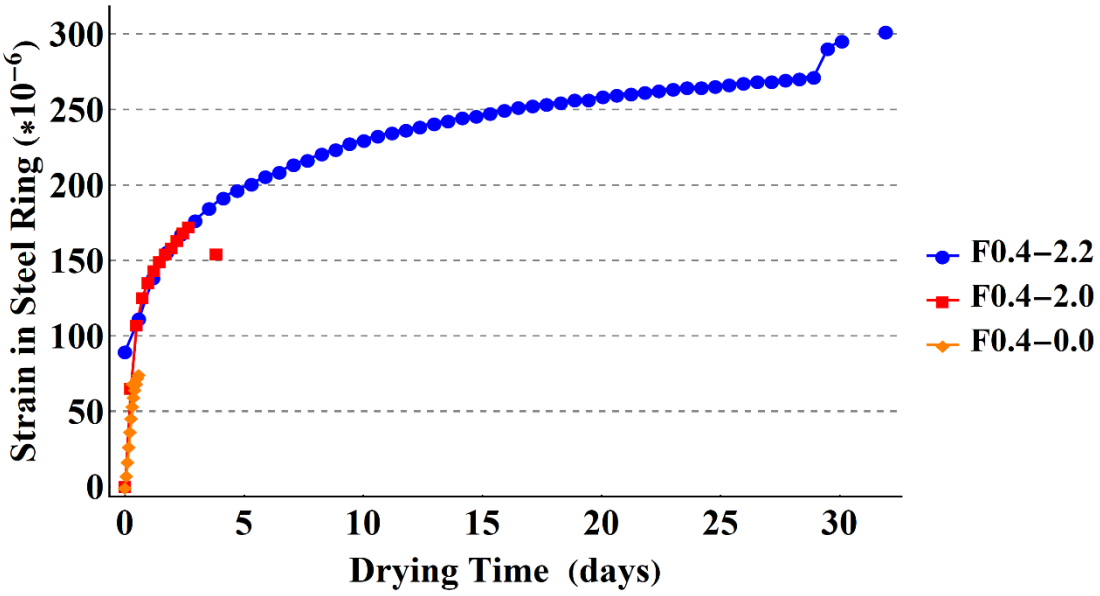

Figure 80: Restrained ring drying shrinkage tests with 0.4 w/c ratio. The RH was dropped to 35% at ~29 days to break the specimens.

An experimental oddity occurred in the F0.4-2.2: the microstrain in the steel remained at 0 until ~0.8 days. The shape of the resulting curve resembled the behavior of the control

mixture (F0.4-2.0) but at a higher microstrain; therefore, F0.4-2.2 was shifted up by 90 microstrain in post-processing to match data with the control mixture as shown in Figure 80. After the specimen was subjected to 50% RH for 29 days with no formation of a macrocrack, the RH was dropped to 35% to break the specimen. The specimen formed a macrocrack at 31.2 days and 301 microstrain in the steel, a time delay factor of 50.5 and a microstrain increase factor of 3.91.

5.3.3 Microfine Cement with CNFs, MCMFs, and Other Fibers

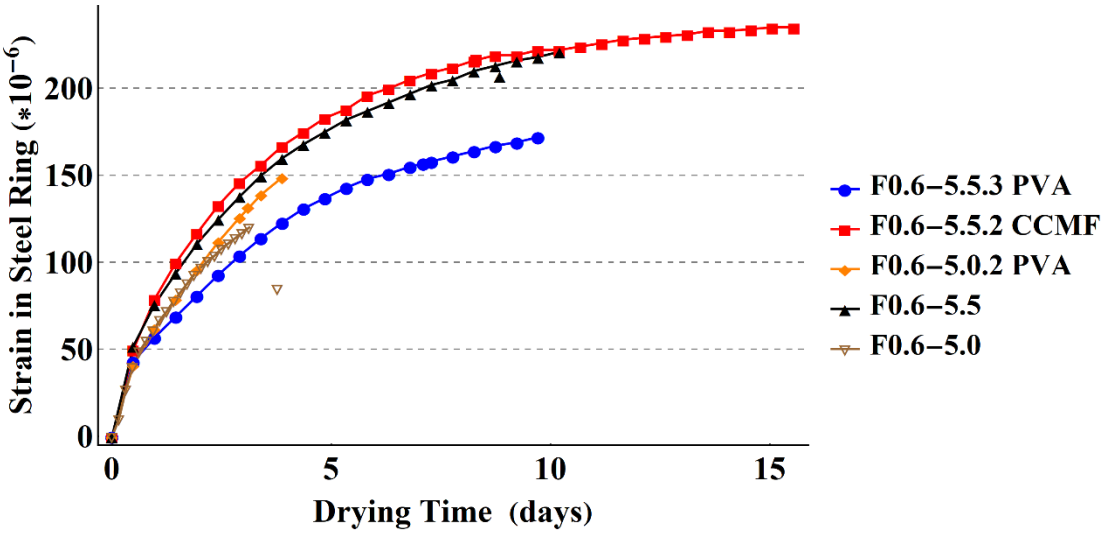

Figure 81: Restrained ring drying shrinkage tests with larger microfibers.

Hybrid microfine cement mortars with and without MCMFs were subjected to restrained ring drying shrinkage tests with longer microfibers as shown in Figure 81: polyvinyl

alcohol (PVA) and chopped carbon microfiber (CCMF). Adding PVA fibers to a 5wt% CNFs mixture added some benefits to ultimate microstrain and time delay in cracking, but the improvements were not as notables as what has been seen combining CNFs with MCMFs. Figure 81 also shows that adding 3wt% PVA fibers to a 5wt% CNFs 5wt% MCMFs mixture increased time delay in cracking but did not greatly influence ultimate microstrain (compared to 5wt% CNFs 2wt% PVA). It should be noted that PVA fibers do not separate as well as CCMFs during mixing and have the tendency to form clumps as shown in Figure 76. Adding CCMFs to the mixtures with 5wt% CNFs 5wt% MCMFs did not significantly effect ultimate microstrain but extend time delay until cracking from ~10 days to ~15 days. There were no clumps of CCMFs in the fresh mixture or the final composite. It should be noted that the CCMFs were prone to fracture during composite break rather than fiber pullout, and the macrocrack that formed in mixtures without PVA fibers had few if any fibers bridging the macrocrack.

5.3.4 Summary of Results and Conclusions

The sudden shift in slopes in the strain vs. time curves in microfine mortar mixtures with CNFs in Figure 71 are theorized to be the result softening caused by the switch from an ‘undamaged’ material to a ‘damaged’ material. The strain behavior in the time period prior to the knee in each mixture was dominated by the properties of the mortar matrix of sand and hydrated cement. During the knee, it is proposed that each mixture began developing microcracks that damaged the integrity of the mortar matrix. Eventually, the proliferation of microcracks in the mortar matrix reached a damage threshold and

subsequently resulted in the formation of a macrocrack in the control microfine cement mortar mixtures. The microfine cement hybrid mortar mixtures, however, sustained the damage due to crack bridging by the well-dispersed CNFs, and the existing microcracks could not propagate to form a macrocrack until more damage was induced.

The addition of MCMFs to the hybrid CNF microfine cement increased shrinkage cracking resistance more than the sum of the benefits from CNFs or MCMFs alone. It is our theory that cement matrix microcracking is bridged by CNFs, creating an apparent macrostrain in the composite that enables microfibers to add cracking resistance to the composite before the microcracks can propagate to form a macrocrack. Fiber composites of up to 5wt% CNFs and 5wt% MCMFs were successfully created and significantly increased the drying shrinkage cracking resistance of the composite. A summary of the results of the restrained ring drying shrinkage cracking tests is provided in Table 12. The mixture used in this research with the greatest shrinkage cracking resistance was a hybrid microfine cement mortar F0.4-2.2; the time delay in cracking was increased by a factor of ~52, and the ultimate microstrain in the steel ring was increased by a factor of ~3.9.

Table 12: Summary of restrained ring drying shrinkage test results.

Cement Type	W/C Ratio	CNFs (wt%)	MCMFs (wt%)	Other Fiber Type	Other Fiber (wt%)	Cracking Time (days)	Cracking Microstrain ($\mu\varepsilon$)	Cracking Time Factor**
OPC	0.4	0	0	--	--	2.2	89	--
OPC	0.5	0	0	--	--	2.8	97	--
OPC	0.5	1	0	--	--	2.7	73	0.96
OPC	0.5	2	0	--	--	3.4	94	1.2
OPC	0.5	3	0	--	--	4.1	102	1.5
MF	0.5	0	0	--	--	0.5	79	--
MF	0.5	1	0	--	--	0.8	89	1.6
MF	0.5	2	0	--	--	1.6	106	3.2
MF	0.5	3	0	--	--	1.8	107	3.6
MF	0.6	5	0	--	--	3.2	121	6.4
MF	0.7	5	0	--	--	3.3	102	6.6
MF	0.5	2	2	--	--	6.5	179	13
MF	0.6	5	5	--	--	10.2	222	20
MF	0.5	0	2	--	--	1.3	112	2.6
MF	0.4	0	0			0.6	77	--
MF	0.4	2	0	--	--	2.7	174	4.5
MF	0.4	2	2	--	--	31.2*	301*	52
MF	0.6	5	5	CCMF	2	15.6	235	31
MF	0.6	5	5	PVA	3	10.2	172	20
MF	0.6	5	0	PVA	2	4.2	155	8.4

*The RH was dropped from 50% to 35% to end the test sooner due to time constraints on the equipment.

**Calculated as the ratio of (mixture cracking time) / (control mixture cracking time)

6. CONCLUSIONS AND FUTURE RESEARCH

6.1 Dissertation Summary

The research contained in this dissertation dictates the effects of high concentrations of CNFs and various microfibers on the mechanical properties of Portland cement mortars with a primary emphasis on drying shrinkage cracking resistance. The first research focus was on dispersing high concentrations of CNFs into OPC and microfine cements using a sonication technique in pure ethyl alcohol to form a pre-mixed hybrid cement/CNF powder. Concentrations of CNFs up to 5wt% were successfully included microfine cement mortar with excellent dispersion, but it was found that geometric clustering inhibited the concentration of CNFs that could be successfully dispersed as a stable mixture in OPC. Both a theoretical model and SEM image analysis of the unhydrated hybrid cement powders proved that geometric clustering is a problem in OPC with high concentrations of CNFs but is not an issue in microfine cement (with CNFs).

The primary research focus in mechanical properties of the composite PCBMs was on drying shrinkage resistance utilizing a modified restrained ring drying shrinkage test. Hybrid CNF/OPC mortar ring tests did not show much change with the addition of up to 3wt% CNFs, but hybrid CNF/microfine cement mortar ring tests revealed a stark

difference with the addition of up to 5wt% CNFs (compared to the control mixture). CNFs bridged microcracking in the microfine cement matrix at the onset of failure, and the composite did not form a macrocrack until the damage from drying shrinkage increased enough to overcome the CNF crack bridging effect; this damage threshold increased with increasing concentrations of CNFs.

The restrained ring drying shrinkage test required additional information to properly characterize the behavior and results, so other experiments were completed to further characterize the materials. Free (unrestrained) drying shrinkage prisms revealed that hybrid OPC and hybrid microfine cement mortars had similar behavior during drying shrinkage but at different rates. Mortar cube elastic moduli testing showed that hybrid OPC mortars can had reduced elastic stiffness compared to control mixtures, and hybrid microfine cement mortars have no significant change in elastic modulus with the addition of CNFs. Flexure prism testing results indicated that hybrid OPC mortars can match control mixture strengths at late ages and high concentrations of CNFs but have decreased strengths at early age and do not gain strength with up to 3wt% CNFs. Hybrid microfine cement mortar flexure test results indicated that the addition of up to 3wt% CNFs can incrementally increase flexure strength by up to 50% at 28 days.

The next step in increasing drying shrinkage cracking resistance was to include microfibers into the hybrid microfine cement mortars. MCMFs were added in matching concentrations with CNFs (e.g. 2wt% and 2wt%, 5wt% and 5wt%), and the resulting

composite had a drying shrinkage cracking resistance that was higher than the combination of either CNFs of MCMFs alone. MCMFs could be mixed into the cements (either OPC or microfine, hybrid or no) during sonication with the CNFs or by tumbling the cement and MCMFs together. Adding MCMFs to hybrid microfine cement mortar extended the time until the formation of a macrocrack by up to 5,200%. Lowering the w/c ratio of the composite was also found to enhance the effects of both CNFs and MCMFs. The addition of microfibers larger than MCMFs could further increase the drying shrinkage cracking resistance, but dispersion was a problem with the longer fibers (especially PVA microfibers).

Finally, some mechanical properties were measured of the hybrid microfine cement mortars with MCMFs. Compressive strength cylinders indicate that adding CNFs and MCMFs to a microfine cement mortar can increase 7-day compressive strengths by up to 56%, but dropping the w/c ratio from 0.5 to 0.4 can increase 7-day compressive strengths by 45%. Izod impact strength tests showed that CNFs and MCMFs do not significantly effect hybrid microfine cement mortars. CMOD testing indicated that the addition of CNFs and/or MCMFs increase peak load, ultimate CMOD, and material cracking toughness.

6.2 Primary Conclusions

The primary objectives of this research were to enhance the efficacy of CNFs and MCMFs in PCBMs and to increase the cracking resistance of the composite material without detriment to other mechanical properties. The information provided in Section 6.1 indicates that the objectives were completed, and conclusions that can be drawn from the research are listed herein:

- Sonicating CNFs and cement together in pure alcohol with a low solids-to-liquids ratio can effectively disperse high concentrations of CNFs throughout the cement, and the resulting hybrid CNF/cement powder can be used in lieu of an ordinary cement in common mixing procedures.
- CNFs in OPC are subject to geometric clustering. High concentrations of CNFs exacerbate the geometric clustering effect and can potentially make the dispersion of CNFs through the cement worse than low concentrations. CNFs are not subject to geometric clustering in the microfine cement used in this research and form a stable mixture at high concentrations up to (and possible exceeding) 5wt%.
- SEM imaging can be used to gain quantitative information for research but is susceptible to bias and should not be the sole source of data, especially in mixtures whose constituents' sizes range over several orders of magnitude.
- Microfine cement mortar and OPC mortar behave similarly during unrestrained drying shrinkage but at different rates. Adding high concentrations of CNFs to

OPC creates a network of CNF agglomeration zones (due to geometric clustering). Adding high concentrations of CNFs to microfine cement slightly coarsens the pore network but does not create a network of CNF agglomeration zones.

- High concentrations of CNFs can prove detrimental to the elastic modulus and flexural strength of hybrid OPC mortars. High concentrations of CNFs have negligible effects on microfine cement mortars and can improve the flexural strength by up to 50%.
- Flexure prisms with both CNFs and MCMFs suggest that their addition to microfine cement mortar can increase the flexural strength by up to 121%, but workability issues and air voids cause uncertainty in any one particular specimen.
- Compressive strengths of hybrid microfine cement mortar are highly susceptible to w/c ratio. The addition of both CNFs and MCMFs can increase the compressive strength by up to 56%, but dropping the w/c ratio from 0.5 to 0.4 can increase the compressive strength by up to 45%.
- The addition of CNFs and MCMFs does not significantly effect impact fracture strength of hybrid microfine cement mortars. Both CNFs and MCMFs improve the flexural peak load, ultimate CMOD, and flexural toughness of hybrid microfine cement mortars.
- Restrained drying shrinkage ring tests revealed that the incorporation of CNFs into OPC mortar proved detrimental to the material at worst and marginally beneficial to the material at best. These effects are attributed to 1) the limit of

achievable dispersion of CNFs through the matrix due to the size disparity between the CNFs and the OPC grains – i.e., the geometric clustering effect – and 2) to the apparent segregation of CNFs out of dispersion during vibration, which may also be induced by the size disparity of the cement grains and the CNFs.

- Restrained drying shrinkage ring tests also revealed that the incorporation of MCMFs into OPC mortar have the potential to delay drying shrinkage cracking time by a factor of up to 5.4 at 6wt% MCMFs, but further research is needed to solidify the results and to determine the cause of flaws in the material.
- The sudden shift in slopes in the strain vs. time curves in microfine mortar mixtures with CNFs are theorized to be the result softening caused by the switch from an ‘undamaged’ material to a ‘damaged’ material. The strain behavior in the time period prior to the knee in each mixture was dominated by the properties of the mortar matrix of sand and hydrated cement. During the knee, it is proposed that each mixture began developing microcracks that damaged the integrity of the mortar matrix. Eventually, the proliferation of microcracks in the mortar matrix reached a damage threshold and subsequently resulted in the formation of a macrocrack in the control microfine cement mortar mixtures. The microfine cement hybrid mortar mixtures, however, sustained the damage due to crack bridging by the well-dispersed CNFs, and the existing microcracks could not propagate to form a macrocrack until more damage was induced.

- The addition of MCMFs to the hybrid CNF microfine cement increased shrinkage cracking resistance more than the sum of the benefits from CNFs or MCMFs alone. It is our theory that cement matrix microcracking is bridged by CNFs, creating an apparent macrostrain in the composite that enables microfibers to add cracking resistance to the composite before the microcracks can propagate to form a macrocrack. Fiber composites of up to 5wt% CNFs and 5wt% MCMFs were successfully created and significantly increased the drying shrinkage cracking resistance of the composite. The mixture used in this research with the greatest shrinkage cracking resistance was a hybrid microfine cement mortar F0.4-2.2; the time delay in cracking was increased by a factor of ~52, and the ultimate microstrain in the steel ring was increased by a factor of ~3.9.

6.3 Future Work

The research presented in this dissertation can be seen as fundamental and not immediately applicable. Future work is required to commercialize high-fiber content PCBMs (both CNFs and microfibers in both microfine cement and OPC), and more fundamental research in the form of modeling is needed for high concentration CNF PCBMs. Possible avenues of research are listed below.

- *Optimization of microfine cement multi-scale fiber-reinforced PCBMs.* As discussed in Section 6.3, the microfine cement used in this research was chosen for its commercial availability. It is likely that the 'optimum' cement grain size

distribution is not what was used. The only concentrations of CNFs used in this research were 1wt%, 2wt%, 3wt%, and 5wt%. 4wt% was not investigated, nor were any concentrations between integers (e.g. 2.5wt%). The only multi-scale fiber-reinforced microfine cement mortars that were studied had equal proportions of CNFs and MCMFs (e.g. 1wt% CNFs and 1wt% MCMFs), but it is likely that the optimum fiber concentrations would have fewer CNFs and more MCMFs (e.g. 2wt% CNFs and 6wt% MCMFs).

- *Extended research of OPC with high concentrations of MCMFs*. Section 5.2.2 discusses the first findings of OPC with up to 6wt% MCMFs pre-mixed into the cement with no loss in workability. 6wt% MCMFs without loss in workability is astounding since most research in the field of FRC caps at ~3wt% fibers. Further work needs to extend to include as many MCMFs as possible without loss in mechanical properties in hopes of creating a high-performance MCMF-reinforced OPC with high cracking resistance pre-mixed and ready for use by general contractors. Since MCMFs increased the compressive strength, flexural strength, and cracking resistance of microfine cement mortars, it is expected that high concentrations of MCMFs in OPC would likewise provide benefits to OPC.
- *Novel distribution techniques for cements with high water demand*. The high water demand of the microfine cement, especially with CNFs, limits the w/c ratios available with current mixing techniques. It has been shown in this research that lowering the w/c ratio can enhance the efficacy of both CNFs and MCMFs in microfine cement mortars. The lowest w/c ratio achievable in the

microfine cement mortar with 2wt% CNFs and 5wt% CNFs was 0.4 and 0.6, respectively, even with 4.0wt% HRWR. A new mixing/distribution technique needs to be developed to lower the w/c ratio below 0.4 with high concentrations of CNFs to maximize the efficacy of the fibers and further improve the mechanical properties (compressive and flexural strengths, impact toughness, flexural toughness, etc.).

- *Experimenting with various microfibers to add ductility.* The MCMFs used in this research add strength and cracking resistance, but they do not add post-crack ductility to the composite. Macrocracks in the mortars in this research do not have fibers bridging across the crack, and the composite still behaves as a brittle material much like the mortars without MCMFs. Another fiber type (or multiple) needs to be added to the composite for ductility.
- *Development of mass-production techniques.* The alcohol/sonication dispersion method described in Section 3.1.3 is extremely time consuming compared to other dispersion methods. Little material can be sonicated per batch of material (e.g. 200 grams of cement with CNFs in 1 hour), and the alcohol must be removed (and preferably recaptured) in a distillation column after sonication. A new technique using the same alcohol/sonication method could be developed that is not a batch process but a continuous feed to speed up material processing.
- *More accurate elastic moduli testing.* Elastic moduli as determined in Section 4.3 were estimated using the displacement of the loading head on the compression

machine. Actual elastic moduli need to be measured using ASTM standard techniques (or other more accurate techniques).

- *Test 28-day compressive cylinders with a different curing method.* 28-day compressive cylinders made with microfine cement had lower compressive strengths than the 7-day compressive cylinders. While we theorize that this is due to chemical interaction between the hydrated microfine cement and the lime water in which the specimens were cured, there is no evidence to support or refute the claim. A better curing method would be sealed specimens or demolded at 24 hours and exposed to 98% RH until time of testing.
- *Increase the number of samples tested.* All experiments were performed on too few samples. One of the largest drawbacks of the hybrid microfine cement is the time to create the material; this limited the number of specimens that could be produced in a timely manner for testing.

7. REFERENCES

1. Crow, J.M., *The concrete conundrum,* in *Chemistry World*. 2008.
2. Koch, G.H., et al., *Corrosion Costs and Preventative Strategies in the United States,* F.H. Administration, Editor. 2001, NACE International.
3. Bazant, Z., S. Sener, and J.-K. Kim, *Effect of Cracking on Drying Permeability and Diffusivity of Concrete.* ACI Materials Journal, 1987. **84**(5): p. 351-357.
4. Aveston, J. and A. Kelly, *Theory of multiple fracture of fibrous composites.* Journal of Materials Science, 1973. **8**(3): p. 352-362.
5. Bentur, A. and S. Mindess, *Fiber Reinforced Cementitious Composites*. 1990: Elsevier Science Publishers LTD.
6. Smilauer, V., H. Petr, and P. Padevet, *Micromechanical Analysis of Cement Paste with Carbon Nanotubes.* Acta Polytechnica, 2012. **52**(6): p. 22-28.
7. ACI Committee 544, *State-of-the-Art Report on Fiber Reinforced Concrete,* in *ACI 544.1R-96*. 2002.
8. Mindess, S., F.J. Young, and D. Darwin, *Concrete, 2nd Edition*. 2003: Pearson Education, Inc.
9. Majumdar, A.J., et al., *Fibre Concrete Materials.* Materials and Construction (Paris), 1977. **10**(2): p. 103-120.

10. Kobayashi, K. and R. Cho, *Flexural behaviour of polyethylene fibre reinforced concrete.* International Journal of Cement Composites and Lightweight Concrete, 1981. **3**(1): p. 19-25.

11. Al-Saleh, M.H. and U. Sundararaj, *Review of the mechanical properties of carbon nanofiber/polymer composites.* Composites Part A: Applied Science and Manufacturing, 2011. **42**(12): p. 2126-2142.

12. Yu, M.-F., et al., *Strength and Breaking Mechanism of Multiwalled Carbon Nanotubes Under Tensile Load.* Science, 2000. **287**(5453): p. 673-640.

13. Mahadik, S.A., S.K. Kamane, and A.C. Lande, *Effect of steel fibers on compressive and flexural strength of concrete.* International Journal of Advanced Structures and Geotechnical Engineering, 2014. **3**(4): p. 388-392.

14. Morris, A.D. and G.G. Garrett, *A comparative study of the static and fatigue behaviour of plain and steel fibre reinforced mortar in compression and direct tension.* International Journal of Cement Composites and Lightweight Concrete, 1981. **3**(2): p. 73-91.

15. Barr, B., A. Asghari, and T.G. Hughes, *Tensile strength and toughness of FRC materials.* International Journal of Cement Composites and Lightweight Concrete, 1988. **10**(2): p. 101-107.

16. Balaguru, P.N. and S.P. Shah, *Fiber-Reinforced Cement Composites*. 1992: McGraw-Hill.

17. ASTM, *ASTM C1018: Standard Test Method for Flexural Toughness and First-Crack Strength of Fiber-Reinforced Concrete (Using Beam with Third-Point Loading).* ASTM International, 1997.

18. ACI Committee 544, *Measurement of Properties of Fiber Reinforced Concrete,* in *ACI 544.2R-89*. 1989.

19. Ramakrishnan, V., G.Y. Wu, and G. Hosalli, *Flexural Fatigue Strength, Endurance Limit, and Impact Strength of Fiber Reinforced Concretes.* Transportation Research Record, 1989.

20. Sanchez, F. and C. Gay, *Performance of Carbon Nanofiber-Cement Composites with a High-Range Water Reducer.* Transportation Research Record: Journal of the Transportation Research Board, 2010. **2142**(-1): p. 109-113.

21. Nasibulin, A.G., et al., *A Novel Approach For Nanocarbon Composite Preparation.* MRS Proceedings, 2012. **1454**: p. 279-286.

22. Konsta-Gdoutos, M.S., Z.S. Metaxa, and S.P. Shah, *Multi-scale mechanical and fracture characteristics and early-age strain capacity of high performance carbon nanotube/cement nanocomposites.* Cement and Concrete Composites, 2010. **32**(2): p. 110-115.

23. Nasibulina, L., et al., *Carbon nanofiber/clinker hybrid material as a highly efficient modificator of mortar mechanical properties.* Materials Physics and Mechanics, 2012. **13**: p. 77-84.

24. Gdoutos, E.E., et al., *Advanced cement based nanocomposites reinforced with MWCNTs and CNFs.* Frontiers of Structural and Civil Engineering, 2016.

25. Li, G.Y., P.M. Wang, and X. Zhao, *Mechanical behavior and microstructure of cement composites incorporating surface-treated multi-walled carbon nanotubes.* Carbon, 2005. **43**(6): p. 1239-1245.

26. Chung, D.D.L., *Cement-matrix structural nanocomposites.* Metals and Materials International, 2004. **10**(1): p. 55-67.

27. Sanchez, F., L. Zhang, and C. Ince, *Multi-Scale Performance and Durability of Carbon Nanofiber/Cement Composites*, in *Proceedings of the 3rd International Symposium on Nanotechnology in Construction*. 2009: Prague, Czech Republic. p. 345-350.

28. Sanchez, F. and C. Ince, *Microstructure and macroscopic properties of hybrid carbon nanofiber/silica fume cement composites.* Composites Science and Technology, 2009. **69**(7-8): p. 1310-1318.

29. Metaxa, Z.S., M.S. Konsta-Gdoutos, and S.P. Shah, *Carbon nanofiber cementitious composites: Effect of debulking procedure on dispersion and reinforcing efficiency.* Cement and Concrete Composites, 2013. **36**: p. 25-32.

30. Shah, S.P., M.S. Konsta-Gdoutos, and Z.S. Metaxa, *Carbon Nanofiber-Reinforced Cement-Based Materials.* Transportation Research Record: Journal of the Transportation Research Board, 2010. **2142**(-1): p. 114-118.

31. Yazdanbakhsh, A., et al., *Challenges and Benefits of Utilizing Carbon Nanofilaments in Cementitious Materials.* Journal of Nanomaterials, 2012. **2012**: p. 1-8.

32. Abu Al-Rub, R.K., et al., *Mechanical Properties of Nanocomposite Cement Incorporating Surface-Treated and Untreated Carbon Nanotubes and Carbon Nanofibers.* Journal of Materials in Civil Engineering, 2012. **2**(1): p. 1-6.

33. Tyson, B.M., et al., *Carbon Nanotubes and Carbon Nanofibers for Enhancing the Mechanical Properties of Nanocomposite Cementitious Materials.* Journal of Materials in Civil Engineering, 2011. **23**(7): p. 1028-1035.

34. Brown, L. and F. Sanchez, *Influence of carbon nanofiber clustering on the chemo-mechanical behavior of cement pastes.* Cement and Concrete Composites, 2016. **65**: p. 101-109.

35. Di Gao, Y.L.M. and L.M. Pend, *Mechanical and Electrical Properties of Carbon-NanoFiber Self-Consolidating Concrete.* Earth and Space 2010, 2010: p. 2577-2585.

36. Luo, J., Z. Duan, and H. Li, *The influence of surfactants on the procssing of multi-walled carbon nanotubes in reinfored cement matrix composites.* Physica Status Solidi (A) Applications and Materials Science, 2009. **206**(12): p. 2783-2790.

37. Kauppinen, E.I., et al., *Direct Synthesis of Carbon Nanofibers on Cement Particles.* Transportation Research Record: Journal of the Transportation Research Board, 2010. **2142**(-1): p. 96-101.

38. Sbia, L.A., et al., *Optimization of ultra-high-performance concrete with nano- and micro-scale reinforcement.* Cogent Engineering, 2014. **1**(1): p. 990673.

39. Chaipanich, A., et al., *Compressive strength and microstructure of carbon nanotubes–fly ash cement composites.* Materials Science and Engineering: A, 2010. **527**(4-5): p. 1063-1067.

40. Stephens, C., L. Brown, and F. Sanchez, *Quantification of the re-agglomeration of carbon nanofiber aqueous dispersion in cement pastes and effect on the early age flexural response.* Carbon, 2016. **107**: p. 482-500.

41. Mo, Y.L. and R. Howser, *Carbon Nanofiber Concrete for Damage Detection of Infrastructure.* 2013.

42. Makar, J.M., J.C. Margeson, and J. Luh. *Carbon Nanotube Cement Composites - Early Results and Potential Applications*. in *Proceedings of the 3rd international conference on construction materials: performance, innovations and structural implications*. 2005. Vancouver, BC, Canada.

43. Peyvandi, A., et al., *Effect of the cementitious paste density on the performance efficiency of carbon nanofiber in concrete nanocomposite.* Construction and Building Materials, 2013. **48**: p. 265-269.

44. Metaxa, Z.S., M.S. Konsta-Gdoutos, and S.P. Shah, *Mechanical Properties and Nanostructure of Cement-Based Materials Reinforced with Carbon Nanofibers and Polyvinyl Alcohol (PVA) Microfibers.* American Concrete Institute, 2010. **270**: p. 115-124.

45. Deng, Y., *Carbon Fiber Electronic Interconnects*, in *Mechanical Engineering*. 2007, University of Maryland. p. 85.

46. Gorss, J., *High Performance Carbon Fibers*, A.C. Society, Editor. 2003.

47. Bal, S., *Experimental study of mechanical and electrical properties of carbon nanofiber/epoxy composites.* Materials & Design (1980-2015), 2010. **31**(5): p. 2406-2413.

48. Zhu, J., et al., *Strain-Sensing Elastomer/Carbon Nanofiber "Metacomposites".* The Journal of Physical Chemistry C, 2011. **115**(27): p. 13215-13222.

49. Ji, L., et al., *Porous carbon nanofibers from electrospun polyacrylonitrile/SiO2 composites as an energy storage material.* Carbon, 2009. **47**(14): p. 3346-3354.

50. Qie, L., et al., *Nitrogen-doped porous carbon nanofiber webs as anodes for lithium ion batteries with a superhigh capacity and rate capability.* Adv Mater, 2012. **24**(15): p. 2047-50.

51. Bortz, D.R., C. Merino, and I. Martin-Gullon, *Carbon nanofibers enhance the fracture toughness and fatigue performance of a structural epoxy system.* Composites Science and Technology, 2011. **71**(1): p. 31-38.

52. Hvizdos, P., et al., *Carbon Nanofibers Reinforced Ceramic Matrix Composites*, in *Nanofibers - Production, Properties and Functional Applications*, D.T. Lin, Editor. 2011, InTech.

53. Musso, S., et al., *Influence of carbon nanotubes structure on the mechanical behavior of cement composites.* Composites Science and Technology, 2009. **69**(11-12): p. 1985-1990.

54. Yazdanbakhsh, A., et al., *Distribution of Carbon Nanofibers and Nanotubes in Cementitious Composites.* Transportation Research Record: Journal of the Transportation Research Board, 2010. **2142**: p. 89-95.

55. Xie, X., Y. Mai, and X. Zhou, *Dispersion and alignment of carbon nanotubes in polymer matrix: A review.* Materials Science and Engineering: R: Reports, 2005. **49**(4): p. 89-112.

56. Konsta-Gdoutos, M.S., Z.S. Metaxa, and S.P. Shah, *Highly dispersed carbon nanotube reinforced cement based materials.* Cement and Concrete Research, 2010. **40**(7): p. 1052-1059.

57. Yazdani, N. and V. Mohanam, *Carbon Nano-Tube and Nano-Fiber in Cement Mortar: Effect of Dosage Rate and Water-Cement Ratio.* International Journal of Material Sciences, 2014. **4**(2): p. 45.

58. Parveen, S., S. Rana, and R. Fangueiro, *A Review on Nanomaterial Dispersion, Microstructure, and Mechanical Properties of Carbon Nanotube and Nanofiber Reinforced Cementitious Composites.* Journal of Nanomaterials, 2013. **2013**: p. 1-19.

59. Metaxa, Z.S., M.S. Konsta-Gdoutos, and S.P. Shah, *Nanoimaging of Highly Dispersed Carbon Nanotube Reinforced Cement Based Materials.* 7th International RILEM Symposium on Fibre Reinforced Concrete: Design and Applications, 2008. **Rilem Publications**: p. 125-131.

60. Li, Q., J. Liu, and S. Xu, *Progress in Research on Carbon Nanotubes Reinforced Cementitious Composites.* Advances in Materials Science and Engineering, 2015. **2015**: p. 1-16.

61. Chen, S.J., et al., *Carbon nanotube–cement composites: A retrospect.* The IES Journal Part A: Civil & Structural Engineering, 2011. **4**(4): p. 254-265.

62. Yazdanbakhsh, A. and Z. Grasley, *Utilization of Silica Fume to Stabilize the Dispersion of Carbon Nanofilaments in Cement Paste.* Journal of Materials in Civil Engineering, 2014. **26**(7): p. 1-10.

63. Mudimela, P.R., et al., *Synthesis of Carbon Nanotubes and Nanofibers on Silica and Cement Matrix Materials.* Journal of Nanomaterials, 2009. **2009**: p. 1-4.

64. Makar, J.M., J.C. Margeson, and J. Luh, *Carbon Nanotube/Cement Composites - Early Results and Potential Applications*, in *3rd International Conference on Construction Materials: Performance, Innovations and Structural Implications*. 2005, National Research Council Canada: Vancouver, B.C. p. 1-10.

65. Metaxa, Z.S., et al., *Highly concentrated carbon nanotube admixture for nano-fiber reinforced cementitious materials.* Cement and Concrete Composites, 2012. **34**(5): p. 612-617.

66. LichaoFeng, E.Y., E.Y. NingXie, and J. Zhong, *Carbon Nanofibers and Their Composites: A Review of Synthesizing, Properties and Applications.* Materials, 2014. **7**(5): p. 3919-3945.

67. Sánchez, M., et al., *Characterization of carbon nanofiber/epoxy nanocomposites by the nanoindentation technique.* Composites Part B: Engineering, 2011. **42**(4): p. 638-644.

68. Lozano, K., J. Bonilla-Rios, and E.V. Barrera, *A study on nanofiber-reinforced thermoplastic composites (II): Investigation of the mixing rheology and conduction properties.* Journal of Applied Polymer Science, 2001. **80**(8): p. 1162-1172.

69. Yang, B., et al., *Improvement of a gram-scale mixer for polymer blending.* Journal of Applied Polymer Science, 2006. **99**(1): p. 1-5.

70. Yazdanbakhsh, A. and Z. Grasley, *The theoretical maximum achievable dispersion of nanoinclusions in cement paste.* Cement and Concrete Research, 2012. **42**(6): p. 798-804.

71. Yazdanbakhsh, A., et al., *Dispersion quantification of inclusions in composites.* Composites Part A: Applied Science and Manufacturing, 2011. **42**(1): p. 75-83.

72. Grasley, Z.C. and A. Yazdanbakhsh, *Quantifying the dispersion of discrete inclusions in composites using continuum theory.* Composites Part A: Applied Science and Manufacturing, 2011. **42**(12): p. 2043-2050.

73. Shah, H.R. and J. Weiss, *Quantifying shrinkage cracking in fiber reinforced concrete using the ring test.* Materials and Structures, 2006. **39**(9): p. 887-899.

74. Grasley, Z. and M. D'Ambrosia, *Viscoelastic properties and drying stress extracted from concrete ring tests.* Cement & Concrete Composites, 2010. **33**: p. 171-178.

75. ASTM, *ASTM C1581: Standard Test Method for Determining Age at Cracking and Induced Tensile Stress Characteristics of Mortar and Concrete under Restrained Shrinkage*, in *ASTM International*. 2009.

76. Hossain, A.B. and J. Weiss, *The role of specimen geometry and boundary conditions on stress development and cracking in the restrained ring test.* Cement and Concrete Research, 2006. **36**(1): p. 189-199.

77. Moon, J.H. and J. Weiss, *Estimating residual stress in the restrained ring test under circumferential drying.* Cement and Concrete Composites, 2006. **28**(5): p. 486-496.

78. Hossain, A.B., B. Pease, and J. Weiss, *Quantifying early-age stress development and cracking in low water-to-cement concrete.* Transportation Research Record, 2003. **1834**(1): p. 24-32.

79. Moon, J.-H., et al., *Quantifying the influence of specimen geometry on the results of the restrained ring test.* Journal of ASTM International, 2006. **3**(8).

80. Dong, W., et al., *Effects of specimen size on assessment of shrinkage cracking of concrete via elliptical rings: Thin vs. thick.* Computers & Structures, 2016. **174**: p. 66-78.

81. Zhou, X., W. Dong, and O. Oladiran, *Experimental and numerical assessment of restrained shrinkage cracking of concrete using elliptical ring specimens.* Journal of Materials in Civil Engineering, 2014. **26**(11).

82. Grasley, Z.C. and M.D. D'Ambrosia, *Viscoelastic properties and drying stress extracted from concrete ring tests.* Cement and Concrete Composites, 2011. **33**(2): p. 171-178.

83. Knoppik-Wróbel, A. and B. Klemczak, *Degree of restraint concept in analysis of early-age stresses in concrete walls.* Engineering Structures, 2015. **102**: p. 369-386.

84. Hogancamp, J. and Z. Grasley, *Dispersion of High Concentrations of Carbon Nanofibers in Portland Cement Mortars.* Journal of Nanomaterials, 2017. **2017**: p. 1-11.

85. ASTM, *ASTM C490: Standard Practice for Use of Apparatus for the Determination of Length Change of Hardened Cement Paste, Mortar, and Concrete.* ASTM International, 2011.

86. Hajibabaee, A., Z. Grasley, and M.T. Ley, *Mechanisms of dimensional instability caused by differential drying in wet cured cement paste.* Cement and Concrete Research, 2016. **79**: p. 151-158.

87. Grasley, Z., *Closed-Form Solutions for Uniaxial Passive Restraint Experiments.* American Concrete Institute, 2010. **270**: p. 17-32.

88. Grasley, Z.C. and C.K. Leung, *Desiccation shrinkage of cementitious materials as an aging, poroviscoelastic response.* Cement and Concrete Research, 2011. **41**(1): p. 77-89.

89. ASTM, *ASTM C109: Standard Test Method for Compressive Strength of Hydraulic Cement Mortars.* ASTM International, 2016.

90. ASTM, *ASTM D256: Standard Test Methods for Determining the Izod Pendulum Impact Resistance of Plastics.* ASTM International, 2010.

91. Grasley, Z., et al., *Relative Humidity in Concrete.* Concrete International, 2006: p. 51-57.

92. Grasley, Z.C., et al., *The Internal Relative Humidity of Concrete: What Does it Mean?* Concrete International, 2006. **October**: p. 51-57.

APPENDIX A: TABLES OF MATERIALS AND MIXTURE PROPORTIONS

Table 13: Table of Materials

Material	Supplier		Acquisition
Ottawa 20-30 silica sand	Humboldt Mfg.	Elgin, IL	Purchase
Type I/II cement	Home Depot	College Station, TX	Purchase
MicroMatrix cement	Capitol Cement	San Antonio, TX	Donation
PR-24-XT-PS CNFs	Pyrograf Products	Cedarville, OH	Purchase
PX35MF0150 MCMFs	Zoltek	Bridgeton, MO	Donation
PX35CF0125-13 CCMFs	Zoltek	Bridgeton, MO	Donation
PVA RECS15 microfibers	Nycon	Fairless Hills, PA	Purchase
Glenium 7700 HRWR	Grace Construction	Cambridge, MA	Donation
Recover retarder	Grace Construction	Cambridge, MA	Donation

Table 14: Fiber concentrations in wt% by mass of cement, vol% by volume of cement, and vol% of total mortar.

W/c ratio	Fibers	Wt%	Vol%	Cumulative wt%	Cumulative vol%	Vol% total mortar*
0.5	CNFs	1	1.97	1	1.97	0.42
0.5	CNFs	2	3.94	2	3.94	0.83
0.5	CNFs	3	5.91	3	5.91	1.24
0.6	CNFs	5	9.84	5	9.84	1.93
0.5	CNFs MCMFs	1 1	1.97 1.97	2	3.94	0.83
0.5	CNFs MCMFs	2 2	3.94 3.94	4	7.88	1.65
0.5	CNFs MCMFs	3 3	5.91 5.91	6	11.8	2.46
0.6	CNFs MCMFs	5 5	9.84 9.84	10	19.7	3.78
0.6	CNFs MCMFs CCMFs	5 5 2	9.84 9.84 3.94	12	23.6	4.51
0.6	CNFs MCMFs CCMFs	5 5 3	9.84 9.84 5.91	13	25.6	4.86
0.6	CNFs MCMFs PVA	5 5 3	9.84 9.84 7.27	13	27.0	5.11
0.4	CNFs	2	3.94	2	3.94	0.89
0.4	CNFs MCMFs	2 2	3.94 3.94	4	7.88	1.77
*All mortars were made with a sand-to-cement mass ratio of 1.75						

APPENDIX B: SEM IMAGES OF CNFS IN CEMENT

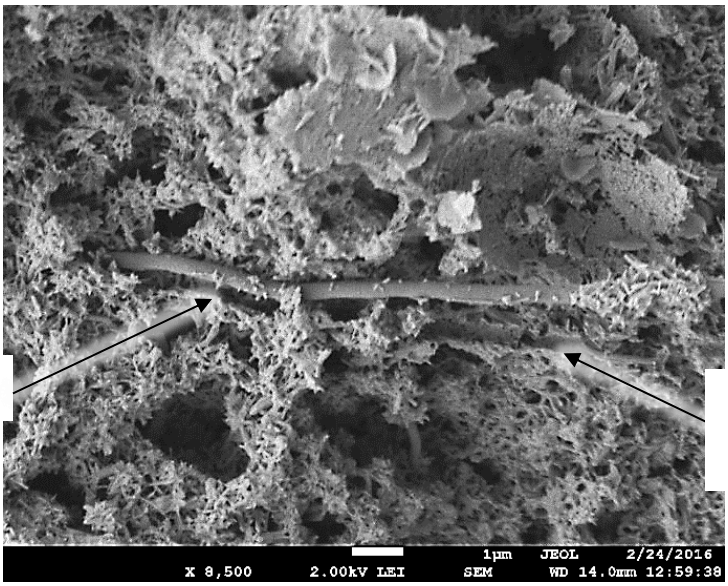

Figure 82: CNF with indentation in cement matrix.

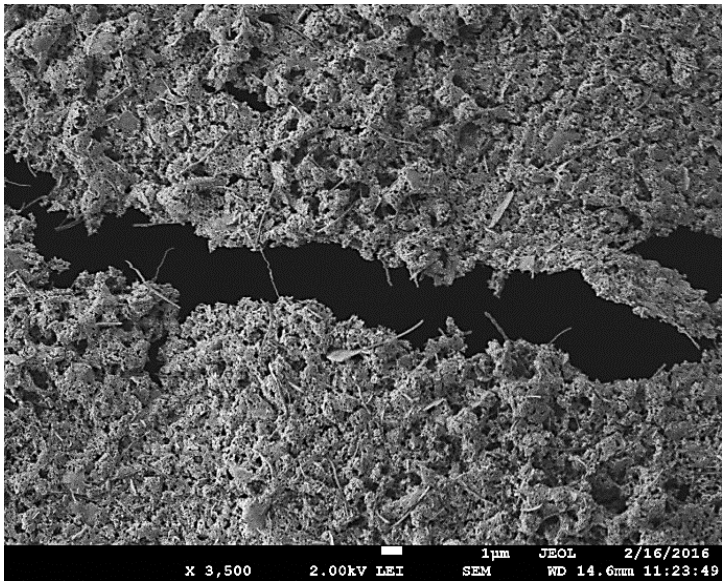

Figure 83: Top crust of 1wt% hybrid OPC hydrated.

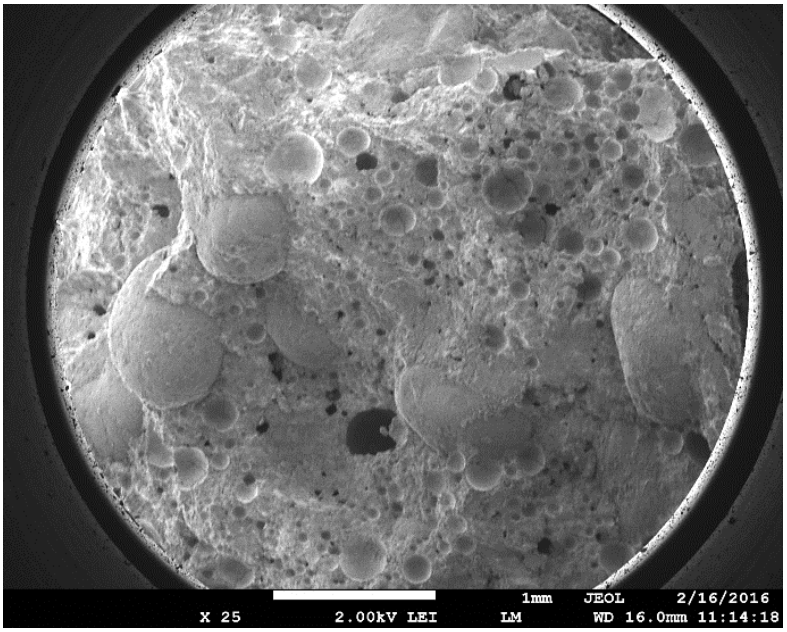

Figure 84: Low-magnification SEM image of bubbles in 1wt% CNF hybrid OPC (this is not the top crust of the material).

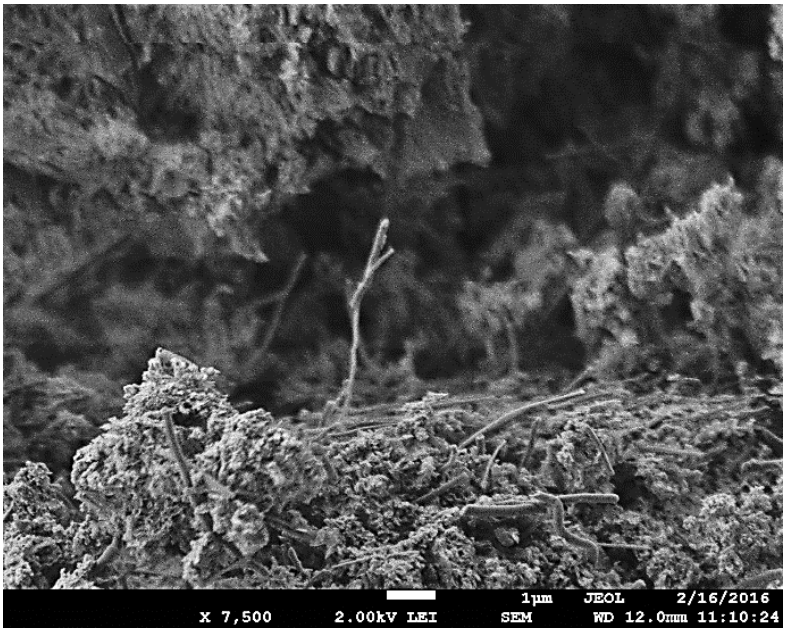

Figure 85: 1wt% CNFs hybrid OPC hydrated with a cluster of CNFs.

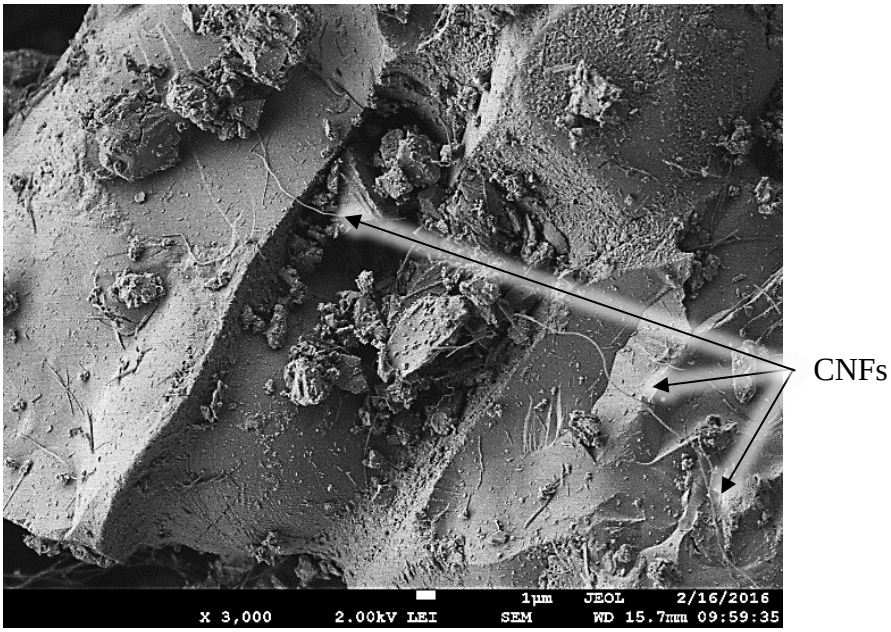

Figure 86: Large OPC cement grain with CNFs on its surface showing the size disparity between CNFs and the largest OPC grains.

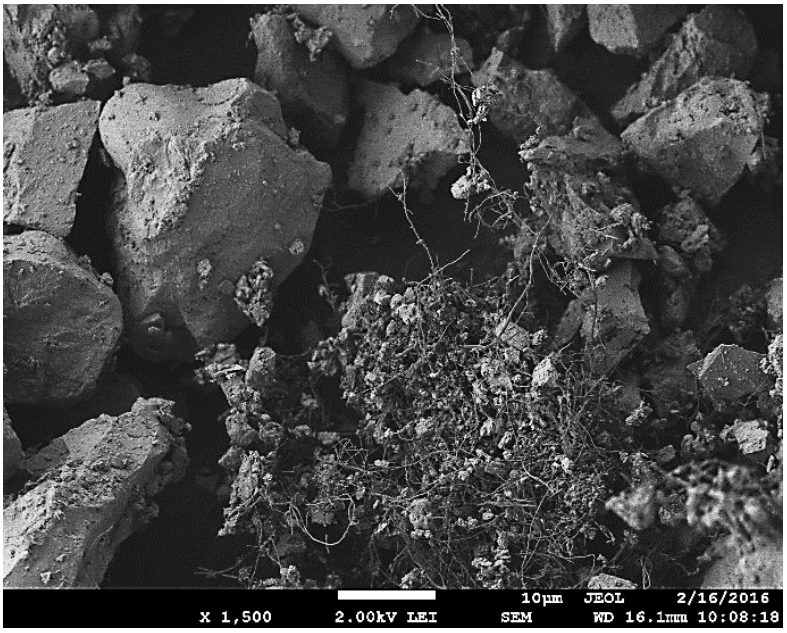

Figure 87: 2wt% CNFs hybrid OPC powder showing a clump of CNFs next to large OPC grains.

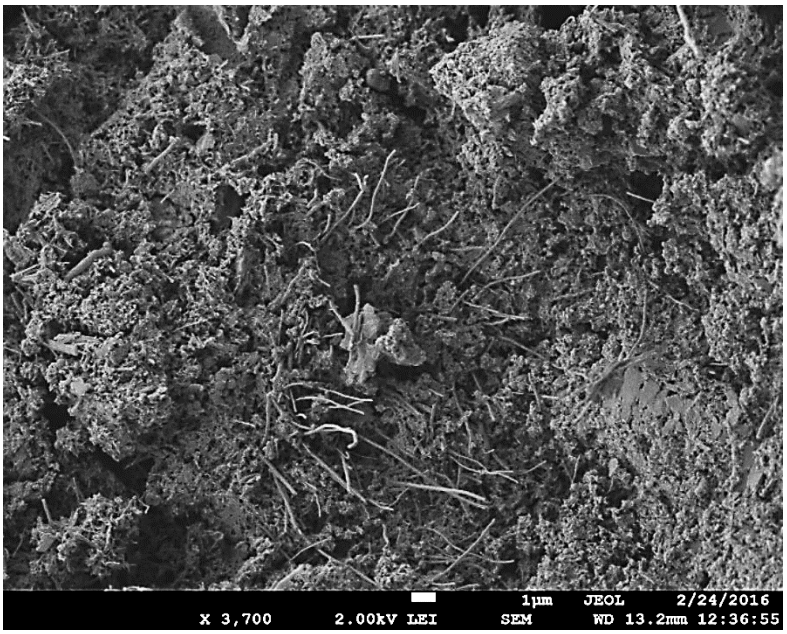

Figure 88: 2wt% CNFs hybrid OPC hydrated showing CNFs.

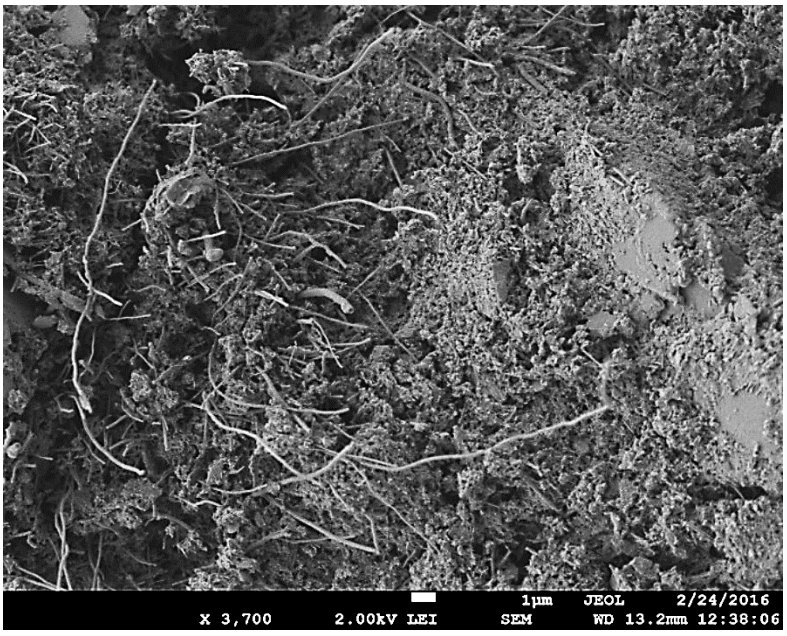

Figure 89: 2wt% CNFs hybrid OPC hydrated showing CNFs.

Figure 90: 2wt% CNFs hybrid OPC hydrated showing CNFs and ettringite in a large crack. CNFs and ettringite are nearly indistinguishable at this magnification.

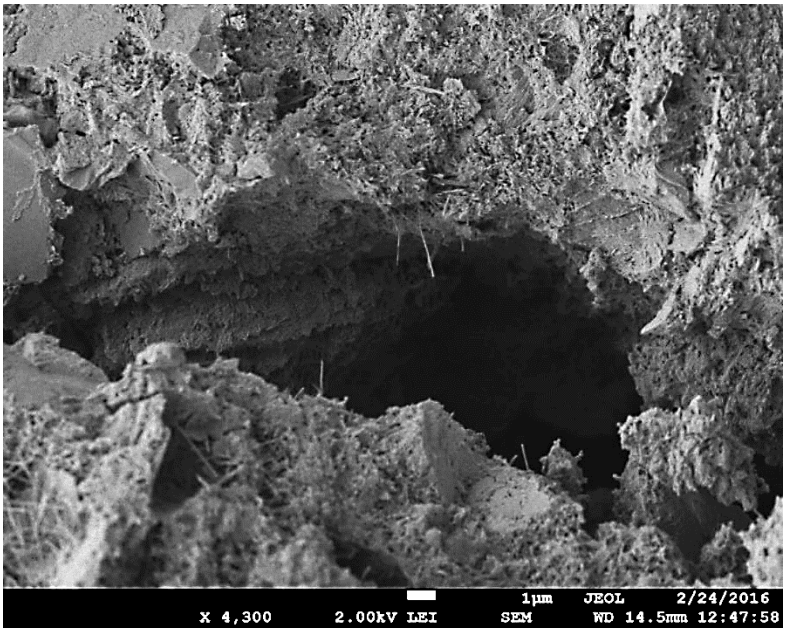

Figure 91: 2wt% CNFs hybrid OPC hydrated showing a crack with few CNFs protruding from the crack surface.

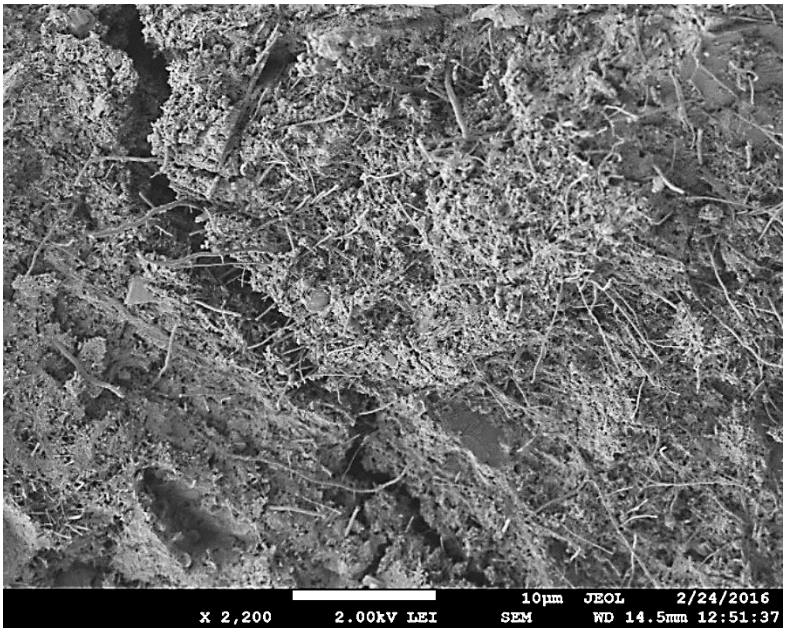

Figure 92: 2wt% CNFs hybrid OPC hydrated showing many CNFs around a crack.

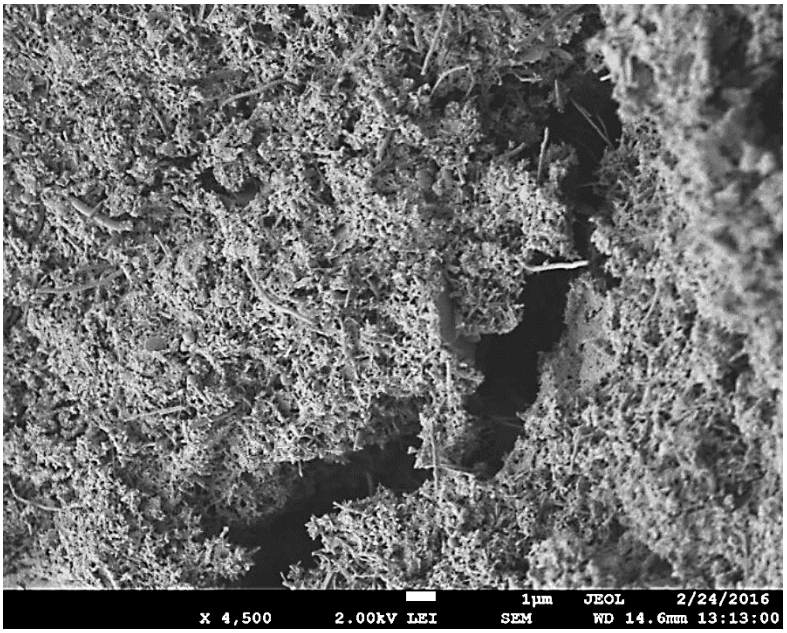

Figure 93: 3wt% CNFs hybrid OPC hydrated showing a crack with few CNFs protruding from the crack surfaces.

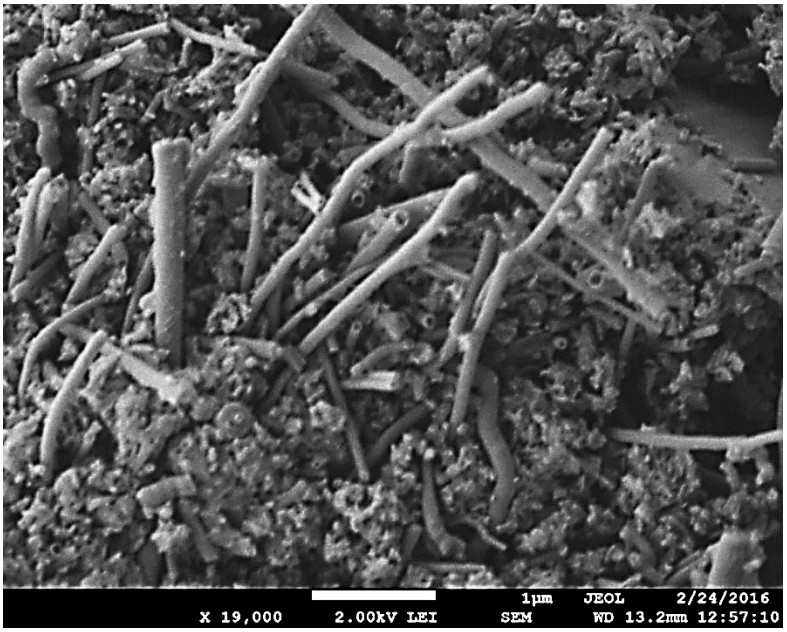

Figure 94: 3wt% CNFs hybrid OPC showing a clump of CNFs.

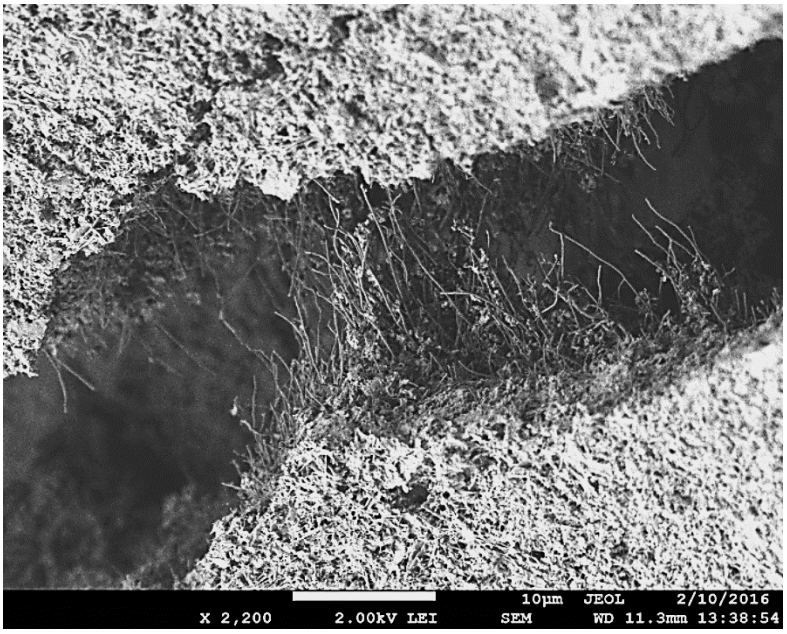

Figure 95: 2wt% CNFs hybrid microfine cement showing a clump of CNFs bridging a crack.

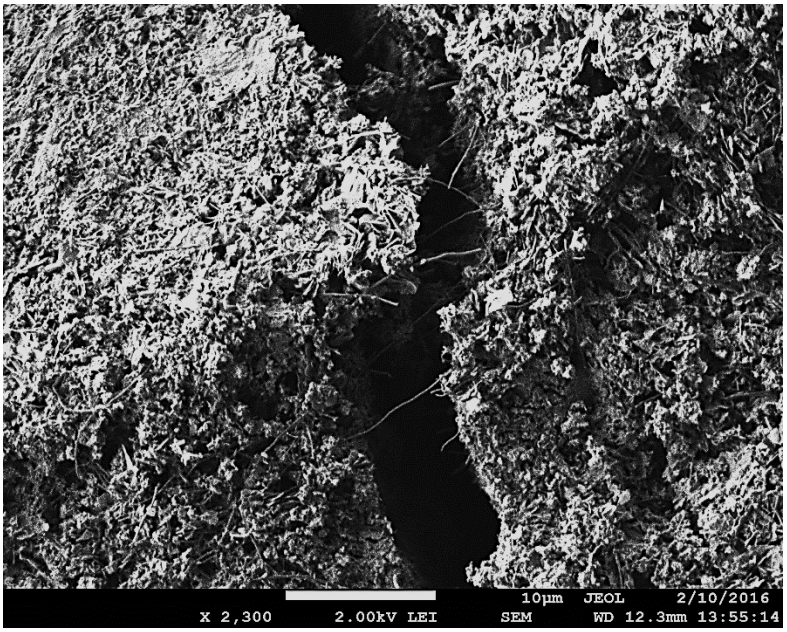

Figure 96: 3wt% CNFs hybrid microfine cement showing CNFs bridging across the crack.

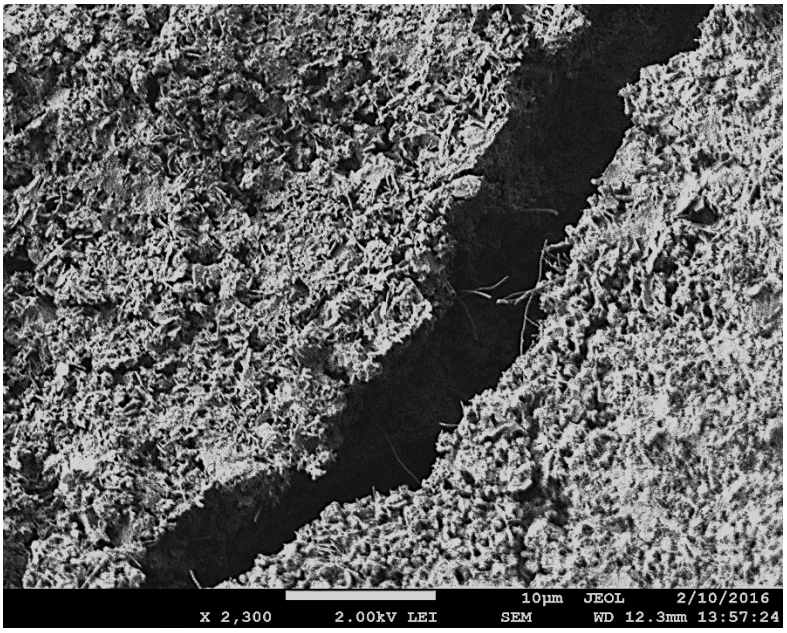

Figure 97: 3wt% CNFs hybrid microfine cement showing CNFs broken during crack formation.

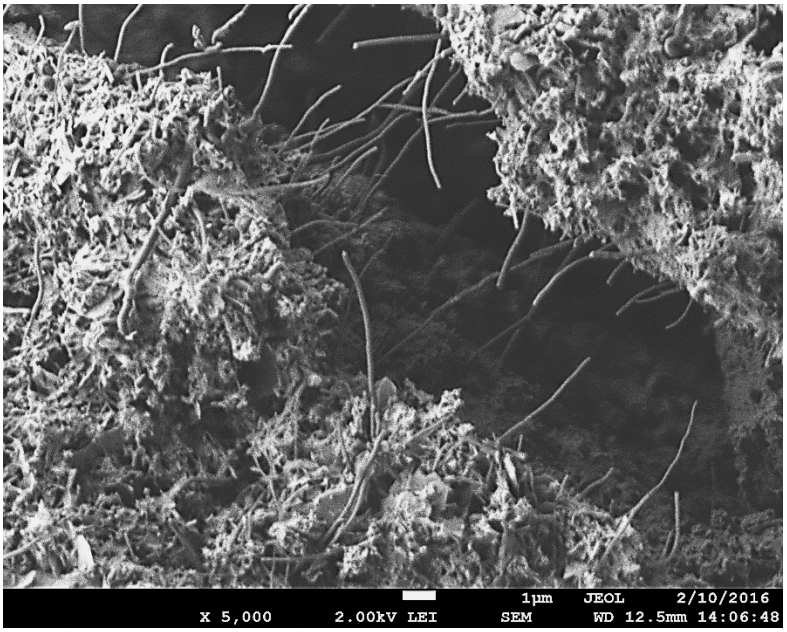

Figure 98: 3wt% CNFs hybrid microfine cement showing CNFs (most broken) bridging a crack.

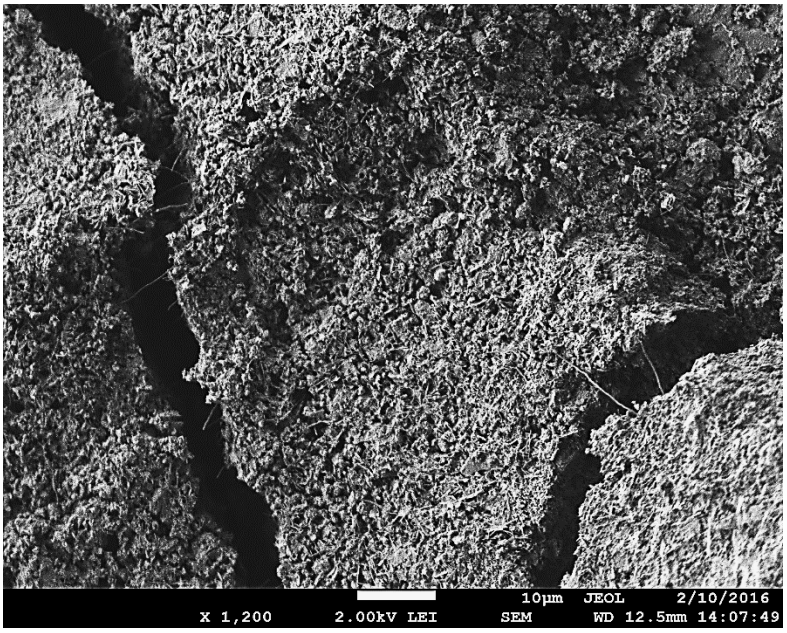

Figure 99: 3wt% CNFs hybrid microfine cement showing CNFs bridging across multiple cracks.

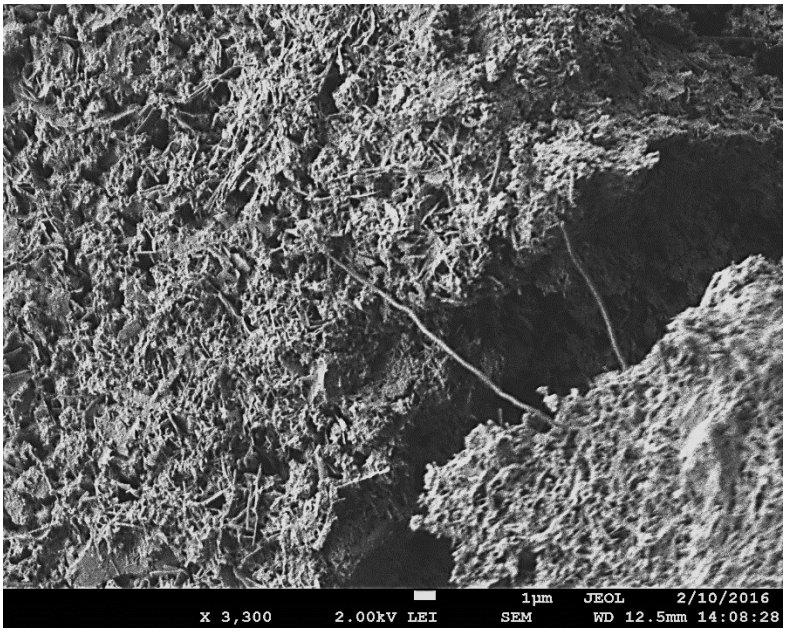

Figure 100: 3wt% CNFs hybrid microfine cement showing CNFs briding a crack with one long fiber embedded on both ends.

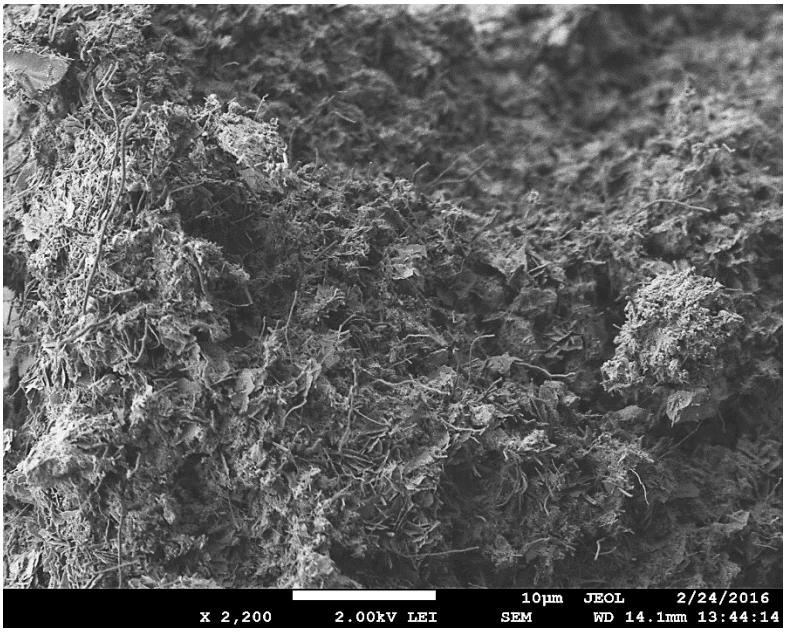

Figure 101: 5wt% CNFs hybrid microfine cement showing a plethora of CNFs.

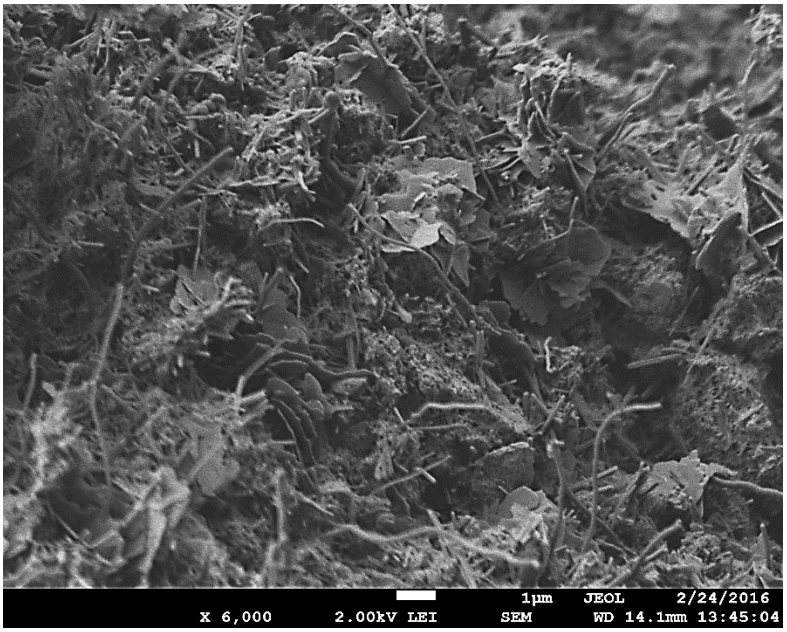

Figure 102: 5wt% CNFs hybrid microfine cement showing and hexagonal calcium hydroxide crystals.

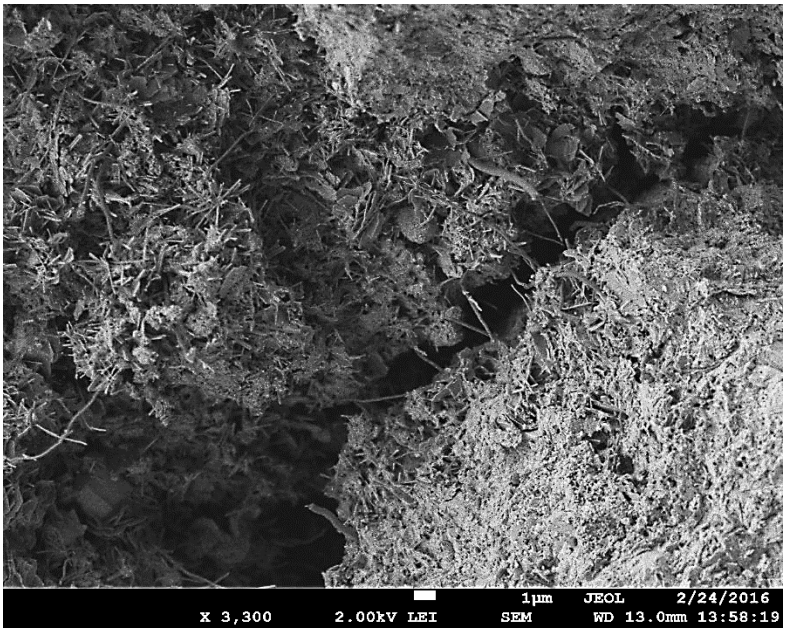

Figure 103: 5wt% CNFs hybrid microfine cement showing CNFs bridging a crack.

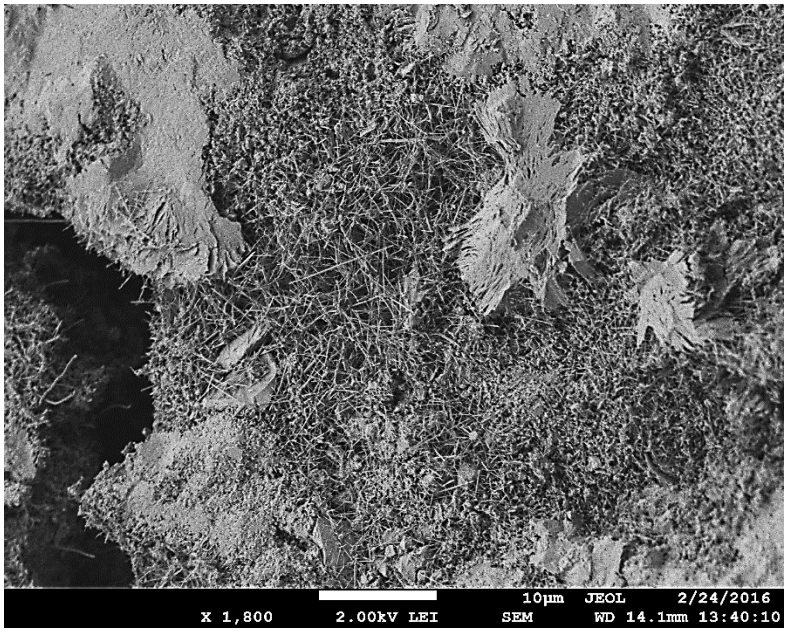

Figure 104: 5wt% CNFs hybrid microfine cement showing a large agglomeration of CNFs (center).